TOMAS BATA UNIVERSITY IN ZLIN
FACULTY OF TECHNOLOGY
Polymer Centre

Pavel Urbánek

Electronic Properties of Thin Polymer Films:
A Study of Structure between Nano- and Microscale

Elektronické vlastnosti tenkých polymerních
vrstev: Studie struktury mezi nano- a mikroškálou

Doctoral Thesis

Programme:	P 2808 Chemistry and Materials Technology 2808V006
Course:	Technology of Macromolecular Compounds
Supervisor:	doc. Ing. et Ing. Ivo Kuřitka, Ph.D. et Ph.D.
Year:	2014

Study programme: P 2808 Chemistry and Materials Technology
Field of study: 2808V006 Technology of Macromolecular
                     Compounds

Supervisor: Assoc. Prof. Ing. et Ing. Ivo Kuřitka Ph.D. et Ph.D.

Content

ACKNOWLEDGEMENT

Abstract

The main goals of the research presented in this thesis are preparation of thin polymer films and study of their optic and optoelectronic properties considering the structural ordering depending on their thickness with fundamental impact on final applications. As reference materials were used both σ- and π-conjugated polymer material, namely polysilanes and derivative of polyphenylenvinylene – MEH-PPV.

A brief theoretical background for conjugated and conductive polymers is reviewed in **Chapter 1**. The possibilities, how to improve their properties by preparation of composites with functionalized nanoparticles, are discussed in *Section 1.2*. Main techniques for thin films preparation and casting are discussed and described in **Chapter 2**. In **Chapter 3** are mentioned and described techniques used for characterization of prepared thin films.

Chapter 4 summarizes the main goals of this thesis.

In **Chapter 5**, the method and conditions for thin films casting from neat MEH-PPV polymer, polysilanes and from composite material are described in more detail and results and experience achieved during the sample preparation are discussed.

In **Chapter 6,** *Section 6.1,* a photoluminescence study of thin films from neat MEH-PPV is reported. In *Section 6.2,* the study of exciton diffusion length in thin MEH-PPV films is presented. Material properties are studied and interpreted from microphysical point of view, photoluminescence changes and inter- or intrachain exciton recombination or changing diffusion exciton length differing in thin and thick films are discussed. These physical properties are most important for practical use and are strongly dependent on the structural ordering in thin films, which has been shown to be tightly related to the thickness of films.

In **Chapter 7**, *Section 7.1*, a comprehensive photoluminescence study of polysilanes is introduced and the results discussed in terms of spectral changes depending on the film thickness. In *Section 7.2*, the UV-degradability study of polysilanes is presented. Not only the polymer deterioration but also self-recovering processes occur in polysilanes films during and after UV irradiation. This study together with

earlier published results support the theory of different conformational ordering of polymer chains depending on the films thickness as in case of π-conjugated polymer.

In **Chapter 8**, the work is targeted on the composite preparation from MEH-PPV and ZnO and CdS nanoparticles and evaluation of improved properties of this material used for final application, i.e. polymer OLED devices and hybrid structures for photovoltaic.

Chapter 9 is framed as a summary of conclusions of this thesis.

In **Chapter 10**, are brought several author's suggestions for future research in the field of semi- or conductive polymers, i.e. σ- and π- conjugated materials in respect to specific conditions and methods which are available in the Centre of Polymer Systems at the Tomas Bata University in Zlin.

Abstract in Czech

Hlavními body výzkumu prezentovaného v této disertační práci je příprava tenkých polymerních filmů a studium jejich optoelektrických vlastností, přičemž je brán do úvahy vývoj strukturního uspořádání polymerních řetězců v tenkých filmech závisející na jejich tloušťce. To má v konečném důsledku zásadní vliv na jakékoliv zamýšlené aplikace. Jako referenční materiály byly použity σ- a π-konjugované polymery, konkrétně polysilany a derivát polyphenylenvinylenu – MEH-PPV.

Krátký teoretický úvod o konjugovaných polymerech představuje **Kapitola 1**. Možnosti, jak zlepšovat jejich vlastnosti pomocí přípravy kompozitního materiálu, kde jako plnivo jsou použity funkcionalizované nanočástice, jsou diskutovány v *Sekci 1.2*. Hlavní techniky přípravy a depozice tenkých vrstev jsou rozebrány a popsány v **Kapitole 2**. V **Kapitole 3** jsou zmíněny a popsány techniky, které byly použity pro charakterizaci připravených tenkých filmů.

Kapitola 4 sumarizuje hlavní cíle této disertační práce.

V **Kapitole 5** jsou zmíněny metody a podmínky během přípravy tenkých vrstev z čistého MEH-PPV, polysilanů a kompozitního materiálu. Jsou zde uvedeny a diskutovány zkušenosti a výsledky získané během depozice tenkých vrstev.

V **Kapitole 6**, *Sekci 6.1*, je uvedena fotoluminiscenční studie tenkých filmů připravených z čistého polymeru MEH-PPV. V *Sekci 6.2* je představena studie závislosti difúzní délky excitonu v tenkých vrstvách na jejich tloušťce. Materiálové vlastnosti jsou studovány a interpretovány z mikrofyzikálního hlediska, v závislosti na tloušťkách filmů dochází ke změnám PL, molekulových a mezimolekulových rekombinací excitonů, jakož i ke změně difúzní délky excitonu. Navíc tyto fyzikální vlastnosti jsou velmi důležité z hlediska praktického použití a jsou silně závislé na strukturním uspořádání v tenkých filmech.

V **Kapitole 7**, *Sekci 7.1*, je uvedena souhrnná PL studie o polysilanech, přičemž jsou diskutovány spektrální změny závisející na tloušťce vrstvy. V *Sekci 7.2* je prezentována UV-degradační studie polysilanů. Zde je nutno podotknout, že v materiálu neprobíhá jenom degradace, ale také se objevuje fenomén „samo-opravy" materiálu v průběhu i po expozici UV zářením. Získané výsledky společně

s dřívějšími pracemi podporují teorii různě uspořádaných polymerních řetězců ve vrstvě závisejících hlavně na jejich tloušťce, obdobně jako v případě π-konjugovaného polymeru.

Část práce prezentovaná v **Kapitole 8** pojednává o přípravě a vlastnostech kompozitního materiálu z polymeru MEH-PPV a nanočástic ZnO a CdS. Takto připravený kompozit byl použit pro zhotovení vzorku aplikace, tj. polymerní OLED diody a hybridní struktury pro fotovoltaiku.

Kapitola 9 je shrnutí závěrů vyplývajících z výsledků prezentovaných v této disertační práci.

Kapitola 10 přináší několik autorových návrhů pro budoucí a následný výzkum v oblasti polo- a vodivých polymerů, tzn. σ- a π-konjugovaných materiálů, s ohledem na specifické podmínky a metody dostupné na Centru polymerních systémů na Univerzitě Tomáše Bati ve Zlíně.

1. Introduction

Conjugated polymers belong to a wide group of novel materials with interesting properties, such a semiconductivity and optical activity, electro- and photoluminescence. This group of materials combines optoelectronic properties of semiconductors with the mechanical properties and processing advantages of plastics [1].

The use of electrically conductive polymers was considered firstly in 1960's. A synthesis route of trans-polyacetylene was discovered. Shirakawa shown that trans-polyacetylene is able to be transformed into the electrical conductive material by doping with I_2 and AsF_5 [2], [3] and after that conjugated polymers were often studied as "conductive" polymers. However, they have not attracted tremendous research interests until 1990 when the electroluminescence (EL) from conjugated polymers was first reported [4]. Polymer electronics grew to a huge area of science and industry and nowadays, conductive polymers represent very interesting class of materials for coming future [5]. The light emitting devices made from polymer, flexible electronic components or photovoltaic applications promise the broadening of current applications [6] because of rising commercial market of such product as organic light emitting devices (OLED) displays, TV screens, solid state lighting [7].

From the physical point of view, they are semiconductors with the optical and electrical properties similar to the traditional inorganic semiconductors. From the chemistry point of view, they are macromolecules, which can be designed and synthesized to achieve the desired chemical and physical properties. From the materials engineering point of view, they are materials with unique, and often low-cost, processing capability and suitable mechanical properties such as flexibility. The combination of these unique characteristics makes conjugated polymers a charming and yet very useful material. One of the great benefits of polymer electronics lies in its low-cost solution processing capability. The polymer materials are dissolved in ordinary solvents and deposited onto the substrate using the simple coating technologies such as spin-coating, ink-jet printing, and screen printing to form the desired structures. In theory, the whole production process of polymer integrated circuits can be a continuous web processing, which will make the

production of polymer electronic devices significantly more cost-effective than traditional silicon semiconductor devices [8].

Of course, before actually being implemented in an application, the chemical, mechanical and electronic properties of these materials must be investigated, because the charge-transport, optoelectronic and other properties of conjugated materials critically depend on the packing of the molecules or chains and the degree of order in the solid state, as well as on the density of impurities and structural defects. Moreover, their final properties are process condition dependent.

1.1 Conjugated polymers

Standard, insulating organic polymers have saturated sp^3 hybridized carbons making up their main chain. In organic conjugated polymers two possibilities exist, how the electron delocalization can be assured. Firstly, the main chains consist of sp^2 hybridized carbons. This configuration results in three σ-bonding electrons, the 2s, $2p_x$ and $2p_y$ and a remaining $2p_z$ electron. In case of two adjacent $2p_z$ orbitals overlap, forming a π-bond, Figure 1a). If the overlap of π-orbitals is along the whole backbone, the delocalization of π-electrons can arise. The π-bonds are dispersed and the polymer becomes conductive. By contrast, the σ-delocalization is caused by overlapping of sp^3 silicon orbitals and is given by β_{gem}/β_{vic}, where the degree of delocalization is a function of this ratio. β_{vic} is the resonance integral of two overlapping sp^3 orbitals on adjacent Si atoms and β_{gem} is the resonance integral on the same Si atom, Figure 1b). Perfect σ-conjugation occurs if the ratio β_{gem}/β_{vic} equals to 1, when the chain is in all-trans conformation. Thus the delocalization is strongly depending on the chain length and its conformation [9].

a)   b)
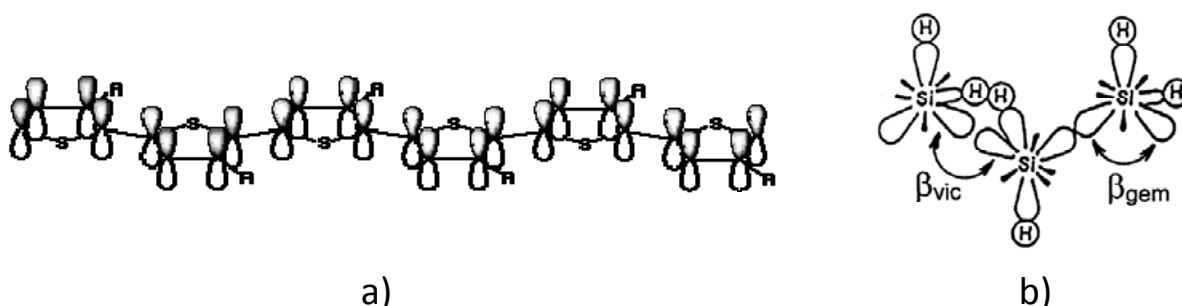
Figure 1 Schemes of a) π-bonds and b) σ-bonds and electrons delocalization.

Thus, we can distinguish two types of conjugated polymers, π- and/or σ-conjugated polymers. However, the both types of material have in common the feature of band structure, which is represented in the Figure 2.
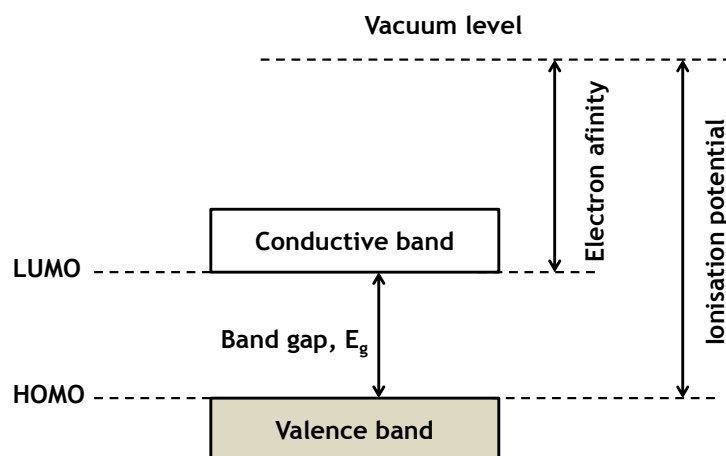
Figure 2 Schematic picture of the band structure in conjugated polymers [10].

Another characteristic property of conjugated polymers is their more or less prevailing one-dimensionality (1-D) of the conjugated electronic structure. Consequently, such materials are ordered and strongly anisotropic [11].

1.1.1 π-conjugated polymers

The characteristic feature of π-conjugated polymers is the π-electron delocalization along the polymer chain [12], depicted in the Figure 3. The π-electronic structure near the Fermi level in conjugated polymers plays a major role in such phenomena as charge carrier injection, interface formation and light emission [13].
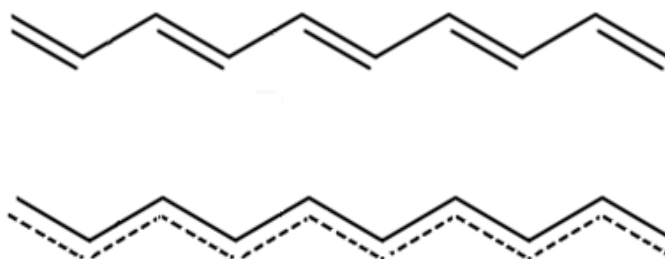
Figure 3 Schematic formula of trans-polyacetylene and its π-electron delocalization [13].

Of course, one-dimensional systems can display a wide variety of instabilities, and these influence the temperature dependence of the electrical conductivity in

addition to other properties. That a 1-D metal is unstable against static lattice distortion was first pointed out by Peierls, so the phenomenon of main chain distortion in conjugated polymers is called as a Peierls distortion. It means that the energy of hypothetical metallic state of polymers is higher than that of polymers with alternating bonds. So, the system lowers its energy and changes the unit cell geometry by dimerization resulting in single – double bond alternation. By this cause the conjugated polymers are transformed into the semiconductors with band gap E_g ranging typically between 1.5 eV and 3.5 eV. The distortion is then manifested by C-C bond length alternation. Two possible orders of alternation exist: (-s-d-s-d- and -d-s-d-s-) and thus two ground energy states are possible. If they have the same energy then ground states are degenerated, and practically, they cannot be distinguished one from the other due to this ground state degeneracy. In case of the difference between theirs ground state, they are non-degenerate and the lower energy state is more probably into existence. The Peierls instability can be viewed as a localization of electrons induced by static lattice distortion.
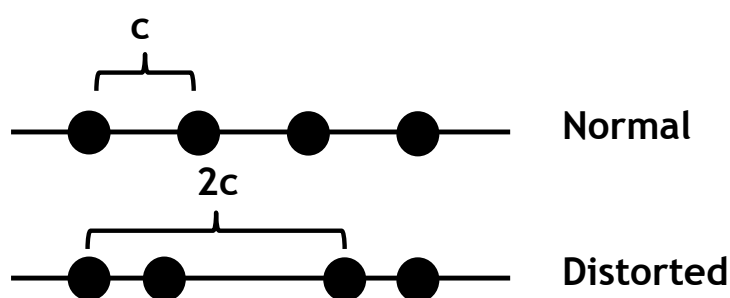
Figure 4 Scheme of Peierls distortion.

Thus conjugated polymer can be generally divided into two groups: degenerated ground state polymer such a trans-polyacetylene, where the ground states are not distinguishable and non-degenerated ground state polymers such a derivatives of poly(p-phenylenevinylene) [13].

Charge carriers

A bond alternation defect (transition region) in degenerate polymers can cause the isolation of an unpaired electron. These types of defects are called solitons. The soliton corresponds in the electronic structure to a localized state in the middle of

the band gap, and if neutral - S^0, soliton has a spin ½. Solitons can be created by the light quantum absorption or by doping inducing charge transfer [14]. In case of negative doping, the negative solitons S^- negatively charged are formed with 2 electrons. For positive doping, the positive solitons S^+ with positive charge are created.
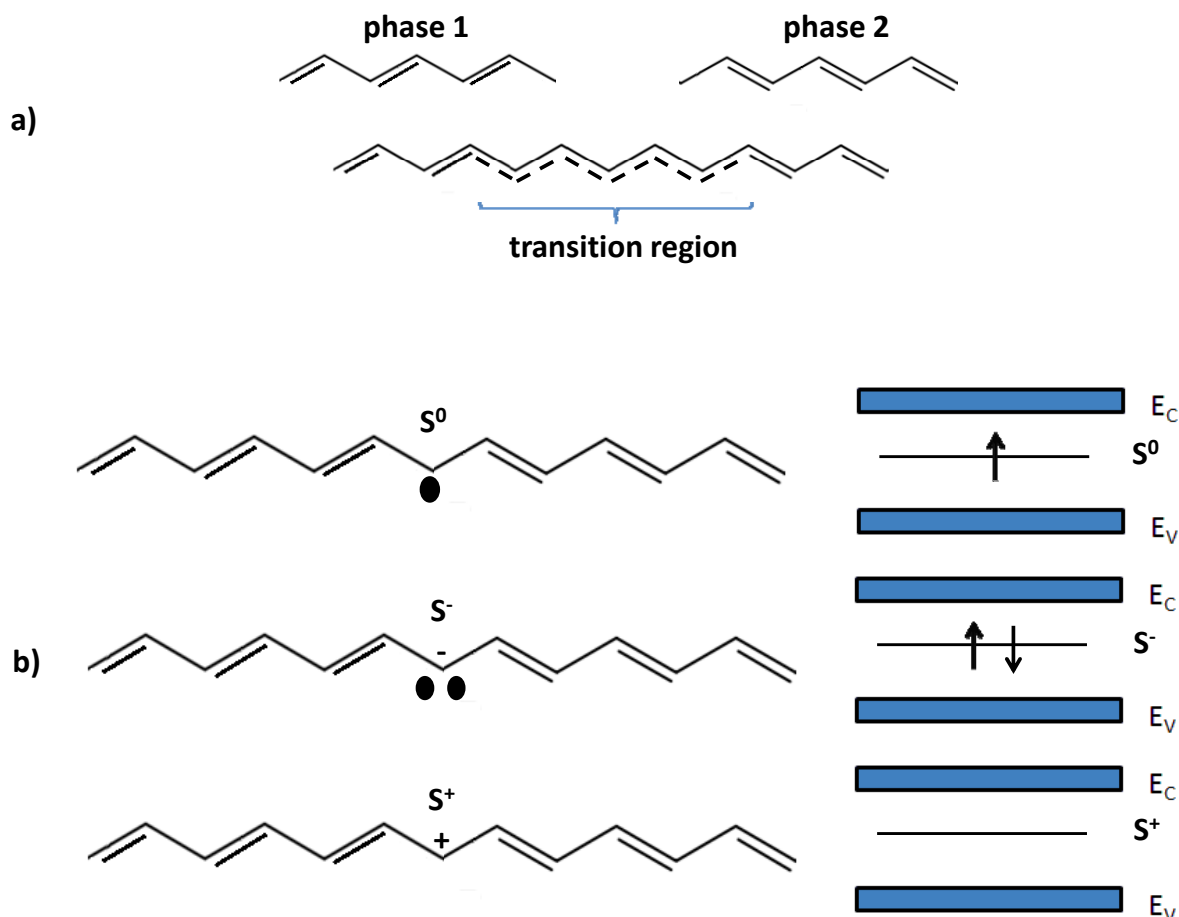
Figure 5 A schematic pictures of the transition region a), and of the three posible soliton states b).

Non-degenerate conjugated polymers have a favorable bond alternation order which can be caused by optical excitation or charge injection. This costs energy and therefore is the defect confined on the shortest possible chain segment in respect to compromise between energy minimization and Coulomb repulsion of localized charges. Charged defects on the chain are called polarons, P^- (negative charge) and P^+ (positive charge) [15]. When two polarons interact, they form a double charged state, which is energetically more favorable in the degenerate state, but not everywhere. These states are called bipolarons, BP^{++} and BP^{--} [16].

Even though bipolarons are energetically more favorable than polarons, per definition, the first charge induced on a non-degenerate polymer chain must be a polaron. In the electronic structure, these defects correspond to two new localized states in the band gap. For a negative polaron, P^-, the state just above the valence band is filled and the state just below the conduction band is half-filled. For a positive polaron, P^+, the state just above the valence band is half-filled and the state just below conduction band is empty. In both cases, there is the density of states at the Fermi level. In the case of bipolarons, two new localized states are formed in the band gap, with both states being doubly occupied for negative bipolarons, BP^{--}, and both states being empty for positive bipolarons, BP^{++}. For the bipolaron case, there is no density of states at Fermi level, since it is situated half-way between the conduction and the top bipolaron state for negative bipolaron, and half-way between the valence band and the lowest lying bipolaron state for positive bipolaron [17].
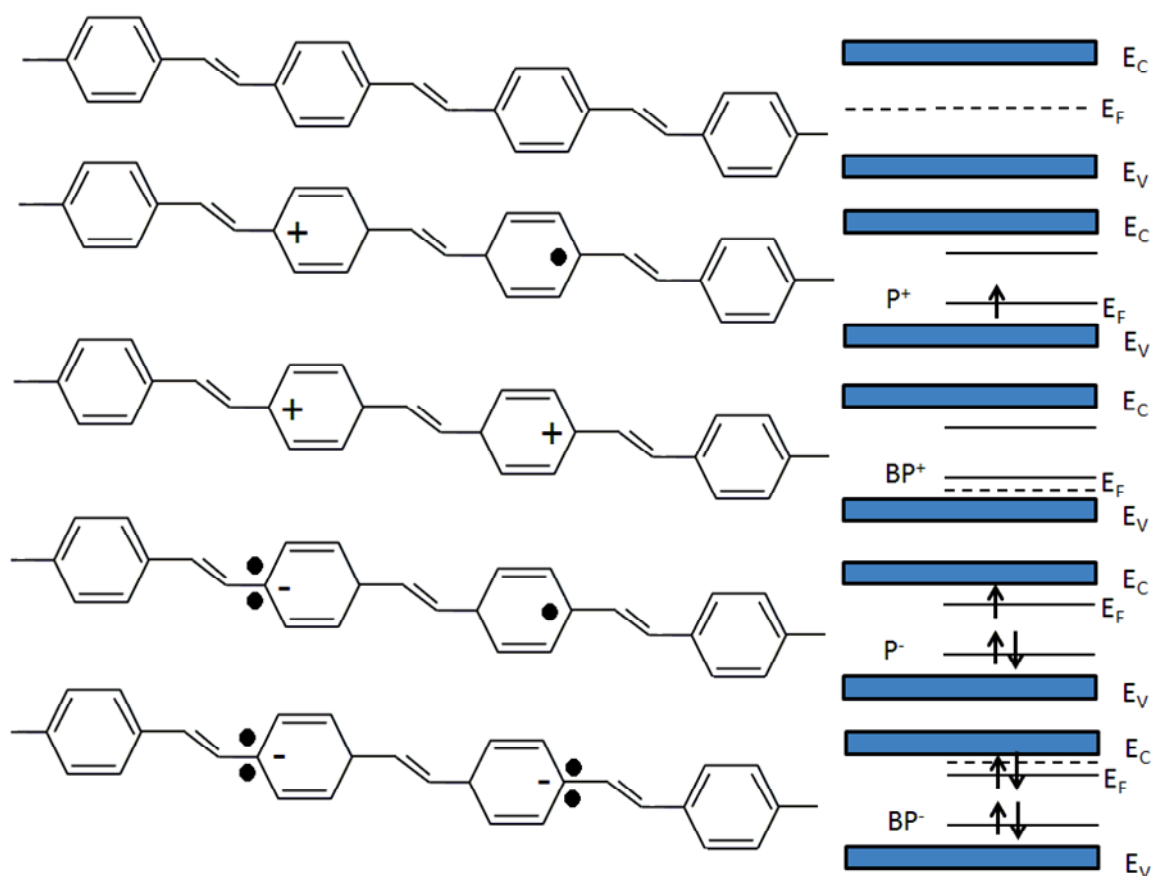
Figure 6 The schematic picture of the possible polaron and bipolaron state in non-degenerate conjugated polymers (E_C – conductive band, E_V – valence band, E_F – Fermi level).

The concept of polarons (and solitons) was further developed in connection with the observation of high electrical conductivity in doped conjugated polymers [18]. It was shown that soliton excitations are possible in *trans*-polyacetylene (tPA) and that these defects could explain both magnetic and optical properties of doped systems. Exactly how these doping induced defects are involved in charge transport, however, not yet settled. Vast amounts of transport data [19] for lightly or moderately doped samples are in agreement with the hopping laws over a wide temperature range. This suggests that once the localized polaron, soliton, or bipolaron states are formed, conduction takes place predominantly through hopping process between these states [20].

Studies on conjugated polymers have recently shifted to the undoped state, predominantly as the undoped state has shown to have very interesting luminescence [21] as well as photovoltaic [22] properties. In the undoped state the number of charge carriers is small and the interest from the point of view of transport is more focused on the mobility of charge carriers. Similar to the situation in molecular crystals, the transport properties of conjugated polymers are also strongly dependent on structural order and the purity of the samples.

Charge transport in disordered polymers is regarded as hopping process between localized states. The confinement of the electronic states is, in this case, a combination of the effect of chain interruptions and the polaronic effect discussed earlier. Thus, to some extent, this type of system is similar to the molecular systems with the molecules replaced by the chain segments over which the electrons can delocalize. However, structural order as well as mobility is much lower in the polymer samples than in organic crystals [23]. In disordered polymer systems, the overlap between the states localized to different chain segments is quite low [24], the separation between chain segments is of variable range, and the segments themselves are of different length and experience variations in the local field. Thus, for this type of systems, the transport is regarded as a low-probability hopping process and hopping conduction is defined as the process in which charge carriers conduct the electric current by thermally activated tunneling from an occupied site to an empty site. More explicitly, the thermal energy that is required for the process to occur is gained from the phonon system [1].

Optoelectrical properties of π-conjugated polymers

As mentioned above, the charge carriers can be implemented in polymer chain by two ways, Firstly, by excitation of electrons (photo or electro). The second way is injection by doping for instance. After excitation the excitons can be formed and one important aspect of the emission properties of conjugated polymers is the assignment of its emissive centers. Apart from the intrinsic chemical composition and macromolecular architecture, the emission wavelength depends on three main parameters: the torsion angle of the conjugated backbone and the presence of conformational, configurational, and morphological disorder and defects (sp^3 bonds, chain ends, aggregates and impurities), which determine the conjugation length [25], and the occurrence of interchain interactions leading to the formation of excimers, aggregates, and/or polaron pairs [26].
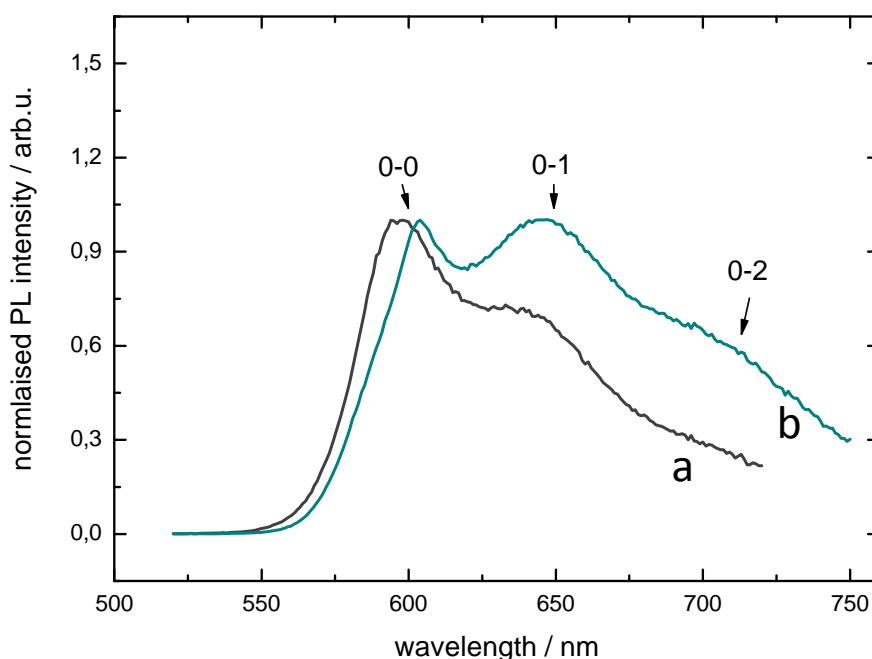
Figure 7 Emission spectra of thin films from MEH-PPV, a) thin film 35 nm; b) thick film 100 nm.

In case of poly[2-methoxy-5-(2-ethylhexyloxy)-1,4-phenylenevinylene] – MEH-PPV, which is known as an orange emitter with spectral peaks at about 600 nm (transition 0-0), at 640 nm (transition 0-1) and at about 720 nm (transition 0-2). Variations in chain configuration and interchain interaction lead to wavelength emission shifts and to changes of peaks intensity ratio, Figure 7. This fact is attributed to conjugation length of polymer chains, whereas the conjugation length

is much longer in thick films (hundreds of nanometers) than in thin films (tens of nanometers) and exciton diffusion length is longer as well and thus, the excitons can travel along the chain and can switch on the other one [27].

1.1.2 σ-conjugated polymers

Another class of conjugated polymers, so called σ-conjugated polymers are interesting group of polymer materials among them polysilanes are the most attractive, but there is more recent group in which germanium atoms form the main polymer chain.

Linear polysilanes, called polysilylenes (PSis), are a group of σ-conjugated polymers with the backbone consisting entirely of silicon atoms. PSis are considered as polymer materials applicable in many electrical, optical and optoelectrical applications because of their unique electronic properties due to the effect of σ-electron delocalization along the main chain [28]and [29].

Polysilanes were firstly synthesized in 1920' by Kipping [30] and [31]. Nowadays, there are principally two ways of synthesis method of silicon based polymers. First one is classical chemical synthesis called Wurtz coupling which allows lead chemical reaction to obtain polymers as a bulk material, which is intended for other processing to form desired structures.
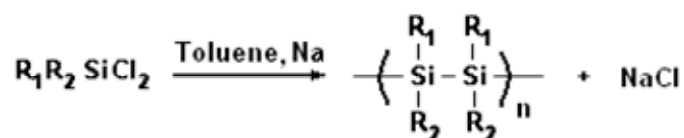
Figure 8 Preparation of polysilane by Wurtz coupling – schematically.

The other way of polysilanes preparation is a broad class of synthesis using catalysts and yielding materials with variable dimensionality, heterogeneity and different microphysical properties. One of these ways is for instance dehydrogenative coupling, schematically shown in Fig. 8 [28].

9
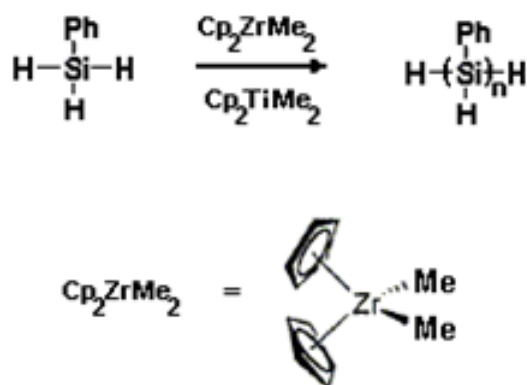
Figure 9 Scheme of dehydrogenative coupling [28].

Newer method for PSis preparation, the electroreductive synthesis is. It was carried out to avoid drastically condition during the Wurtz coupling. The main point of the electroreductive synthesis is the radical mechanism of reaction, see Figure 10.
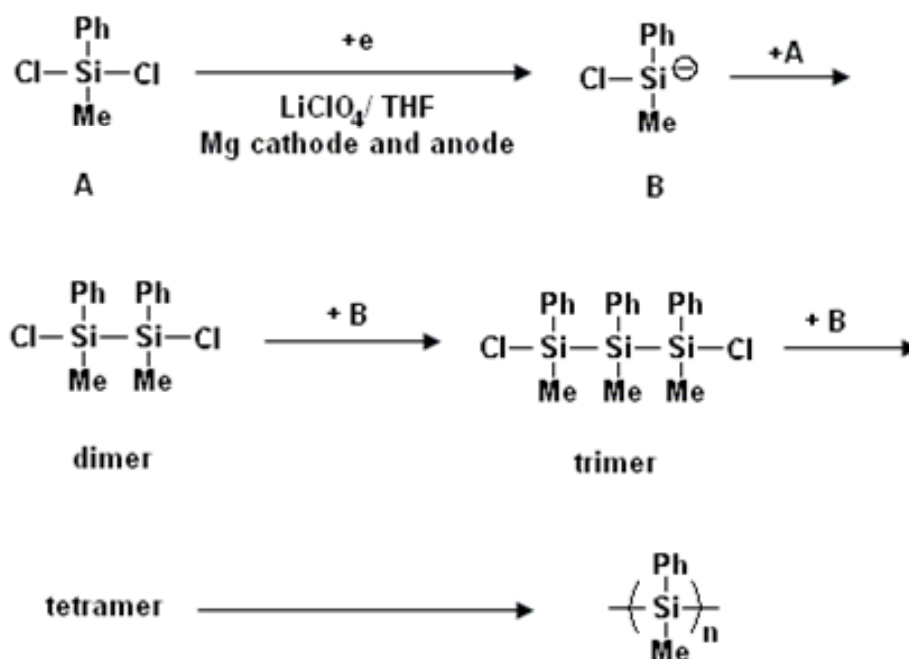
Figure 10 Electroreductive synthesis of polysilanes.

In case of good reaction conditions (sonification of solution, monomeer concentration) and good electrodes, it is possible to achieve polysilanes with polymerization degree of 31 000. On the other hand, the yield is too low. Higher yields (more than 80 %) were achieved in case of polymerization degree at 9 000 [32].

Optoelectrical properties of σ-conjugated polymers

PSis chains, with two organic substituents on each silicon atom, behave as one-dimensional system with weak intermolecular interaction, whereas side groups influence the physical and electrical properties of polysilanes, which are related to their optical activity, which results in UV/VIS absorption and electron excitation [33], [34]. The absorption spectrum of a solid film of a typical polysilylene, poly[methyl(phenyl)silylene] (PMPSi), consists of three main typically broad and structerless peaks with maxima at 330 nm, 270 nm and 195 nm. It was reported [34] that the first transition, at 330 nm, is related to delocalized σ–σ* transitions, the peak at λ = 270 nm is associated with π–π* transitions in the benzene ring. In addition to the σ–σ* and π–π* types of absorption band, a very weak tail in the visible region was observed [34]. The electron excitation plays an important role because it can be accompanied by photoluminescence as a consequence of excitonic deactivation [35].

The luminescence spectrum shows for a purely linear PMPSi only one sharp peak at about 360 nm with a small Stokes's shift caused by excitonic deactivation [36]. As the fluorescence emerges from the longest segments, it gives the energy of these segments - 3,44 eV [10]. If there is a strong coupling of excitation on the lattice, then the luminescence within the absorption manifold will be broadened, because the structurally relaxed state will be emitting state. Regardless of the wavelength of the excitation in a system consisting of a chain of electronically coupled chromophores (segments), in which the excitation energies vary with the size of the segment and the ambient environment, excitation of any average state will be followed by energy transfer to lower lying acceptor states (segments) that can fluoresce. This leads to spectral diffusion unless the excitation energy is so low that only the lowest lying acceptor states will be excited. Imperfection, defects and branching points on the main chain in polysilanes are usually manifested in a broad visible luminescence with low intensity. Quantum efficiency of fluorescence in the solid film is quite high, about 0.15 [36].
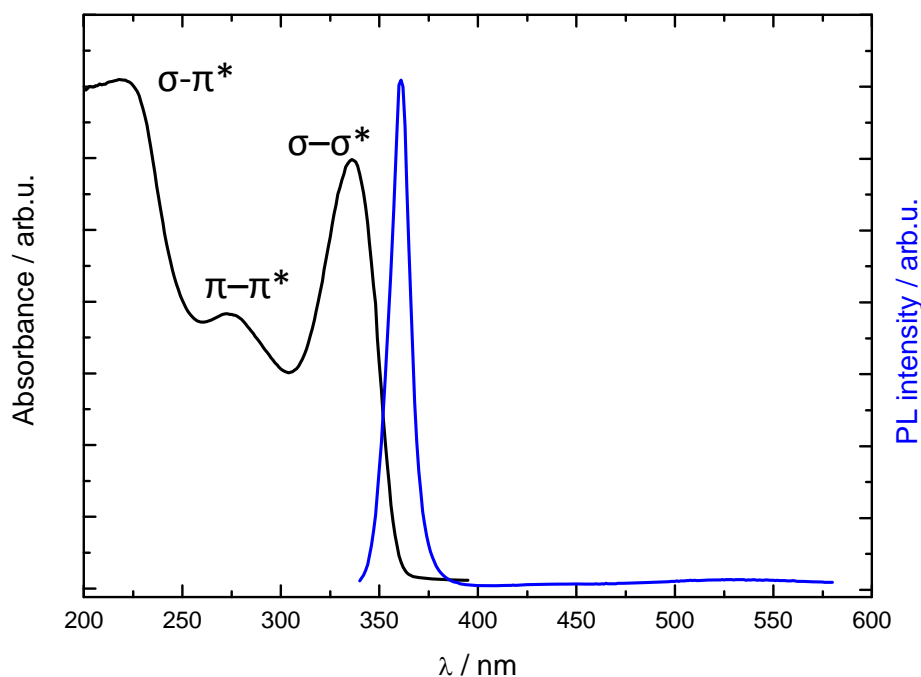
Figure 11 Absorbance and photoluminescence spectra of PMPSi thin films.

Degradation of polysilanes

The degradation of material is always one of the most important material criteria because it is determining for the final material application. Polysilanes are especially vulnerable to UV radiation, and thus the UV degradation is a process, which is studied by a broad group of method. Among them, the PL studies in UV and visible region are very useful as they provide for structural information too.

The phenomenon of UV degradability and metastability in polysilylenes is related to the electron excitations of σ bonds, forming weak Si-Si bonds. The photoscission of the Si-Si bonds then proceeds via thermal activated reactions with the surrounding medium of weak bonds (WB). The weak Si-Si bonds constitute the deep electron states situated (0.45–0.55) eV above HOMO level depending on the energy of the excitation photons [37]. It was proved by theoretical calculations that, σ*-σ star recombination leads to Si-Si bond scission. The process occurs due to traveling of exciton to segments with the lowest energy where they radiatively recombine and the Si-Si bond is degraded (in Figure 12). These calculations were verified by experimental study [38].

12
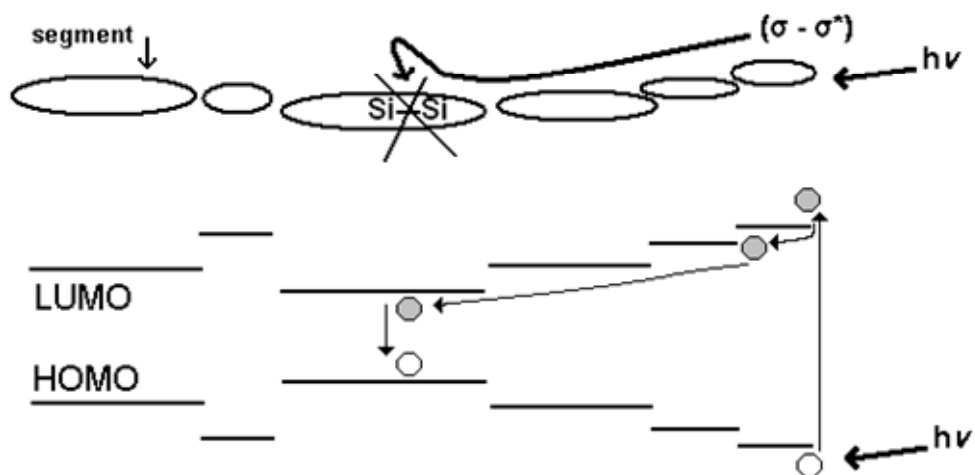
Figure 12 Schematic of scissoring of Si-Si bond.

In the absence of oxygen, we can describe the photodegradation of PSis with the aid of chemical equations in a scheme in Figure 13. Absorption of the UV radiation and occurrence of radicals is in solid phase reversible process, whereas the WBs are created before the formation of silyl radicals (Equation 1 in the Figure 13). These radicals can after that recombine and new Si-Si bonds can arise [39]. But the reverse reaction, radical coupling, must be enhanced by the rigid of Si skeleton of the silicon network structure because of the low diffusibility of the radical site. Equations 2 a 3 in the Figure 13 describe the situation the silyl radicals do not have appropriately condition for the recombination resulting into the Si-Si bond forming. Then, after Si-Si bond scission, group with double bonds on the Si atom arise. These double bonds are very unstable, thus Si atoms are bonded by methylene group [39], [40].
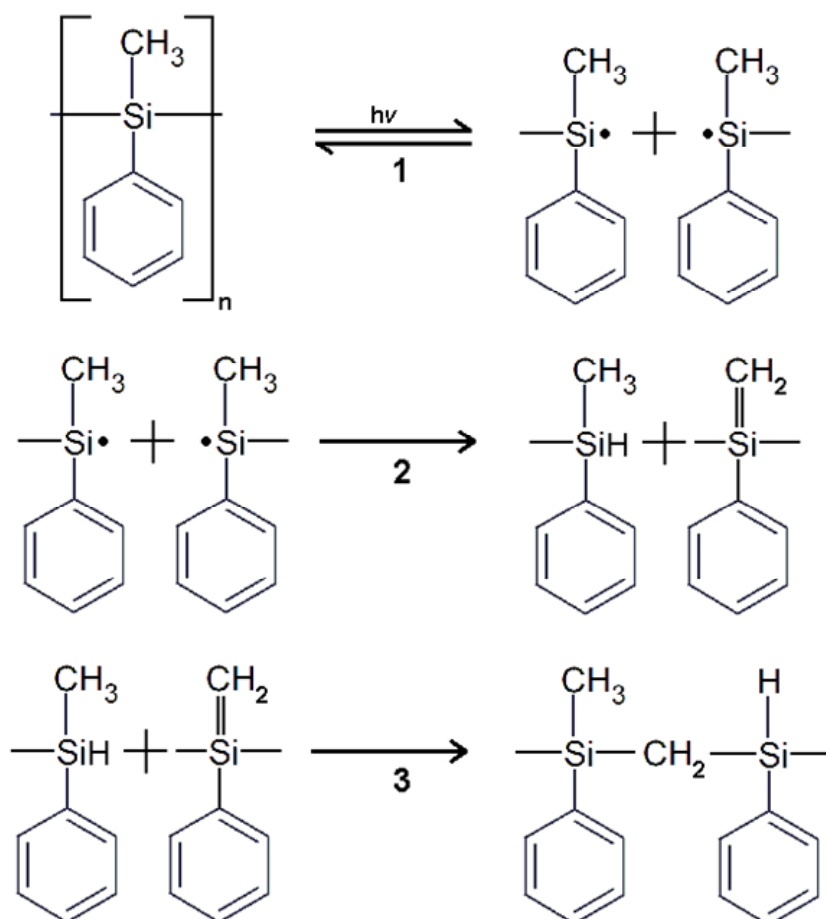
Figure 13 Schematic photodegradation of PMPSi without presence of oxygen.

In case of photodegradation in presence of oxygen, the process proceeds according to the Figure 14. The PSis polymer scissoring is based on radical transformation of the Si-Si bonds and the pending methyl groups, which leads to silyl radicals **(1)** in the Figure 14. If silyl radicals interact with silyloxyl **(5)** in oxygen atmosphere, siloxane arises **(6)**. The formation of silanol **(4)** is via silylperoxyl **(2)** and hydroperoxide **(3)**. In case of methylene radicals formation **(7)** arising from PSis by an interaction with silyls **(1)**, the peroxyl radical **(8)** can be created, which recombine into the hydroperoxide on the side group **(9)**. The carbonyl species **(10)** arise because of higher stability then hydroperoxide [38]. These changes on the polymer main chain can be successfully retarded using phenolic UV absorbers and oxalanilides protecting the polymers by the excited-state intramolecular proton transfer mechanism retarded the formations of siloxane moieties in air.

14
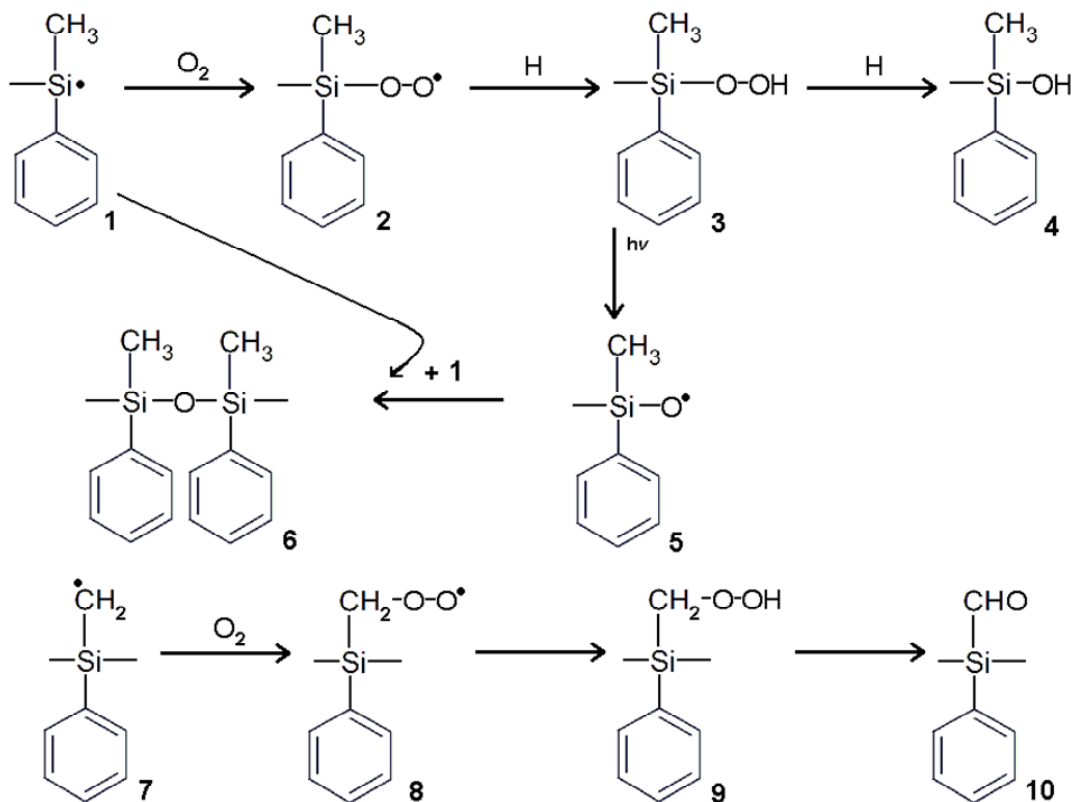
Figure 14 Schematic photodegradation of PMPSi in the presence of oxygen.

1.2 Composite materials for thin films

The charge carrier transport and recombination strongly influence the light emission and photovoltaic performance of organic light emitting diodes and solar cells, respectively. Since semiconducting organic polymers are low mobility materials with low quantum photogeneration efficiency in their pristine phase, bulk heterojunction concept is introduced for an efficient charge generation and for a long carrier lifetime and for instance, blending of two thiophene-based PPE-PPV polymers having identical conjugated backbone decorated with different volume fraction of hydrophobic alkoxy- side chains has led to enhanced charge carrier mobility and improved photovoltaic performance [41].

The polymer mixing with improving fillers can be considered as a reasonable alternative. Composite materials play important role in case of solar cells because the energy harvesting based on polymer devices with inorganic nanoparticles is very promising and has great potential as mentioned above. Most of conductive polymers are p-type semiconductors. To improve theirs properties, it is favorable to dope them by n-type semiconductive materials such ZnO or CdS.

15

Polymer solar cells that only consist of a conducting polymer alone have low minority carrier mobility, for example, MEH-PPV has a high hole mobility, but a low electron mobility [42]. The intrinsic carrier mobility imbalance in MEH-PPV severely limits the performance of pure-polymer-based cells. To overcome this imbalance, a second material is incorporated to act as an electron acceptor and as a pathway for electron transport. Then the efficiency of polymer-nanoparticles heterojunction solar cells can achieved up to 5 %. When the size of the nanoparticles is smaller than that of the exciton in the bulk semiconductor, the lowest energy optical transition is significantly increased in energy due to quantum confinement. The electron affinity of CdS is in the range 3.8 – 4.7 eV; hence, it is a suitable material to act as electron acceptors when combined with conjugated polymers, when the electron affinity of the conjugated polymers is in the range 2.5 – 3.0 eV [43].

Another material which can be successfully used in purpose to improve properties of conductive polymers is ZnO. Zinc oxide is a promising semiconductor that has a wide direct band gap of 3.37 eV and a very large exciton binding energy of 60 meV at room temperature. Thus, ZnO materials have been regarded as very attractive candidates for the next generation of UV light emission devices [44]. Nevertheless, the p-type doping of ZnO is always a bottleneck since wide band gap materials usually show a poor doping efficiency. It is an important barrier for the application of ZnO based UV LEDs. Thus, the p-n heterostructures consisting of n-type ZnO as the active layer and other p-type materials have been introduced, but still lack high efficiency. On the other hand, ZnO nanowires, ZnO nanorods or ZnO nanoparticles – in other words low-dimensional nanostructural ZnO has attracted great interest because of its unique physical and chemical properties. For example, ZnO or other semiconductor nanowires or nanorods can offer additional advantages for optoelectronic device applications due to the increased junction area, enhanced polarization dependence, and improved carrier confinement in one dimension. In order to realize UV electroluminescence, a device was reported based on ZnO nanorods/MEH-PPV heterostructure in which the polymer MEH-PPV was used as the electron injection layer [45].

2. Thin film preparation techniques

Presently, a rich group of deposition technique is available. However, only some of them combine good processability of polymer solution, low cost, quickness, repeatability and high quality of prepared films. Spin coating and ink-jet printing are two methods belonging to this group and fulfilling requirements mentioned above.

2.1 Spin coating

The process of applying a solution or dispersion to a horizontal rotating disc, resulting in ejection and evaporation of the solvent and leaving a liquid or solid film, is called spin coating, and has been studied and used since the beginning of the 20th century. Spin coating is a unique technique in the sense that it is possible to apply a highly uniform film to a planar substrate over a large area (Ø 30 cm) with a highly controllable and reproducible film thickness. The importance of spin-coating is manifested in its widespread use in science and industry. It is thus desirable to gain detailed understanding of the spin-coating process from both an experimental and a theoretical point of view. The spin-coating technique applies to inorganic, organic and inorganic/organic solution mixtures. Spin-coating is used in various applications such as coating of photoresist on silicon wafers, sensors, protective coatings, paint coatings, optical coatings and membranes [46].
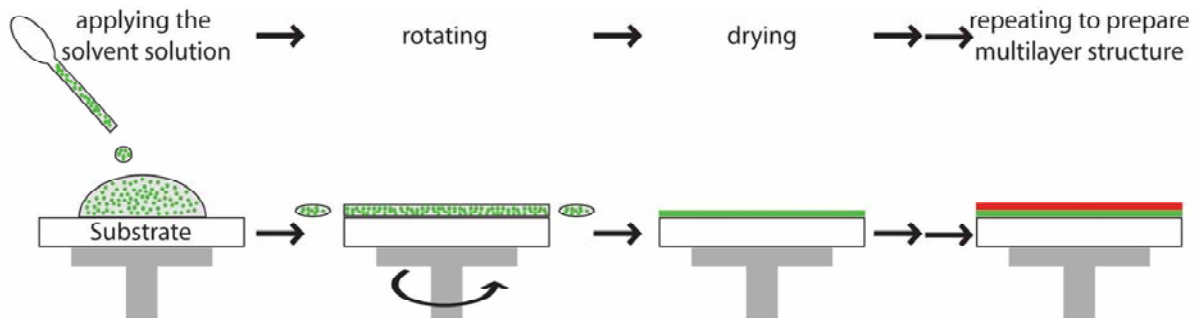
Figure 15 Scheme of spin coating deposition method.

Depositing a viscous fluid on a horizontal rotating disc produces a uniform liquid film. During deposition the disc should either be static or be rotating at a low angular velocity, where after the disc is rapidly accelerated to a high angular velocity (spin speed or equivalently spin rate). The adhesive forces at the liquid/substrate interface and the centrifugal forces acting on the rotating liquid result in strong sheering of the liquid which causes a radial flow in which most of

the polymer solution is rapidly ejected from the disc, see Figure 15. This process combined with subsequent evaporation of the liquid causes the thickness of the remaining liquid film to decrease. For a solution, e.g. a polymer solution, the evaporation process causes the polymer concentration to increase (and thus the viscosity) at the liquid/vapor interface, i.e. a concentration gradient is formed through the liquid film, which, after evaporation of most of the remaining solvent, consequently results in the formation of a uniform practically solid polymer film [47].

The steeply rising focus on nanotechnology as the next industrial global technology also supports the continued and extended use of a well-proven technology capable of producing nanometer scale objects in one dimension over large areas through a simple process. Nanotechnology can be seen as a shift in focus from bulk properties to interface interactions. This is again reflected in the renowned interest in uses of spin-coating during the last decade where engineered interface interactions are exploited to direct internal molecular organization of polymer thin films, resulting in highly anisotropic materials properties [48].

2.2 Ink-jet printing

Inkjet printing has been one of the most studied printing technologies not only for printed electronics but even for biological science in the field of microbiological patterning. This is somewhat surprising, since inkjet printing as a whole is a relatively new and developing technology for high speed, low cost printing. The reasons for the popularity of inkjet can be summarized as follows:

Compatibility − Inkjet printing allows the use of very low viscosity inks (1-20 cP). This is a tremendous advantage of inkjet printing over more conventional analog printing techniques such as gravure printing, screen printing, etc. Many of the materials have somewhat limited solubility, which limits the achievable mass loading in stable ink formulations. Additionally, for many of the inks, the addition of binders is unacceptable, since these binders poison the electronic functionality of the ink. As a result, inkjet has tremendous advantages in this regard [49].

Digital input − since inkjet allows for digital input, it allows for on-the-fly design changes. This is very important in research, since it allows for very rapid

prototyping. Given the early stage of printed electronics, therefore, it is not surprising that inkjet has been so popular. A long term advantage of digital input technology is that it may allow for such operations as on-the-fly distortion correction, which may enable more accurate alignment over large area substrates.

Non-contact printing — since inkjet does not use contact between the substrate and the printing head, it is relatively free from the main disadvantages of contact printing, namely degradation of the print quality over time due to abrasion of the print form, and also yield loss due to particles.

Resolution — currently, it is possible to obtain commercial inkjet heads with resolution of 20 microns, and research mode heads have also been demonstrated with resolution better than 10 microns. In comparison, most analog print technologies produce features of worse than 30 microns (though some techniques have shown sub-10 micron resolution in research or controlled environments).

As a consequence of the above advantages, inkjet has received substantial attention as a means of realizing printed electronics. Unfortunately, to this point, inkjet has struggled to successfully make the transition from research to manufacturing. The reasons for this illustrate clearly the disadvantages and concerns with inkjet printing [50].

Inkjet printing functions include the following:

-       creation of an ink stream or droplets under pressure

-       ejection of ink from a nozzle orifice

-       control of drop size and uniformity

-       placement of drops on the recording surface.

Inkjet printers fall into two basic categories: continuous jet and impulse jet (drop-on-demand).

2.2.1 Continuous printing

Continuous inkjet systems operate by forcing pressurized ink in a cylinder through nozzles in a continuous stream (Figure 16).
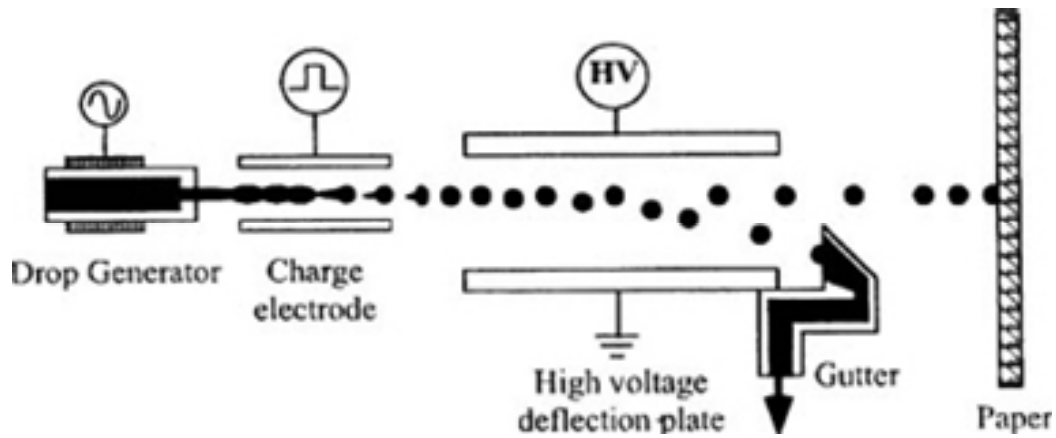
Figure 16 Continuous ink-jet printing system [49].

The ink stream is unstable, breaking into individual droplets either naturally or through some applied stimulation such as ultrasonic vibration. Electrostatic deflections used to control the droplets, which either reach the page in the desired pattern or are deflected into a gutter or catcher [50].

2.2.2 Impulse jet printing (Drop-On-Demand)

In contrast to continuous jet printers, drop-on-demand (DOD) ink delivery systems create drops only as needed, thereby eliminating the need to control excess droplets. These systems are inherently binary; either a drop is ejected for placement on the receiver sheet or it is not. There are two basic method of activating the ink droplets. The earliest impulse jet models used piezoelectric transducers that squeeze the ink chamber or impulse the chamber at one end (Figure 17 b).
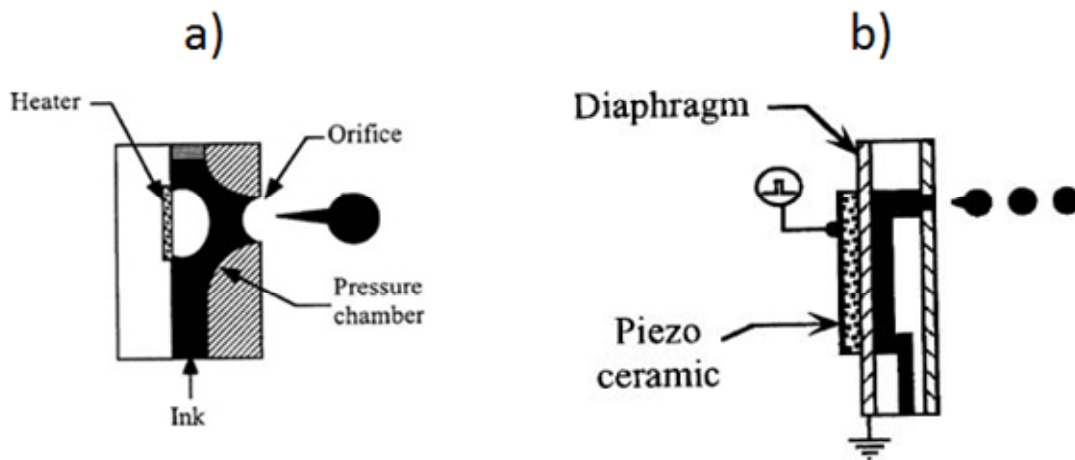
Figure 17 Impulse jet printer systems – a) thermally activated, b) piezoelectric activated [49].

The alternative approach, thermal activation of ink drops is gaining popularity. A heater creates a bubble of ink vapor that forces ink drops from the nozzle (Figure 17 a).

Most of newer inkjet printers use impulse jet technologies to address general-purpose printing applications. Advantages include mechanical simplicity, low hardware cost, and simplified logic. However, there are disadvantages as well: DOD printers are more sensitive to shock and vibrations and have slower dot ejection rates. In addition, market acceptance has been slow, partly because of early reliability problems due to nozzle clogging from dried ink or substrate dust [51].

3. Overview of experimental techniques

3.1 UV-VIS absorption spectroscopy and fluorimetry

Spectroscopic characterization of prepared films is of prime importance because structural information is reflected in molecular and electronic spectra and are in focus of interest of this work.

From the definition, the spectroscopy is a science discipline dealing with interactions of electromagnetic radiation with matter.

In case of UV-VIS spectroscopy, the interaction of light and matter can be easily described as a loss of intensity of transmitted light, whereas all reflections and scattering are neglected or corrected. During the pass through the thin films with thickness l, light intensity decreases governed by the Lambert's law (Equation 1),

$$I = I_0 e^{-\alpha l}$$

Eq. 1

where I_0 is the light intensity from the source, a is the absorption coefficient of the material. This relation could be expressed in other way, with the aid of absorbance A. The relationship between absorbance and intensity of light is following:

$$A = -\log \frac{I}{I_0}$$

Eq. 2

The plot of absorbance depending on the wavelength is called absorption spectrum.

Due to studying of the optical absorption of the molecular compounds, it is possible to achieve information about electronic structure because the UV-VIS spectroscopy measures the probability and energy of exciting a molecule from its ground electronic state to an electronically excited state (promoting an electron from an occupied to an unoccupied orbital). The wavelength of an electronic transition depends on the energy difference between the ground state and the excited state. It is a useful approximation to consider the wavelength of an electronic transition

to be determined by the energy difference between the molecular orbital originally occupied by the electron and the higher orbital to which it is excited [52].
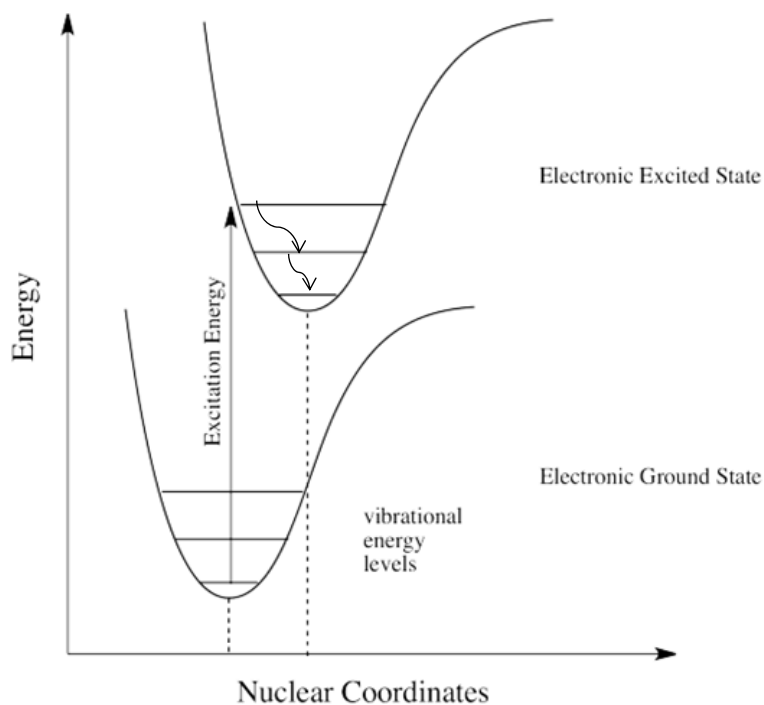
Figure 18 A scheme of an optical excitation from ground electronic state to the excited electronic state, so called Franck/Condon diagram.

During the excitation, most of the electronic transitions are accomplished before nuclei can found their new positions. The electronic transition is in order below 10^{-15} s and the nuclei movement is in about 10^{-11} s. Such vertical transition is called Franck/Condon transition. After excitation, system is not in equilibrium and thus, there is a radiation-less relaxation between vibrational levels. When the electron has time for to relaxation to the lowest vibrational level a photon is emitted and molecule goes to the ground electronic state. This process is called generally luminescence.

Luminescence is usually illustrated by Jablonski diagram (Figure 19). Jablonski diagram is often used as a starting point for discussing light absorption and emission.

The singlet ground and first electronic states are depicted as S_0 and S_1, respectively. At each of these electronic levels the fluorophores can exist in

a number of vibrational levels. Following light absorption, several processes usually occur.
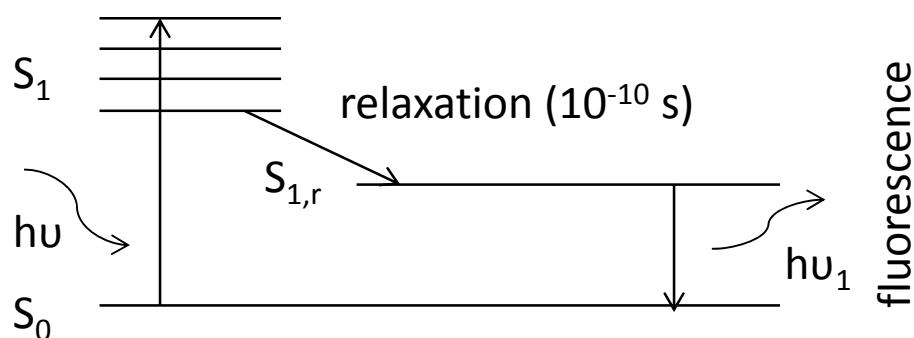
Figure 19 One example form of Jablonski diagram.

A fluorophore usually excited to some higher vibrational level of S_1. With a few exceptions, molecules in condensed phases rapidly relax to the lowest vibrational level of S_1. This process is called internal conversion and generally occurs in 10^{-12} s or less. Since fluorescence lifetimes are typically near 10^{-8} s, internal conversion is generally complete prior to emission. Hence, fluorescence emission generally results from a thermally equilibrated excited state, that is, the lowest energy vibrational state of S_1 [53].

Energy losses between excitation and emission are observed universally for fluorescent molecules in solution. One common cause of the Stoke's shift is the rapid decay to the lowest vibrational level of S_1. Furthermore, fluorophores generally decay to higher vibrational levels of S_0, resulting in further loss of excitation energy by thermalization of the excess vibrational energy. In addition to these effects, fluorophores can display further Stoke's shift due to solvent effects, excited-state reactions, complex formation, and/or energy transfer.

The Stoke's shift is also observable in case of polymers, where is the difference in energy between the peak in the optical absorption relative to corresponding PL peak. Emission takes place from a relaxed electronic state that is different from the one involved in absorption process. Next reason for Stoke's shift in polymers can be a migration of the exciton along the main polymer chain to segments with the longest conjugation length, where the exciton recombines and the emission with longer wavelength occurs [53].

For the PL study, the spectrofluorimeter FLS 920 with Xenon lamp as a source of radiation from Edinburgh Instruments was used. This fluorimeter was equipped with blue sensitive single photon counting detector and two grid monochromators. The PL spectra and PL decay were measured in steady state configuration. Used excitation wavelength was 330 nm, emission was observed at 360 nm. All PL measurements were carried out in vacuum ensured by Cryostat-optistat from Oxford Instrument.

3.2 Surface photovoltage measurements

The technique modified for determination of exciton diffusion length in thin polymer films is called surface photovoltage method. The model is performed assuming a layer with a neutral bulk and one space charge region (SCR) at the free surface. After illumination excitons are created both in the bulk and in the SCR. The model considers that the bulk/SCR interface is the place where the charge separation occurs. The opposite surface is supposed to be a sink for excitons, which represents their losses by surface recombination.

To obtain the SPV signal from the bulk the continuity equation is solved. The second contribution to the signal comes from the SCR taking possible recombination in account. Total SPV signal is a sum of the both contributions. The SPV measurement at various wavelengths gives information on the diffusion length of excitons in the bulk and on the SCR thickness. The usual way of diffusion length evaluation by the SPV technique assumes a thin SCR with negligible losses of photogenerated carriers [54].

Consequently, it fails in samples with a thick SCR. The advantage of the SPV model used here, against PL exciton annihilation, is its applicability to arbitrary thickness of the layers and its possibility to apply it to samples with arbitrary thickness of the SCR and of the bulk. From the photoelectric point of view the polymer layer acts as a thick or as a thin in different parts of the spectrum. For example if the polymer bulk thickness d is 100 nm, the exciton diffusion length L is 20–30 nm, and with the measured absorption coefficient a, there is a large wavelength region where the polymer layer cannot be considered as a thin layer according to the definition given by the following inequalities: $d \leq L, ad \leq 1$ which hold for thin layers [55] - [58].

The transport of excitons in the bulk is controlled by diffusion equation

$$\frac{d^2 \Delta n(x)}{dx^2} - \frac{\Delta n(x)}{L^2} = -g(x)/D.$$

Eq. 3

$\Delta n(x)$ is the excess excitons concentration at depth x in the bulk, L is the exciton diffusion length, D is the exciton diffusion coefficient. In the case of multiple reflections, neglecting interference effects, the photogeneration rate $g(x)$ can be expressed as

$$g(x) = \alpha(1 - R_1)I_0 \{\exp(-\alpha x) + R_2[\exp(-\alpha(2h - x)]\}/[1 - R_1 R_2 \exp(-2\alpha h)]$$

Eq. 4

where a is the absorption coefficient, I_0 is the photon flux density impinging on the polymer layer, h represents the total thickness of the layer, R_1, R_2 are the reflectance from the illuminated and the bottom surfaces, respectively. To find the photogenerated current two boundary conditions are required:

At the free surface

$$Dd\Delta n(x)/dx\big|_{x=0} = s\Delta n(0)$$

Eq. 5

at the SCR/ bulk interface

$$\Delta n(d) = 0$$

Eq. 6

where d is the thickness of the bulk , s is the surface recombination velocity.

The diffusion current density from the bulk at the boundary with the SCR is

$$J_b = eDd\Delta n(x)/dx\big|_{x=d} =$$
$$- a_1 \alpha L/(1 - \alpha^2 L^2)\{\frac{[(1 - S)\exp(-d/L) - (1 + S)\exp(d/L)]\exp(-\alpha d) + 2(\alpha L + S)}{(1 + S)\exp(d/L) + (1 - S)\exp(-d/L)} - \alpha L \exp(-\alpha d)\}$$
$$+ a_2 \exp(-\alpha w)\alpha L/(1 - \alpha^2 L^2)\{\frac{(1 + S)\exp(d/L) - (1 - S)\exp(-d/L) + 2(\alpha L - S)\exp(-\alpha d)}{(1 + S)\exp(d/L) + (1 - S)\exp(-d/L)} - \alpha L\}$$

Eq. 7

$$a_1 = eI_0(1 - R_1)/(1 - R_1 R_2 \exp(-2\alpha h))$$

Eq. 8

$$a_2 = eI_0(1 - R_1)R_2 \exp(-\alpha h)/(1 - R_1 R_2 \exp(-2\alpha h))$$

Eq. 9

$$h = d + w$$

Eq. 10

$$S \equiv sL/D$$

Eq. 11

where w is the thickness of the SCR.

The current density, J_s, from the SCR is given by integration of the exciton photogeneratation rate over thickness of the SCR:

$$J_s = a_1 G \exp(-\alpha d)\int_0^w \alpha \exp(-\alpha x)dx + a_2 G \int_0^w \alpha \exp(-\alpha x)dx =$$

$$a_1 G \exp(-\alpha d)(1 - \exp(-\alpha w)) + a_2 G(1 - \exp(-\alpha w))$$

Eq. 12

The factor $G \in {<}0,1{>}$ represents recombination losses in the SCR and characterizes contribution of photogenerated charges to the current [57]. The terms in J_b and J_s multiplied by a_1 represent the SPV signal generated by photons spreading in the direction of the impinging light, those multiplied by a_2 come from the reflected photons. Total photocurrent density for illumination from the bulk side is the sum of (7) and (12).

$$J = J_b + J_s$$

Eq. 13

The experimentally verified linear relation between the photovoltage and the light intensity leads to proportionality between the photovoltage V and the photogenerated current density J.

$$V \sim J$$

The measurement was performed in a contactless arrangement – illuminated glass/ITO top electrode was separated from the polymer film by a Mylar film, the scheme of measurement is depicted in Figure 20. The samples were irradiated by low-intensity monochromatic light chopped with a low frequency 11 Hz which was sufficiently low to obtain saturated pulses of the photovoltage not influenced by relaxations. An alternating voltage was photoinduced on the capacitor-like sandwich structure, which was measured by lock-in amplifier. The measured PV spectra were recalculated for constant impinging photon flux density and corrected for the transparency of the glass/ITO/Mylar. PV spectra were obtained at room temperature in air.
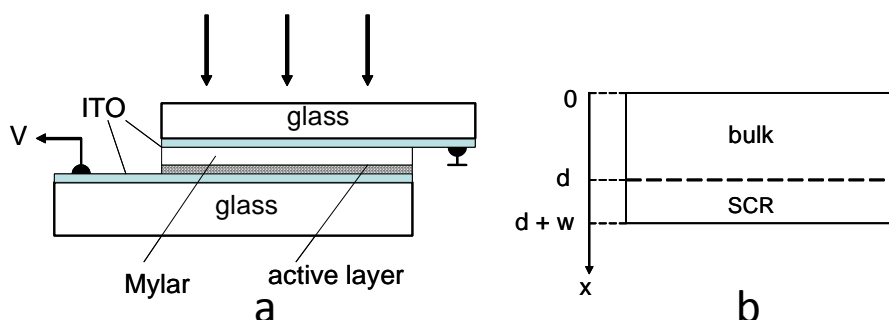
Figure 20 Schematic setup of the samples for SPV measurements – a) and illustration of bulk and SCR area – b); courtesy of [56].

The samples were illuminated from the side of the bulk.

3.3 Atomic force microscopy

Atomic force microscopy (AFM) is a method to see the shape of a surface in three-dimensional (3-D) detail down to the nanometer scale. AFM can imagine all materials – hard, soft, synthetic or natural (including biological structures such as cells and biomolecules) – irrespective of opaqueness or conductivity [59], [60].

AFM is more powerful than only an analytical tool. Major goal of microscopy is to differentiate objects or regions on materials such as metals, semiconductors, ceramics, minerals, polymers, or other organics entities. A common property metric is the rigidity or stiffness of a material, sensed as the resistance to the tip pushing in.
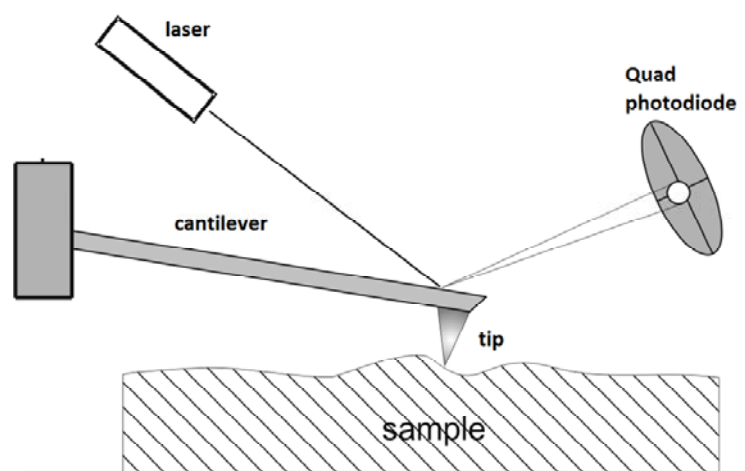
Figure 21 Schematic illustration of the core components of AFM - according to [61].

On the other hand, lateral force measurements in contact mode can be highly sensitive to material composition and structure, and thereby provide material contrast. This naturally includes the ability to image surface contamination [62]. Sliding friction can be sensitive to spatial variations in crystallinity [63] and viscoelasticity [64] and can be used to probe changes due to gaseous environment, down to nanometer scale [65].

The images of the thin film surfaces listed in this work were made by AFM microscope NanoR(TM) from Pacific Nanotechnology. Thin films were prepared on polished Si substrates.

3.4 FTIR spectroscopy

Infrared spectroscopy (IR, or today mostly used Fourier transformed infrared spectroscopy – FTIR) is one of the basic spectroscopic methods well established for polymer characterization [66]. To obtain infrared spectrum is very rapid and simply. But the interpretation and assignment of vibrational bands cannot be

simply feasible task because symmetry, mechanical coupling, Fermi resonance, hydrogen bonding, steric effects, electronic effects, isomerism, physical state, and solvent and temperature effects all contribute to the position, intensity, and appearance of the bands in the infrared spectra of the compounds. Lowering the temperature usually makes the bands sharper and better resolution can be achieved, especially in solids at very low temperatures. However, there is a possibility of splitting due to crystal effects, which must be considered when examining the spectra of solids under moderately high resolution. Polar solvent can cause significant shifts of group frequencies through solvent-solute interactions, such as molecular association through hydrogen bonding [52].

On the other hand, nowadays various sources of IR spectra exist and moreover, the expertise with manifold experience allows the assessment and assignments of vibrational band in IR spectra of polymer.

3.5 Profilometry

Surface metrology is based on the measurement of surface profile – profilometry. This technique, commonly used in mechanical engineering, permits the quantification of surface geometry, typology as well as topology of roughness [67].

Two main approaches can be considered for surface relief characterization: mechanical or optical. Mechanical profilometry has been used succesfully to evaluate the characteristic of polished and smooth surfaces. With that type of method, it is possible to produce very accurate results for laboratory investigations [68]. Mechanical profilometry is not suitable for large surfaces, but in our case, it deals with only micrometer scale.

The principle of mechanical profilometry is that mechanical unit (stylus) walks along surface being in contact with surface. The conditioner gives an electric tension proportional to the vertical displacement of the stylus. Finally, the calculation system associates the position (x, y) and the altitude z of the stylus in order to represent the measured profile of the surface and to calculate the geometric parameters.

For all thickness measurement, the Taylor-Hobson profilometer (called Talystep) was used. The resolution of this instrument is 1 nm in vertical z-axis. The

thicknesses of all measured films were achieved and they are mentioned in further text, where is necessary.
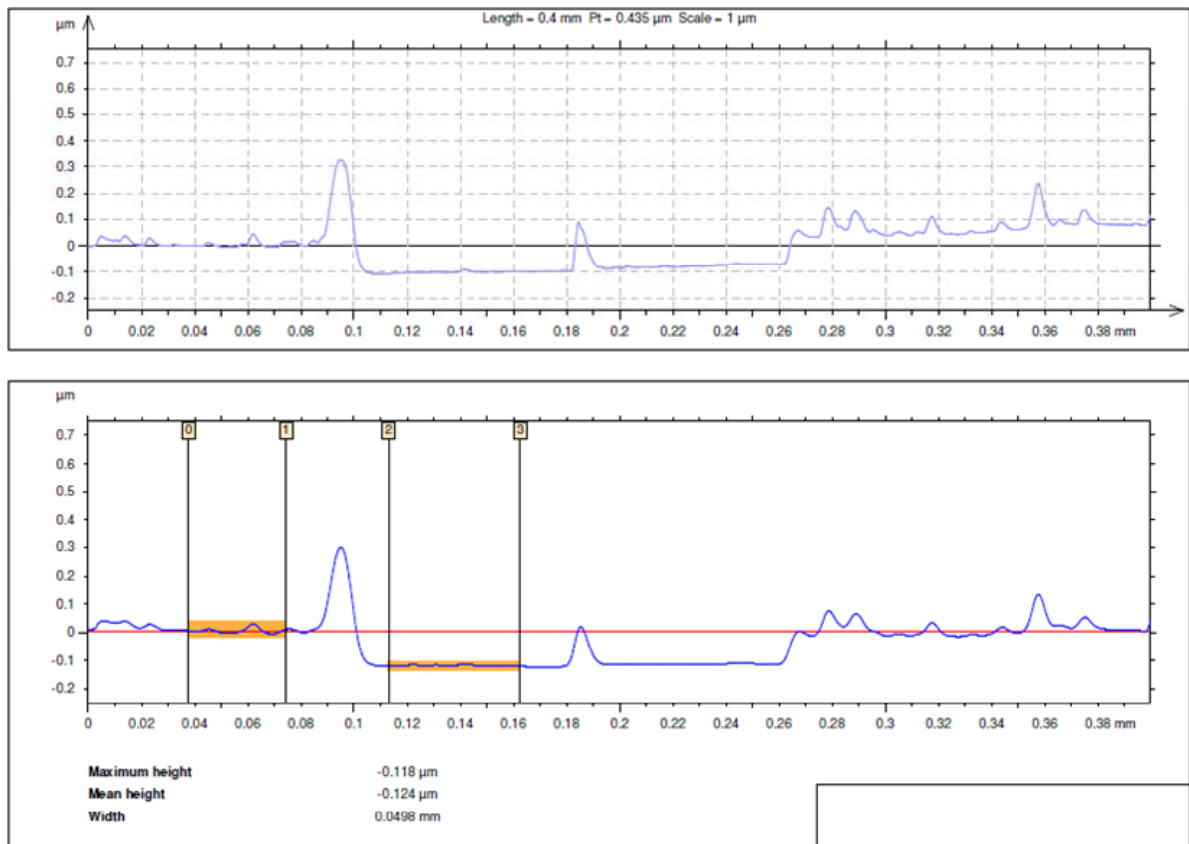

Figure 22 Example of surface profile of thin film.

4. Aims of doctoral thesis

The main goals of the dissertation entitled "Thin polymer films - material study between nano- and microscale" can be summarized into following parts:

1. Preparation of thin films with variable thickness from both, π- and σ-conjugated polymers, mainly from MEH-PPV and polysilanes (PMPSi and copolymer P[DMSi-MPSi]) respectively, whereas the viscosity and concentration of solutions, spin rates during spin coating are under investigation as parameters influencing the final thickness of samples. The thickness shall vary from several nanometers to micrometers to cover whole range from nano- to microscale.

2. Study of optoelectrical properties of prepared polymer thin films in dependence on thickness with special attention paid to the explanation of the threshold effects observed between nano- and microscale. Moreover, to study the manifestation of thickness influence on the previously reported self-recovering and self-healing of σ-conjugated polymer due to the phenomenon of metastability, which are typical for this kind of material.

3. Attempt to prepare composite material with improved optic and optoelectronical properties due to addition of functional nanoparticles filler to the π-conjugated polymer matrix. Such composite/tes shall be considered for use in preparation of polymer OLED devices and/or for photovoltaic performance.

5. Sample preparation

Both type of conductive polymers (π- and σ-conjugated) were deposited on the substrates by spin coating method. The series of drop cast films were prepared with the purpose to confirm the independence of polymers behavior on the casting method. The spincoater Laurell WS-650-MZ-23NPP was used in all castings.

All films were dried and annealed after deposition in a vacuum oven under following condition: p=100 mbar; T=100 °C; hold at 100 °C for 4 hours, then left to cool down, duration time of whole cycle was 16 hours.

The thickness, measured by mechanical profilometer with 1 nm resolution, was in the range from several to hundreds nanometers for spin-coated samples and up to 900 nm for drop cast samples. Individual thicknesses will be specified in further text, with reference to appropriate measuring techniques and data evaluation.

5.1 MEH-PPV films

As the importance of inter- or intrachain interaction in thin polymer films depending on the polarity of used solvent is more and more discussed, the films were prepared from solutions in different solvents to confirm or wipe out the facts that interaction in thin films have origin in the character and quality of the solvent [69]. Thin MEH-PPV films were deposited from solutions in three different solvents; firstly from solvent mixture of chloroform and toluene, next solvent was pure toluene and the last one was dichlorobenzene (DB). Spin rate varied from 2000 rpm to 6000 rpm. The thickness dependence of prepared films on the spin rate during spin coating is plotted in the Figure 23. Used solution concentration in this case was approximately 1 % (exactly 10.0 mg of polymer in 1 ml of solvent).

As substrates, both uncoated quartz glass (QG) and quartz glass coated by indium tin oxide (ITO) were used. Quartz glass was used for UV/VIS absorption measurements and for fluorimetry, ITO coated glass was used for SPV and fluorimetric measurements.

The mixture of chloroform and toluene was chosen for further film preparation due to the good processibility and very homogenous layer formation.
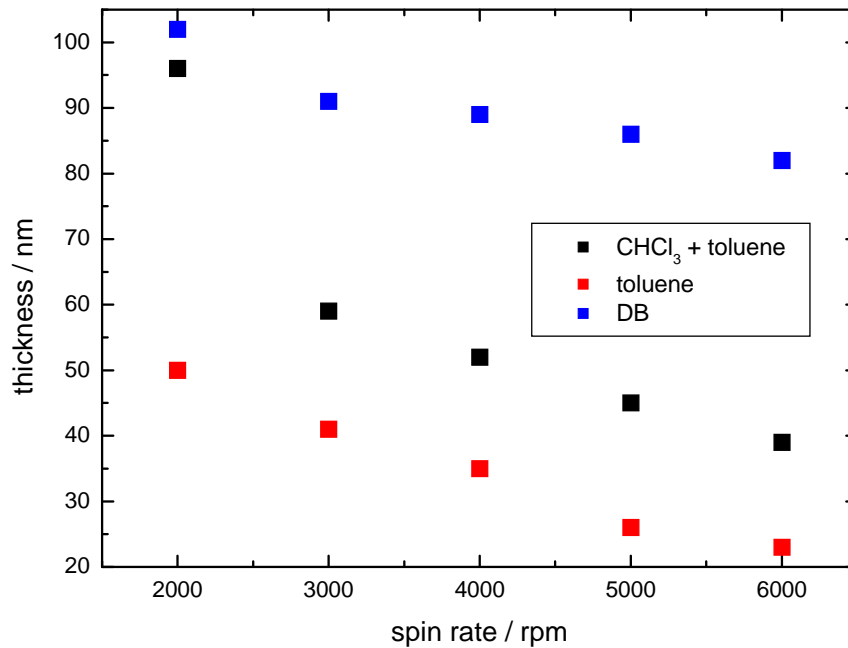
Figure 23 The thickness dependence of prepared films on the spin rate and used solvent.

Toluene has a preferential interaction with the MEH-PPV polymer backbone which imposes a rigid straight open conformation on the backbone chain while the polar chloroform molecules can solvate the polymer's side groups. It is expected that this solvent mixture formulation facilitates adoption of more planar conformations of the polymer chain during formation of cast thin films [70]. Based on these facts, a set of experiments with different concentration of polymer in this solvent was carried out. The obtained results are graphically summarized in the Figure 24.

Preparation conditions are important for homogeneity and optical quality of films as many problems must be avoided (see the Figure 25). In case of MEH-PPV, for instance - uncoated area, swirl patterns, comets, streaks or flares. Three last-mentioned are easy to be eliminated. It is enough to decrease the spin rate and to filter the solution appropriately. To avoid the other troubles with film coating, it is necessary to cast sufficient volume of solution, to clean substrates precisely, to adjust the adequate viscosity of solution and so on. Thus, the spin rate 3500 rpm and concentration of solution 1 % were chosen to achieve the best quality films.

From technological point of view, achieved data can be useful for thin films formation and deposition, because we are able to predict the final thickness of layer if we know the concentration and the viscosity of solution.
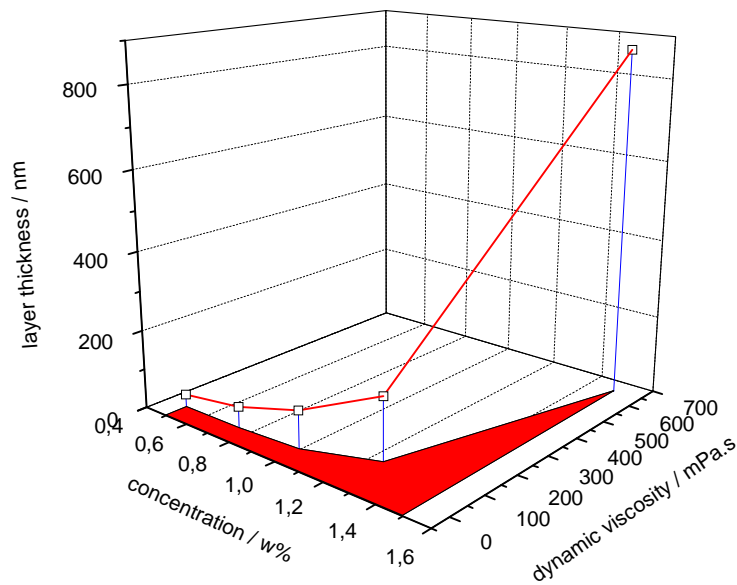
Figure 24 The technological parameters for thin film preparation from MEH-PPV in the mixture of solvents (CHCl$_3$ and toluene), used spin rate 3500 rpm.
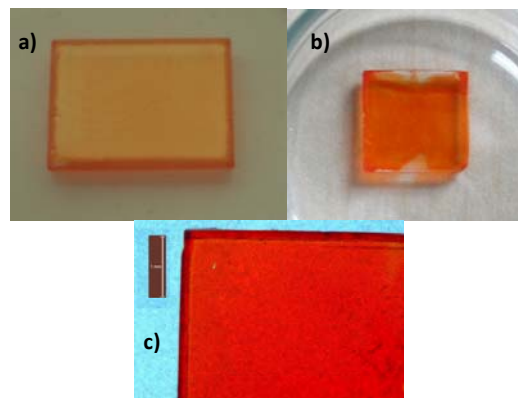
Figure 25 Examples of prepared films from MEH-PPV: a) high quality and homogenous film, b) uncoated area on the substrate due to the low volume of solution during casting c) a detail of high quality film – homogeneity of the film up to the edge of the substrate, 40x magnified.

5.2 Polysilanes films

Two types of polysilanes, concretely, a homopolymer PMPSi and a copolymer P[DMSi-MPSi] were chosen for the structure study between nano- and microscale. Thin films were cast from solution in toluene. QG and silicon wafers were used as substrates. QG was used for UV/VIS absorption measurement, silicon substrate was used for PL, PL decay and metastability and self-recovering measurements. The topography of thin films on Si substrates was measured by AFM method.

Figure 26 The thickness dependence of prepared films on the spin rate and concentration of cast solution during spin coating, PMPSi – left graph, P[DMSi-MPSi] – right graph. Quartz glass used as substrate.

Figure 27 The thickness dependence of prepared films on the spin rate and concentration of cast solution during spin coating, PMPSi – left graph, P[DMSi-MPSi] – right graph. Used substrate – Si wafer.
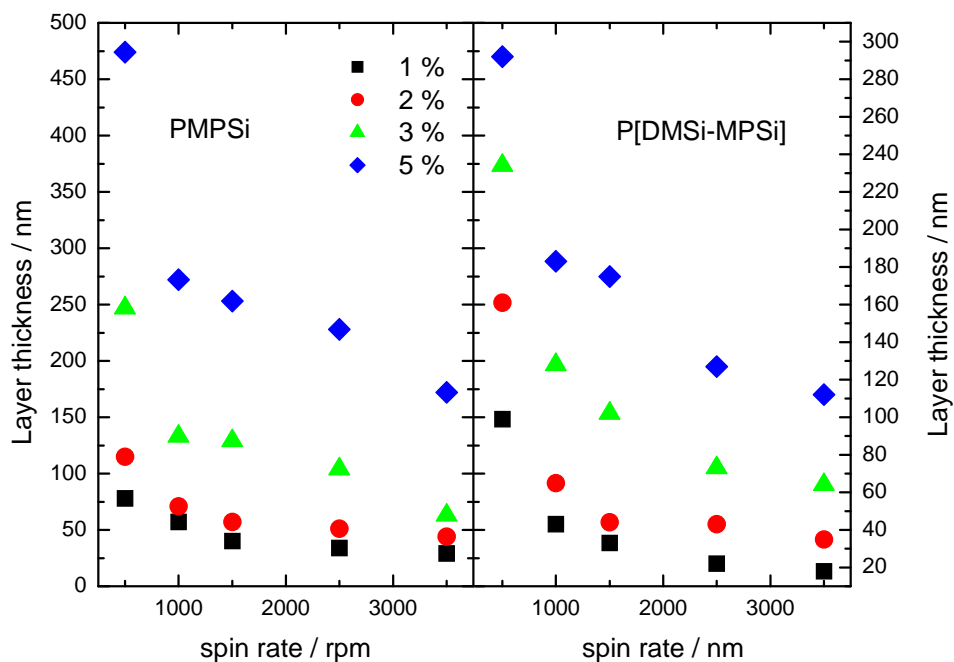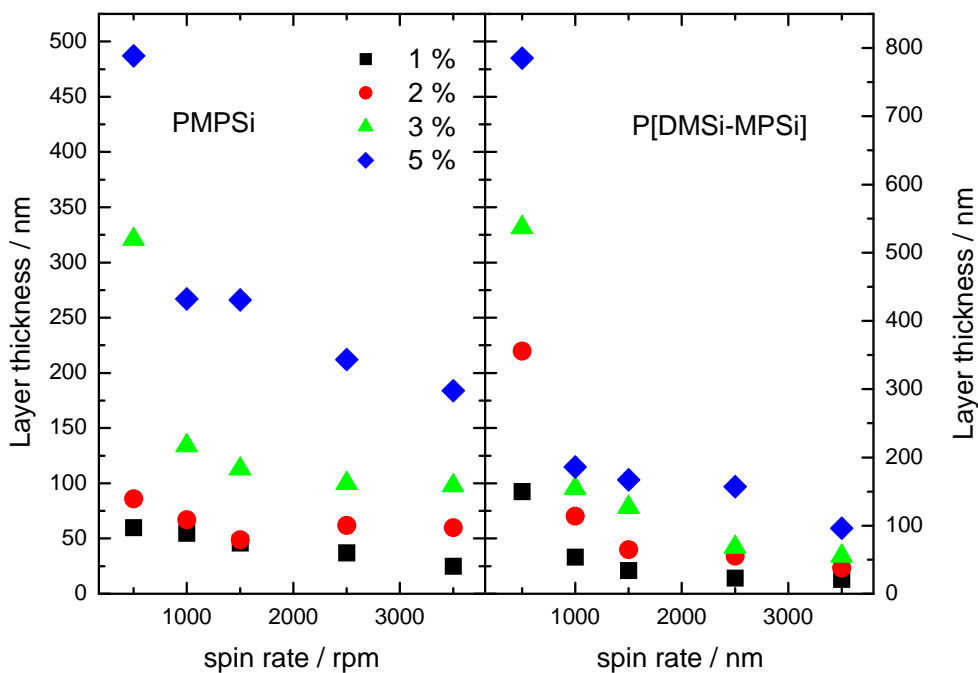
In the Figure 26, the dependence of thickness of prepared films from both PMPSi and P[DMSi-MPSi] on the spin coating condition is plotted. In this case, quartz glass substrate was used. The same kind of dependence is plotted in the Figure 27, but in that case, Si wafer was used as a substrate. Both materials show typical behavior common to almost all polymers used for spin-coating. Similarly to the case of MEH-PPV and based on the experience gathered during the study, it is possible to estimate the behavior of PSis during the film preparation, it means that the final film thickness can be predicted if the concentration of deposited solution and spin rate by spin coating are set up within the known range.

5.3 MEH-PPV/ZnO composite

The preparation of thin composite films is non-trivial and was originally developed in this study. It involves three steps and was performed in our case as follows: The first step was preparation of neat MEH-PPV solution. Concentration of this solution was 1 %, used solvent a mixture of $CHCl_3$ and toluene. The solution was stirred for several hours for good dissolving of polymer. From this solution were coated thin films as neat MEH-PPV references. The next step was the addition of ZnO nanoparticles. ZnO nanoparticles containing solutions were prepared by addition of ZnO in appropriate amounts to target concentration ranging from 7,5 % to 40 % related to weight of polymer. The solutions were sonicated after addition of ZnO nanoparticles. An ultrasound bath Elma Transsonic Digital S was used. After sonication, thin films were prepared by spin coating method on quartz glass substrate which is the third step of the process.

6. Study of MEH-PPV films

MEH-PPV is attractive for their high absorption coefficient in the visible part of the spectrum and can be used as light emitting diodes, lasers, organic thin film transistors and photovoltaic cells [71]. Despite this high versatility for optoelectronic application, some questions underlying the construction or optimization of practical devices based on these materials remain controversial or needing better explanation. There exists a discrepancy between described behavior in the solution and in the form of thin and thick films which needs to be more linked together to obtain a complex view of the problem. Moreover, effects of second order are often manifested in experimental observations, and the photophysical properties and final device performance are found to be extremely sensitive to processing parameters such as choice of solvent, solution concentration, spin coating conditions and heat temperature treatment program. All these parameters are considered to influence the polymer chain orientation and microstructure of obtained solid films [72] - [74].

The chains orientation and structure in thin films can be investigated at different levels, first, the molecular structure of the macromolecules; second, the chain packing and orientation of the macromolecules with respect to substrate; and third, the degree of crystallinity, phase composition and orientation and size of crystalline domains in thicker films [75].

The conformation of macromolecular chain and stacking of these chains differ in thin and thick films and both from solutions. The optoelectronic properties of thin films made from these materials by solvent casting are affected by relatively subtle variation in intra- and interchain interactions in the conjugated polymer. PL study is a useful tool to reveal these differences because observed radiative exciton recombination correlates with microstructure of the material. A typical room temperature steady state PL emission spectrum of MEH-PPV consists of three more or less resolved superimposed peaks corresponding to the intrachain transitions between the ground state with several vibrational energy levels and the excited state. The two main emission peaks in the luminescence spectrum of MEH-PPV can be identified as 0-0 peak at higher energy for exciton recombination caused by the transition from the 0th vibronic excited state to the 0th vibronic ground state and

the 0-1 peak at lower energy exciton recombination from the 0th vibronic excited state to the 1st vibronic ground state. The third peak is denoted 0-2 for exciton recombination from the 0th vibronic excited state to the 2nd vibronic ground state. This higher mode and eventually other higher modes are usually less intense. The intensities of these luminescence peaks, namely 0-0 and 0-1, can be successfully linked with the polymer chain ordering and stacking in the thin film structure [76] – [81]. Single molecule experiments have shown that in dilute solutions or in case of single isolated macromolecule of MEH-PPV on a solid substrate, the photoexcitation creates only one electronic space, a singlet intrachain exciton, which has a high degree of anisotropy. The prevailing intensity of 0-0 peak over the others testifies for increasing conjugation length. Similar behavior is manifested for molecular films with low level of surface coverage or for very thin films. Significantly higher intensity of the 0-0 peak with respect to 0-1 peak is often observed and interpreted as a consequence of steric hindrance from chain packing. The suppression of torsional motion, which is present in bulk films samples, causes an increase in effective conjugation length too and results into the hypsochromic shift of the 0-0 peak maximum. On the other hand, when two π-conjugated polymer chains interact side by side in a π-stack the delocalization of exciton appears not only along the chains but also between chains. However, the coupling between chains leads to a destructive interference in the interchain coherence and intensity of 0-0 emission disappears with the increasing stack ordering in aggregation. Therefore, the photophysical properties of π-stacked polymers are given by a competition between intrachain coupling inducing increase of 0-0 intensity and interchain coupling causing decrease in the 0-0 peak intensity within the vibronic progression. The dense chain packing leads to relative increase of 0-1 peak intensity in comparison with the peak 0-0 [81] – [85].

The structure of polymer thin film is closely related to its function. Knowledge of the transport mechanism in organic devices is important in optimizing their performance. The diffusion length is one of the important parameters for the function of e.g. solar cells. For the diffusion length determination we have used the surface photovoltage method. Compared to the most frequently employed method of the luminescence quenching [86] - [89] which needs a set of samples differing only in their thickness the adapted SPV method has not such demands.

6.1 PL study

From the Graphs a) and b) in the Figure 28, it can be seen that 0-0 peak is red shifted with increasing thickness. The spectral intensity for the second peak (0-1) relatively increases with increasing thickness. These trends are manifestation of the intrachain conjugation length increase and of the interchain π-delocalization increase with increasing film thickness.
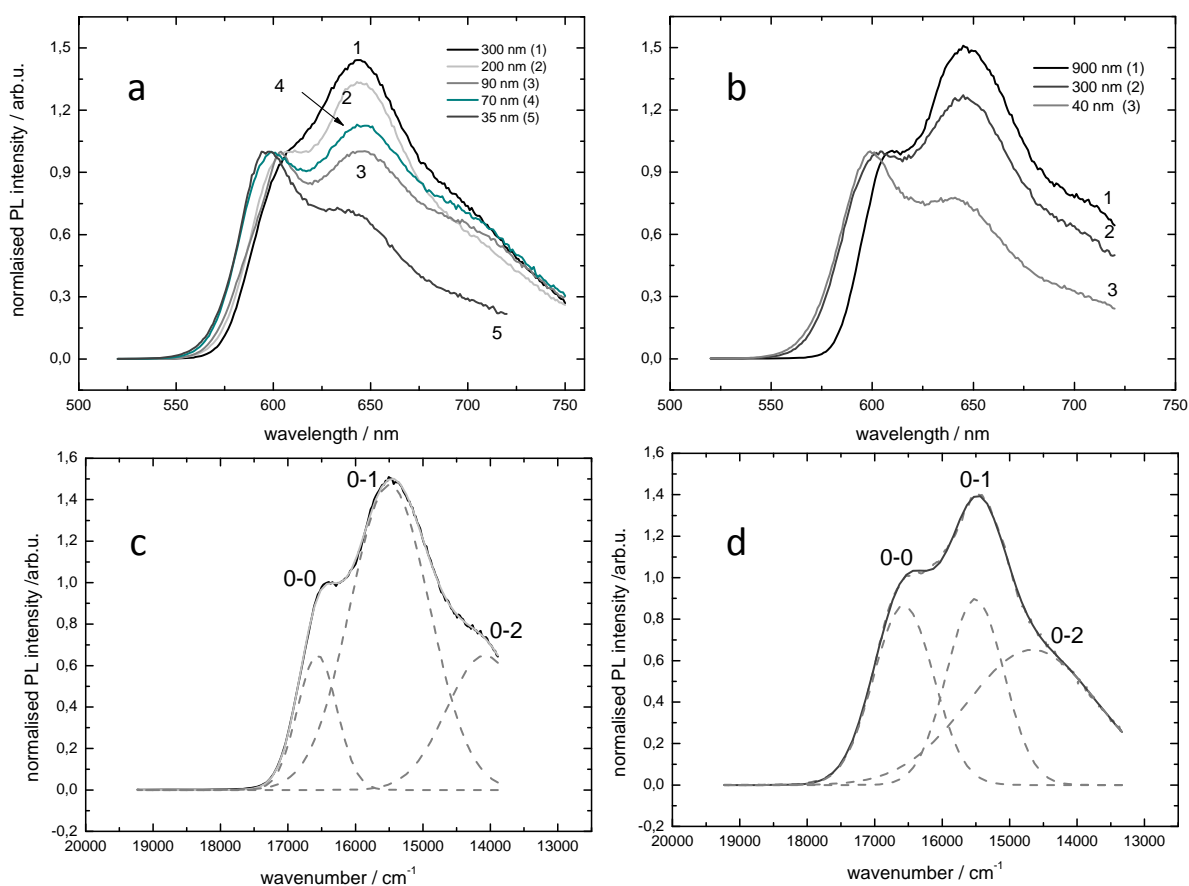
Figure 28 Emission spectra of MEH-PPV and their analysis. Emission spectra of a) spin cast films, b) drop cast films. Fitting of the emission peak by three Gaussian profiles: c) example of the best peak deconvolution d) example of the worst peak deconvolution, see the overlap of the second and third peak.

The PL emission spectra were analyzed in more detail. Each spectrum was plotted in wavenumber scale and deconvoluted into three vibronic bands by fitting the emission peak with three Gaussian profiles. Figure 28 c) shows the example of such analysis on the best resolved spectrum with the use of software Origin 7.0. On the other hand, many recorded spectra were not so well resolved and it is clearly seen in Figure 28 d), that the 0-0 peak has much better resolution than the second (0-1) and third (0-2). The large overlap of the two latter peaks result in some ambiguity

of intensity value obtained for the peak 0-1 separately. However, if the fits for the peaks 0-1 and 0-2 are taken together, the situation improves significantly. The relative intensity of both peaks with respect to the 0-0 peak is linked to the interchain interaction in π-stacks. Therefore, the ratio R_I between the 0-0 peak area and the sum of 0-1 and 0-2 peak areas defined by Equation 14 was chosen to be observed as the parameter sensitive to intra- and interchain ordering in this study.

$$ R_I = \frac{I_{PL}^{0-0}}{I_{PL}^{0-1} + I_{PL}^{0-2}} $$

Eq. 14

The evolution of R_I with the increasing film thickness is plotted in Figure 29. It can be seen, that there is a critical thickness of prepared films, where the dependence of peak area ratio on the film thickness changes significantly its slope. The thickness threshold lies approximately at 150 nm.

In more detail, the 0-0 peak shift is shown in the upper graph in the Figure 33, where the 0-0 peak maximum positions are plotted in dependence on the film thickness. The position of the peaks is unambiguously related to the conjugation length of MEH-PPV polymer segments. The longer is the polymer chain segment over which the conjugation spreads, the higher wavelength of light emitted by a radiative exciton recombination on such segment can be observed.
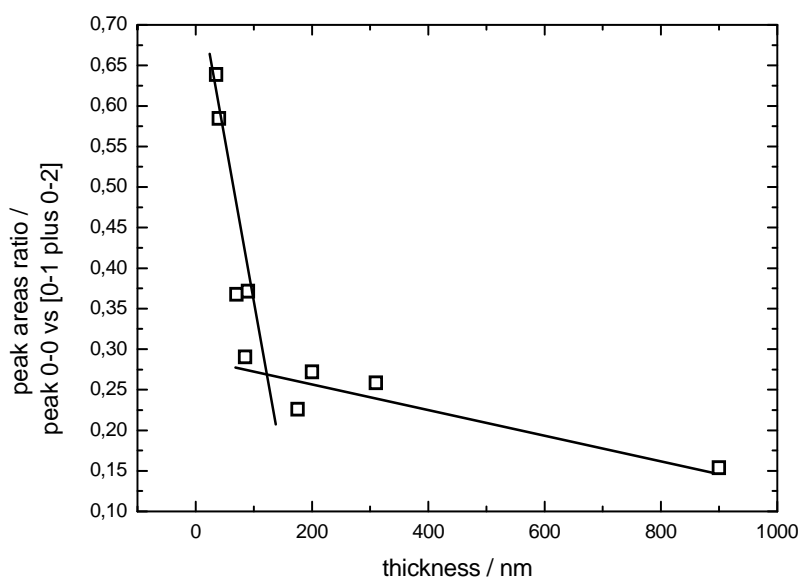

Figure 29 The dependence of the peak area ratio R_I on film thickness. Experimental points are shown as open squares; the straight lines help to find the threshold only.

The concentration of these segments may be relatively low and not reflected in the absorption spectra significantly as the energy transfer after absorption from a distribution of excited conjugated segments proceeds to the longer ones. Again here, a significant change of slope or even the saturation can be observed above 150 nm in the plot.

The consideration, that behavior mentioned above is independent on the solvents used during the film deposition, was verified by investigation of PL of films prepared from the polymer solutions in different solvents. The same features of optoelectrical properties of MEH-PPV films depending on the layer thickness are depicted in the Figure 30.
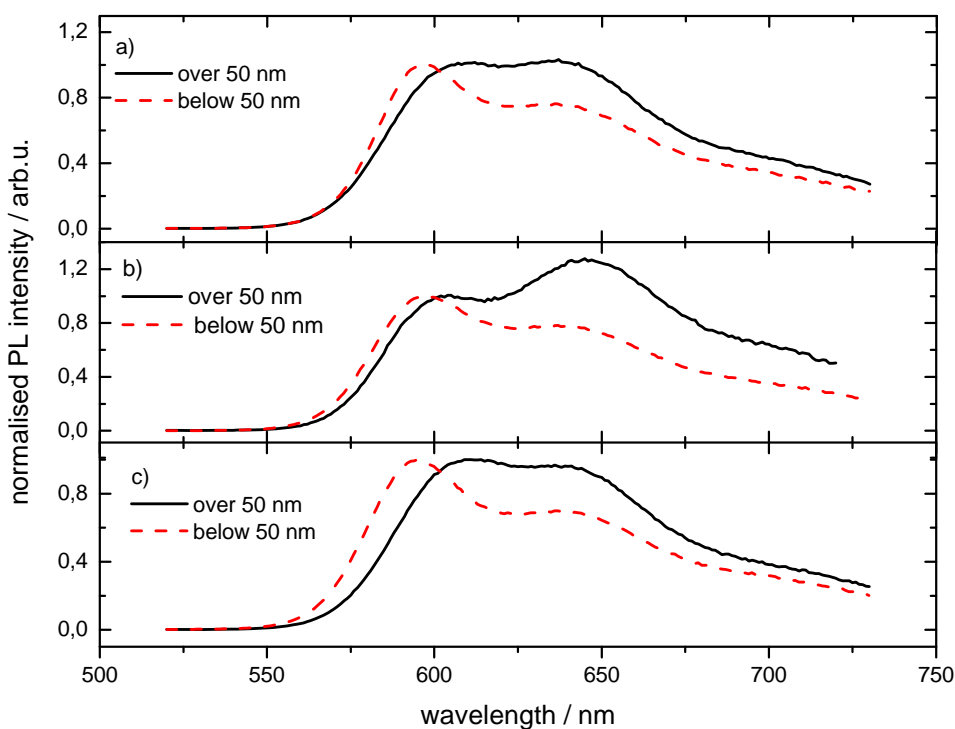

Figure 30 Emission spectra of MEH-PPV films prepared from solutions in different solvents with thickness over and below 50 nm: a) CHCl$_3$ + toluene, b) dichlorobenzene, c) toluene.

6.2 Exciton diffusion length in MEH-PPV films

The conformational order and in π-conjugated polymer stacks must influence the exciton diffusion length. Therefore, SPV method can be used with advantage to determine this behavior because it is independent on the film thickness. So, it is sensitive on the changes of diffusion length varying with thickness.
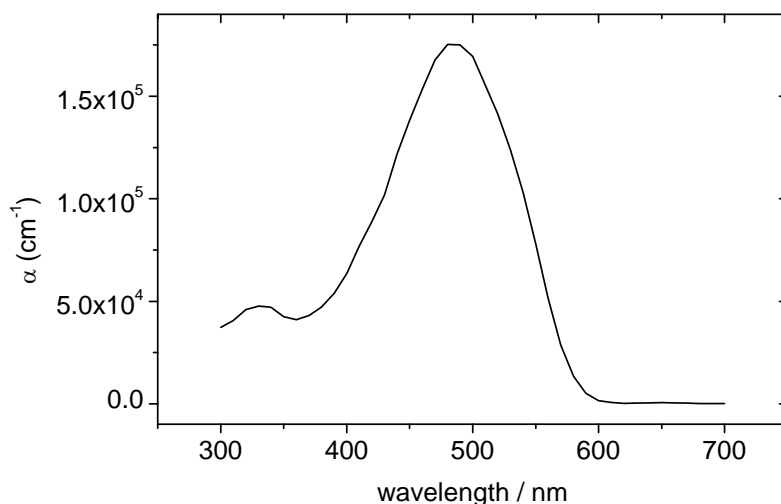

Figure 31 Spectral dependence of the absorption coefficient.

A necessary prerequisite for SPV processing is shown in the Figure 31 where a representative absorption spectrum of the MEH-PPV thin films is plotted. The spectra of photovoltage are plotted in Graphs a-f in the Figure 32. While the form of the a-c curves approximately copies the spectral dependence of the absorption coefficients (Figure 31), the feature of the d-f curves is different; the strong decrease of the signal at the wavelength corresponding to the maximum of absorbance is a consequence of a low ratio of the diffusion length and the bulk thickness [57]. The diffusion lengths were evaluated using the theory included in Appendix 1. Reflectance measured for all individual thicknesses and absorption coefficients shown in the Figure 31 were used for the theoretical spectra calculation. The diffusion lengths of excitons were obtained by fitting the theoretical SPV spectra (full lines) to the experiment (points). The mathematical fit is in good accordance to measured spectra in all cases. Obtained values of the exciton diffusion length are shown in the lower graph in Figure 33 for comparison

with the dependence of 0-0 peak maximum position on film thickness. It can be seen that exciton diffusion length of photovoltaic active MEH-PPV material is influenced by thickness in similar manner as in case of PL spectra. The critical film thickness estimated from SPV measurements at which the exciton diffusion length changes steeply is at about 150 nm.
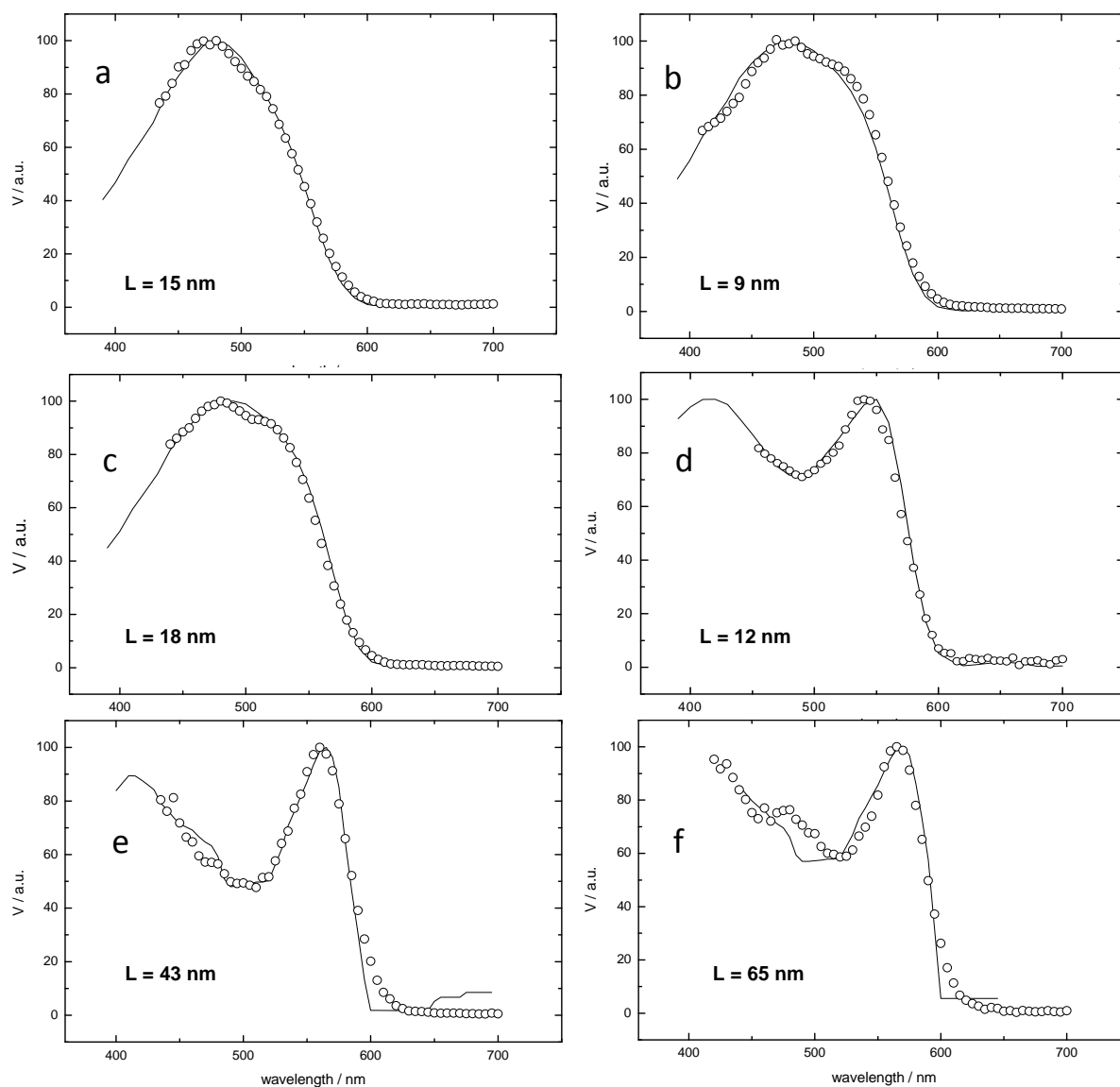
Figure 32 SPV spectra of the MEH-PPV films (points – experiment, full lines – theory). The film thicknesses were as follows: a – 19 nm, b- 53 nm, c – 85 nm, d – 134 nm, e – 235 nm and f – 310 nm. The fitted diffusion lengths (L) are marked inside of individual figures.

Although a rapid increase of conjugation length of at least some polymer chain segments with the film thickness was confirmed for films thinner than 150 nm, the excitons remain still mainly localized. It is consistent with observed negligible

change of the exciton diffusion length with increasing thickness of the film in this interval. Above the critical thickness the exciton diffusion length increases significantly which indicates higher degree of interchain interaction and testifies for higher molecular ordering and denser chain packing in contrast to thinner films. Thus, the photovoltaic measurement corroborates the hypothesis of threshold thickness for optoelectrical properties implying non-trivial polymer film structure dependence on the film thickness.
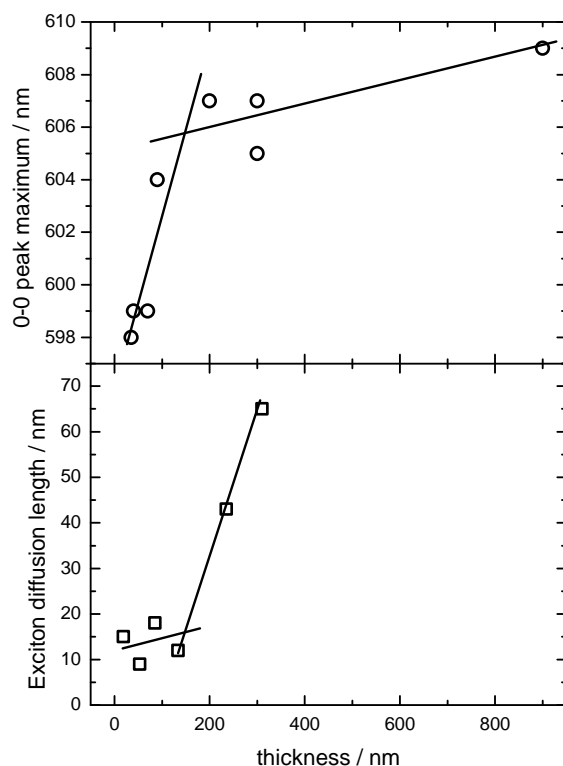

Figure 33 Analysis of emission 0-0 peak maximum wavelength for MEH-PPV films, plotted as circles in the upper graph and dependence of the exciton diffusion length plotted as squares in the lower graph. Both graphs have common x-axis for film thickness. Experimental points are shown as open symbols; the straight lines help to find the threshold only.

7. Study of polysilanes films

7.1 PL study

Intrinsic photoluminescence is a characteristic feature of PSis and it is strongly dependent on the structure of the material. A PL emission spectrum of a real polysilane, deposited as a thin film, is typically composed of two distinctive features as exemplified in Figure 34 a): a very intensive main sharp PL band situated at the wavelength 360 nm and two merged weak broad emission bands manifested in the region from 420 to 520 nm. The sharp band is attributed to the σ^*-σ exciton radiative recombination which is an intrachain transition.

Figure 34 Emission spectra of polysilane thin films with a different thickness, λ_{ex}=330 nm, a) PMPSi, b) P[DMSi-MPSi].

The broad band at 420 nm is related to the radiative recombination of charge-transfer states, or to the recombination of excitons trapped on chain imperfections, or other impurities generated by the photolysis of the polymer, for example cross-link points, dangling bonds, etc. The other broad band at 520 nm is related to a weak bond (WB) formation due to the photodegradation in the material structure. A WB is a Si-Si bond of inferior quality having a longer bond distance between silicon atoms than regular Si-Si bonds in the PSis main chain. The WB is stabilized by the surrounding polymer matrix; however, it is amenable to the thermal annealing. Exciton diffusion, free electron-hole pair formation, their trapping in WBs and their subsequent radiative recombination by tunnelling are

responsible for the weak emission at 520 nm [90], [91]. Excitation spectra show two maxima in Figure 35 (curve 1), one at 330 nm (due to σ-σ* transition) and another one at 275 nm due to π-σ* transition as there is a strong π*-σ* mixing which is a manifestation of the phenyl side group presence in the polymer structure. The PL of PSis is strongly related to their structure and responses sensitively to polymer degradation by a change of the UV emitted light intensity and by manifestation of several emission broad bands in the visible region of the spectra. Moreover, the excitation spectra can be collected as well and interpreted in terms of structural changes, too. PL has been already shown as a useful tool for the structural investigation of PSis [80], [92], [93].
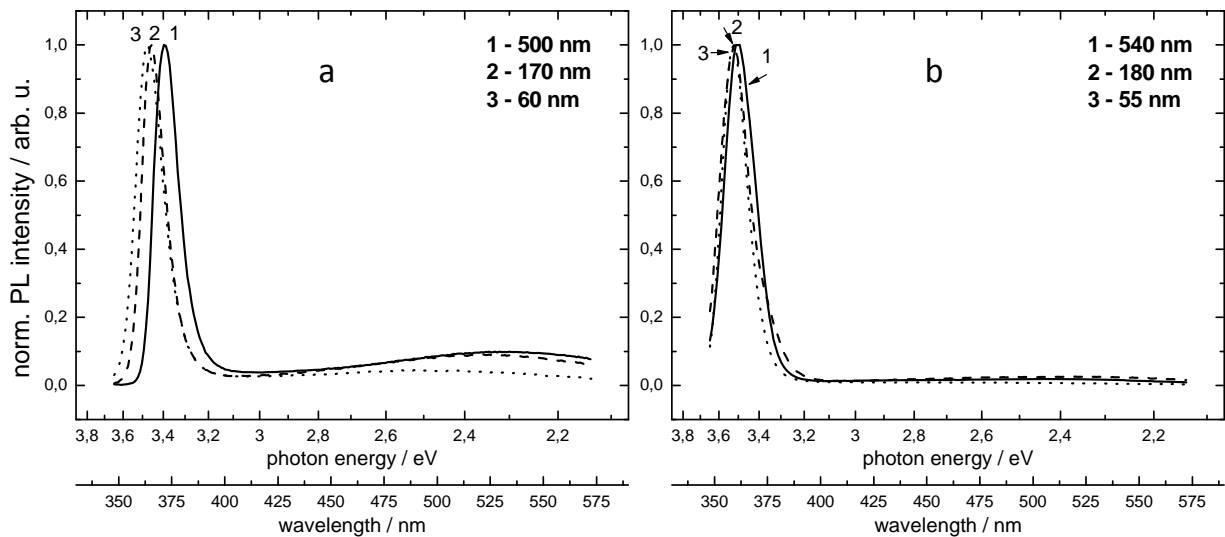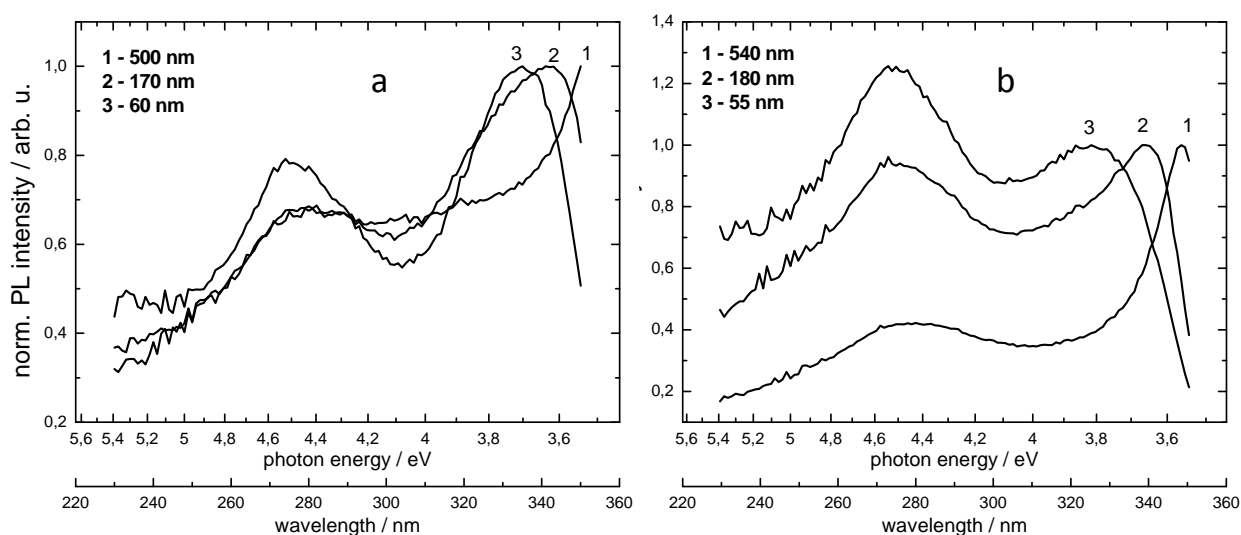

Figure 35 Excitation spectra of polysilane thin films with a different thickness, λ_{em}=360 nm, a) PMPSi, b) P[DMSi-MPSi].

The chromophore responsible for the absorption of a light quantum is a conjugated segment of the main silicon chain of PSis. The energy of this σ-σ* transition depends straightforwardly on the conjugation length of the delocalized σ-orbital system. Once formed, the exciton travels along the main chain until it is trapped on the longest segment, which has the smallest band gap and lowest energy, where a radiative recombination occurs and a photon is emitted. On the other hand, in case of a non-radiative σ*-σ transition, one of the sigma bonds dissociates, which leads to a scission of the Si-Si chain. Nevertheless, the recovery of the material was observed under certain conditions instead of a progressive deterioration of the

material structure. Such "selfhealing" effects are referred to as metastability [94], [95].

Table 1 Excitation and emission maxima of polysilanes in thin film depending on their thickness.

PMPSi			P[DMSi-MPSi]		
Thickness / nm	excitation maximum λ_{exmax} / nm	emission maximum λ_{emmax} / nm	Thickness / nm	excitation maximum λ_{exmax} / nm	emission maximum λ_{emmax} / nm
1100	355	360	785	351	356
578	355	360	537	348	355
487	355	360	356	345	356
474	355	360	186	339	353
421	350	360	167	338	352
272	348	360	157	332	353
253	347	359	154	332	353
228	344	358	150	340	354
172	342	359	127	334	350
104	337	357	114	335	353
71	337	357	96	334	349
63	337	357	68	326	349
57	337	357	65	326	352
57	335	356	55	326	348
51	337	357	55	326	349
44	337	357	54	326	352
40	335	355	38	326	347
34	335	354	34	326	348
29	335	354	21	326	348
0	334	347	0	326	345

In case of PMPSi the small shift of emission maxima depending on the film thickness is clearly seen. The thicker the film is the more the UV emission peak is shifted towards a lower energy due to the increasing length of the polymer chain segment

at the site of recombination. However, the effect is pronounced only a little and, in case of P[DMSi-MPSi], the shift of emission maxima cannot be clearly observed. Broad bands at 450 and 520 nm, as mentioned above, are caused by imperfections and by the WBs formation. The shifts of σ-σ* transitions dependent on the thickness are transparently carried out in Table 1. The zero thickness means excitation and emission maximum obtained for polysilanes in solution, where the molecule is in form of statistical tangle.

On the other hand, in both cases, PMPSi and P[DMSi-MPSi], large shifts of excitation maxima related to the σ-σ* transition in the region at about 330 – 350 nm are manifested in Figure 35. With the increasing thickness of films, the excitation maxima shift markedly to a lower energy, i.e. to higher wavelengths. These shifts are accompanied by a change of the ratio of the PL intensity between two main excitations bands (peaks). Considering the excitation peak at 275 nm remaining relatively unchanged, it can be concluded that the intensity of the σ-σ* transition band strongly increases with the film thickness as well.

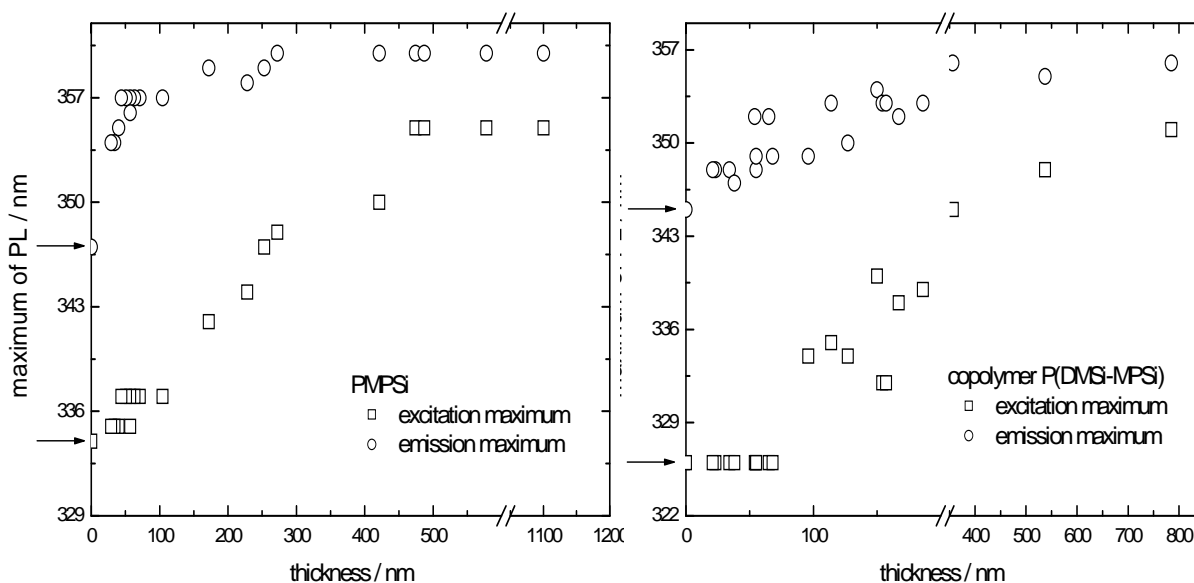**Figure 36 Thresholds in PL excitation and emission maxima of polysilanes.**

The microstructural interpretation framework of emission and excitation spectra can be summarized (and justified) as follows: The wavelength of the maximum in UV emission peak depends directly on the length of the conjugated segment where the radiative recombination of the exciton takes place, i.e. the longer segment,

the longer wavelength. Defects of the polymer structure influence crucially the PL of the material. Conformational defects which can be defined as any deviation from ideal all-trans conformation cause shortening of the conjugation length. The smallest conformational defect can be defined as a kink on the polymer backbone and indeed it decreases the conjugation length although it does not restrain the exciton from travelling along the chain. Imperfections or deviations from purely linear covalent polymer chain structure as branching or crosslinking points dramatically decrease the intensity of the UV emission and change the ratio between UV and visible emission intensity [96], [97], [98]. Analysis of the visible part of emission spectra allows theoretically distinguishing between the polymer chain structural defects and weak bonds as discussed above. However the peaks in visible region are quite broad, overlap to a reasonable extent and thus make the interpretation more difficult in this issue. Excitation spectrum resemble to some extent the absorption spectrum, actually it is its subset in some sense. The absorption of a photon is a fast (vertical) process therefore the excitation spectrum gives information about the conformation at the site of light quantum incidence with the chromophore [53] although only those absorption events that lead to a radiative recombination are recorded. Thus it is possible to investigate the microstructure of the PSis materials at two distinguished sites i.e. at the absorption site and at the recombination site while the distance of these two sites in space (and in time too) is simply due to the exciton diffusion. Though one might argue that this interpretation framework is simplified and limited to one-dimensional approach only and that there are strong interchain interactions in conjugated polymers this is not appropriate in this case. Interchain aggregation influences significantly electronic structure of π-conjugated polymers [75], [76] through interaction of the delocalized π-electron systems in case of so called π-stacking. Slightly similar situation can be observed just in non-substituted σ-conjugated PSis. Creation of two or three dimensional structures from $(SiH_2)_n$ chains gives rise to the interchain interactions which significantly influence the electronic properties of the material. On the other hand, methyl and phenyl substituted PSis show signs for very weak interchain hydrogen bonds in two or three dimensional structures only while the stability of the solid phase is due to cooperative effects of such weak bonds. Consequently, the electronic structure of the polymer backbone chain in

comparison with the one dimensional structure is hardly influenced [99]. Thus the microstructure of alkyl and aryl substituted PSis can be successfully understand and interpreted in terms related to polymer chains as quasi one dimensional structure that keep such character even in solid phase and this approach is relevant for the whole context discussed above.

In both cases, PMPSi and P[DMSi-MPSi], large shifts of excitation maxima related to the σ-σ* transition in the region at about 330 – 350 nm are manifested in Figure 35 and the structural sensitivity of PL investigation method in excitation spectra is not smeared by the above discussed exciton diffusion. Similarly to PL emission, the data are plotted in Figure 36. The wavelength at the maximum in excitation spectrum is 334 nm for PMPSi and 326 nm for P[DMSi-MPSi] so the copolymer has larger Stokes' shift in solution. This suggest that P[DMSi-MPSi] has shorter conjugation length of segments in average in solution, and that the increase of conformational order is relatively bigger for P[DMSi-MPSi] than for PMPSi during formation of the solid thin film. The thinnest PMPSi film in our study was 20 nm thick and its UV emission maximum was at 335 nm which suggest that not much changed between solution and thin film. Similarly, the wavelength 326 nm was observed for P[DMSi-MPSi]. This valeue remains practically constant up to the sample thickness of approximately 80 nm for both materials. It can be assumed, that a relatively unordered structure prevails in thin films below 80 nm with conformations similar to that of the coils in solution. It can be ascribed to certain rigidity of the PSis molecules which are relatively short. It can be observed, that the emission maximum wavelength slightly rises which testifies for presence of longer conjugated segments with increasing film thickness. In other words, the distribution of the conjugation length of PSis chain segments extends to higher range and enriches by longer segments while keeping its center still at the position typical for in solutions. With the thickness of films increasing over 80 nm, the excitation maxima for σ-σ* shift markedly to a lower energy, i.e. to higher wavelengths. It means that much more ordered phase is formed and that the distribution of the segmental conjugation length shifts towards higher values and the Stokes' shift becomes smaller for both polymers. Taking the exciton travelling mechanism to the longest available conjugated segment o into account, the distribution of the conjugation length not only shift but most likely becomes also

much narrower, similarly to the FHWM of the σ-σ* peak in excitation spectra in Figure 36. These shifts are accompanied by a change of the ratio of the PL intensity between two main excitations bands (peaks). Considering the excitation peak at 275 nm associated mostly with the phenyl side groups localization, in other words π-σ* absorption remaining relatively unchanged, it can be concluded that the intensity of the σ-σ* transition band strongly increases with the film thickness, hence the concentration of longer conjugated polymer segments with perfect conformation increases extremely with the thickness as well and the amount of non-radiative recombination events decreases complementary. Saturation can be observed in all these dependencies at the film thickness above 500 nm. Films thicker than 500 nm have constant emission and excitation maxima and very small Stokes' shift about 5 nm.

To summarize, the structural ordering in thin PSis films has two stable regions and a transition or threshold region in dependence on the film thickness. Films that are thinner than 80 nm resemble the polymer in solution to some extent. Films which are thicker than 500 nm show marks of well-developed structure with high share of linear polymer segments in ideal conformation maximizing thus the σ-conjugation length of the segments. The range between 80 and 500 nm shows transitive behavior with strong dependency of the micro-structure on the thickness.

7.2 UV degradability of PSis

The photodegradation of polysilanes by the UV radiation decreases the intensity of the exciton PL band. The time dependence of PL decay is in accord with the idea of the scission of longer Si-Si segments [80]. However, there is a discrepancy between thin and thick films in the photodegradation process. The fundamental PL studies were measured on thin films (thickness about 10 nanometers) and the degradation studies were carried out on thick films (1 and more μm) and the self-recovering effects were observed on thin [94], [95] films in a vacuum and thick films [90] as well, even under oxidative atmosphere without the issue of thickness being discussed at all. On the other hand, the rarely observed phenomena of PL decay retardation in thick films were explained by photo- and prephotobleaching mechanisms, suggesting that the scission of Si-Si bonds is slowed down by the

thermal consumption of the absorbed energy by Si-Si segments in thick films and, moreover, a sponge-like structure of degraded material with a diminished absorption of UV light arises, formed with the degradation beam penetration, and the front of such zone propagates through the thickness of the material until reaching the substrate, thus making the degradation of PSis virtually slower [96], [97], [100].

Degradation curves for both PMPSi and P[DMSi-MPSi] are shown in the Figure 37 and 38, respectively. As degradation agent, the excitation beam (wavelength 330 nm) was employed directly. Graphs show degradation process for films with different thickness. The exponential decay of PL intensity in case of thin films (thickness about 100 nm) during first 200 s of irradiation of thin films is faster for thin films made from PMPSi. The rest of degradation (second part, after 200 s) proceed similarly for both types of material. In all cases, the degradation process ends in total damage of the thin layer for both used polysilanes.

Another degradation pattern was observed for thick films (more than 500 nm). In case of PMPSi, slower degradation compared to thin films occurs. This can be caused by the metastability mechanism, which is competitive to degradation, similarly as in case of laser degradation studies reported earlier [34], [39].
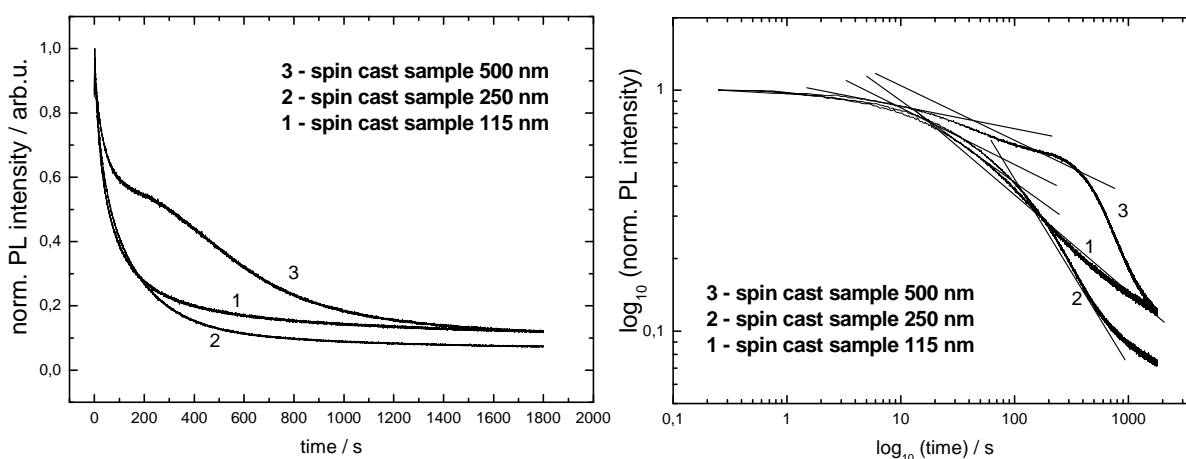

Figure 37 PL decay of PMPSi; excitation wavelength 330 nm, emission at 360 nm.
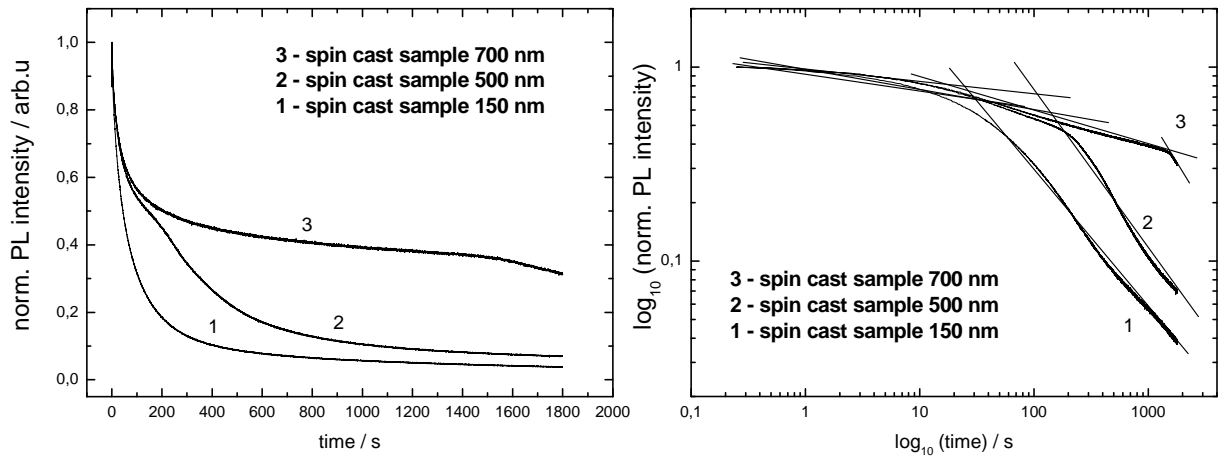
Figure 38 PL decay of P[DMSi-MPSi]; excitation wavelength 330 nm, emission at 360 nm.
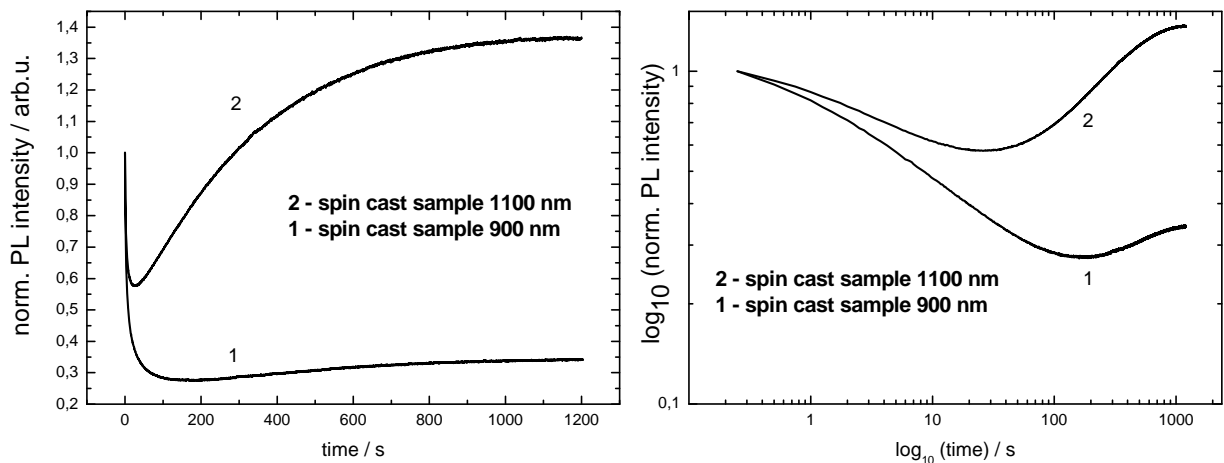

Figure 39 PL decay of P[DMSi-MPSi]: self-recovering and metastability; excitation wavelength 330 nm, emission at 360 nm.

However, these mechanisms are not able to overwhelm the deterioration process under used condition and resulted just in slowdown of the decay. Thick PMPSi film cast from toluene solution undergoes slow degradation and exhibit a reasonable slowdown at 60 % at about 200 s followed by second decay above 300 s, although even here, self-healing and PL enhancement during degradation was not observed. Much stronger effect was observed for copolymer P[DMSi-MPSi] (see Fig. 39, curves 1 and 2). The degradation process is more complicated. After certain time (20 s – 1100 nm and 200 s – 900 nm) a break point is observed and PL intensity rises again, thus the degradation curve has a broad minimum. Similar curve shape as in Fig. 39 curve 1 was observed in previous work where PMPSi was excited by a laser beam at 266 nm [34], [39]. The return starts at 55 % of initial PL intensity for 1100 nm thick

sample and at 25 % for 900 nm thick sample. Moreover, for the thicker sample (1100 nm), the saturation even exceeds the initial PL intensity.

Table 2 shows slopes of linear fits plotted into PL decay curves in log-log scale for films, where the self-healing and PL recovering were not observed on. It is obvious that PL decay is in the first part (till 200 s) the slowest for the thickest films.

Table 2 Slopes and intersects of linear fits in PL decay curves of polysilanes in log-log scale.

PMPSi				P[DMSi-MPSi]			
Thickness / nm		Slope	Intersect	Thickness / nm		Slope	Intersect
500	A	**-0,13**	0,05	700	A	**-0,06**	-0,01
	B	-0,73	1,46		B	-0,16	-0,07
					C	-0,73	1,89
250	A	**-0,34**	0,31	500	A	**-0,16**	0,07
	B	-0,59	0,75		B	-0,9	1,74
115	A	**-0,37**	0,33	150	A	**-0,16**	0,04
	B	-0,38	0,3		B	-0,71	0,88

Generally, the degradation shows different behavior with increasing thickness of the film and it is slower for thicker films. Moreover, in case of copolymer, the increased thickness results not only in retardation of degradation but also to recovery having breakpoint on degradation curves. Observed patterns resemble more annealing than degradation as PL intensity is recovered to 100 % or even improved up to nearly 140 % of its initial value in case of thickness 1100 nm. As well as in the spectroscopic study, the degradation correlates with film thickness and, as possible explanation, the threshold ordering in polymer phase with better conformational structure of polymer chains is suggested. Better alignment of chains would lead to lower free volume in polymer phase which supports weak bond creation and their relaxation into regular bonds. In next, denser polymer packing reinforces the cage effect of surrounding chains hindering movements of chain ends with free radicals after eventual scission, thus inducing their recombination in oxygen free environment. This could be also the underlying mechanism of PL increase over the initial value, as the structure might be even improved via scission

and recombination of chains in more energetically favorable conformations thus improving the delocalization length of PSi's segments.

a)   b)
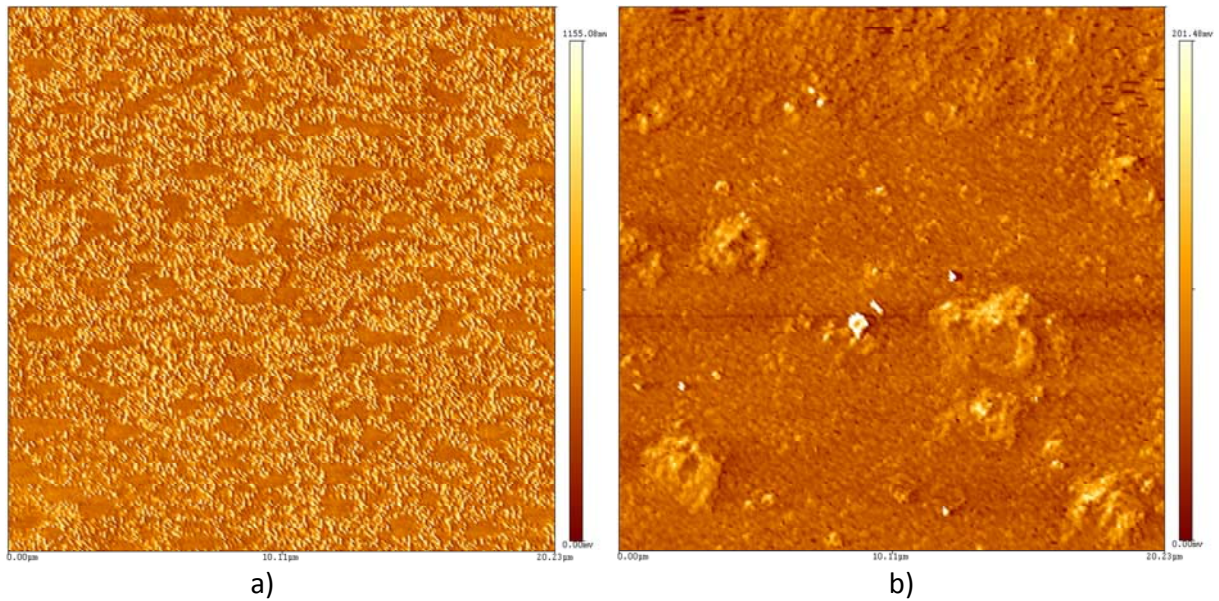
Figure 40 Topography of P[DMSi-MPSi] thin a) and thick b) films in lateral force mode scanned by AFM.

The different conformations and different chain packing in thin and thick films can be supported by AFM lateral mode investigation. Figure 40 shows that in case of thin film the topography and lateral scan differ significantly in comparison with thick films (Figure 40 b). The AFM method in lateral scope mode is a suitable instrument for structure determination [63], [64], [101] - [104], and the obtained results confirm our conclusion that the structure influencing optoelectronic properties in thin and thick films is significantly different.

8. Thin composite films and hybrid structures

The preparation of polymer-inorganic composite has been increasingly studied due to the novel synergy effects as well as enhanced optical and electronic properties in comparison with their purely polymer counterparts [105]. It was demonstrated that the power conversion efficiency of organic solar cell can be improved by addition of ZnO into the active layer [106], [107]. Similarly in OLEDs, it was not only higher power conversion but also more homogenous lighting with higher intensity of light emitting devices what was achieved [108]. As can be seen in the Figure 41, the addition of ZnO nanoparticles into the MEH-PPV matrix causes the PL arising of ZnO under low-energy excitation source in our samples. These phenomena were observed just in case the layers were deposited onto the QG/ITO substrates. This suggests that the contact of composite with an electrode material (ITO) allows the extended recombination of holes and electrons and the emissive recombination is more probable.
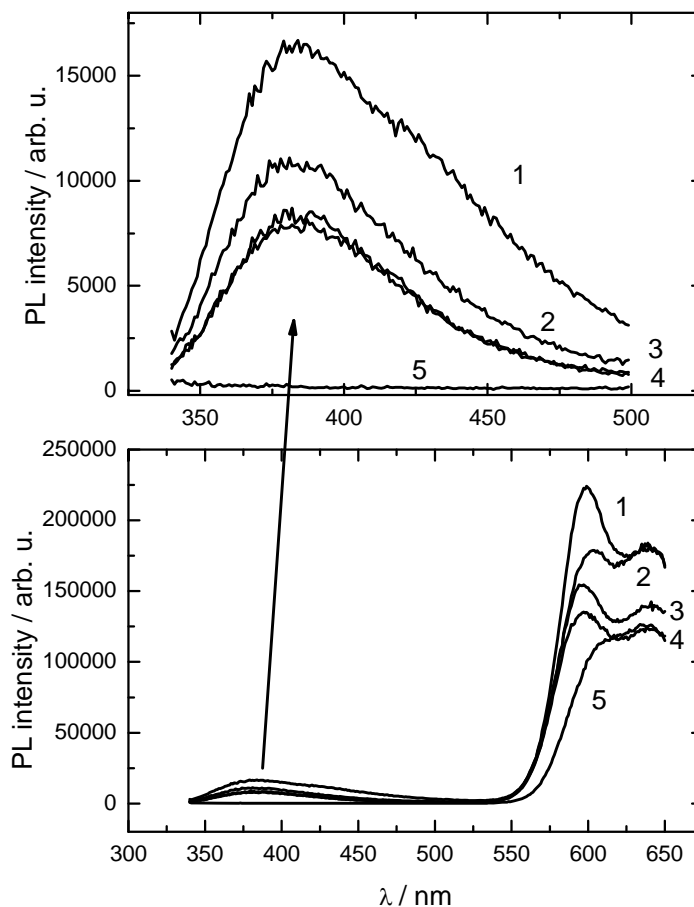

Figure 41 Effect of ZnO nanoparticles on the optoelectrical properties in MEH-PPV/ZnO composite. Different content of ZnO (NP) in the composite: 1 – 40 %, 2 – 30 %, 3 – 20 %, 4 – 10 %, 5 – neat MEH-PPV.

These facts were considered in our work on the materials covered by the Patent Nr. 304387, see Appendix I, where the patent and utility model related are both introduced to this work. The presence of ZnO nanoparticles in MEH-PPV polymer matrix enhances transport of electrons to recombination centers on polymer chains due to n-type semiconductivity and thus, the higher efficiency of EL lighting is achieved. Comparison of neat MEH-PPV device and the device with composite emissive layer is in the Figure 42.
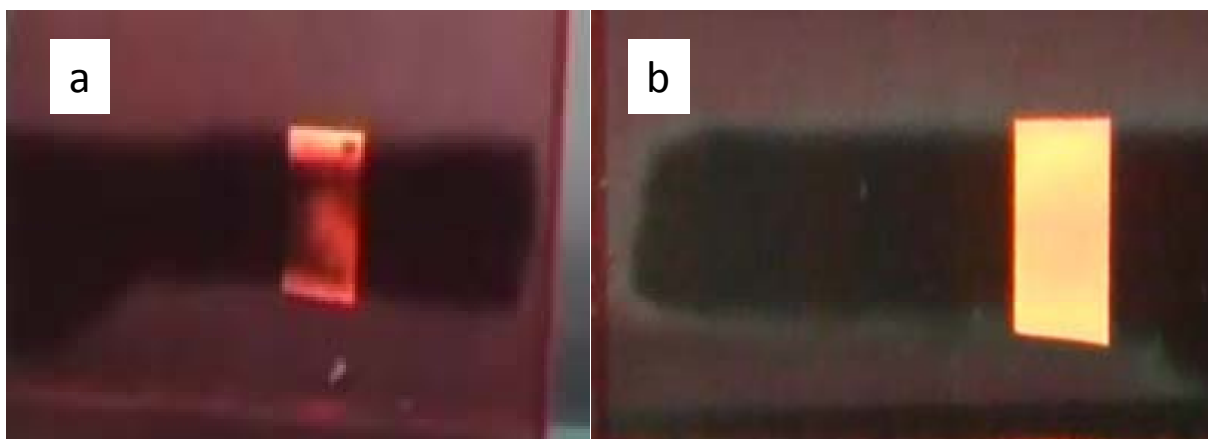

Figure 42 OLED devices with emissive layer deposited from a) neat MEH-PPV, b) composite MEH-PPV/ZnO.

Figure 43 shows EL spectra recorded for OLEDs prepared from neat MEH-PPV and from composite material, the same samples were measures as in the above figure.
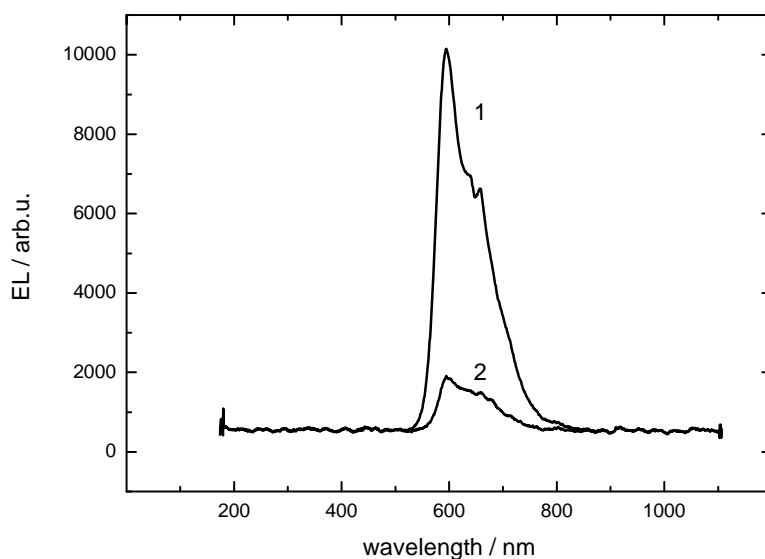

Figure 43 Comparison of EL of OLED devices prepared from 1 – composite MEH-PPV/ZnO, 2 – neat MEH-PPV.

The impact of hybrid structure, i.e. polymer matrix and nanoparticles, on the performance of the material was demonstrated in the field of photovoltaic as well.

The paper, introduced in Appendix II, demonstrates an application of photovoltaic effect in the research of nanomaterials and hybrid structures of polymers with nanoparticles. Photovoltage measurement was utilized for estimating the size of CdS and ZnO nanoparticles and diagnostics of hybrid structures with MEH-PPV, namely nano-CdS/MEH-PPV and nano-ZnO/MEH-PPV. Nano-CdS/MEH-PPV and nano-ZnO/MeH-PPV hybrid structures were prepared, and influence of the particles on charge transport was shown by the PV spectra measurements.

9. Conclusions of thesis

Conclusion of Chapter 6

Throughout this Chapter, it was argued that the microstructure of the thin conjugated polymer film may vary with the film thickness in a non-trivial way and that it is allied to different levels of manifestation of non-localized (aggregate states) and localized (intrachain) transitions. The competitive interplay between these two modes due to electronic-vibrational coupling is governed by the development of intrachain ordering and by the ordering level of π-stacking of polymer chains of MEH-PPV. It have been shown that the microstructure changes from the dominant chain conformations promoting intrachain interaction in thin films of tens nm up to the structure with increased ordering of nanocrystalline domains and prevailing chain stacking which is manifested by higher degree of interchain interaction in the films with thickness of hundreds nm. Moreover, a thickness threshold in all investigated aspects of the films at the thickness about 150 nm was observed. PL emission changes suddenly its character from prevailing intrachain interaction to the behavior promoted by π-stacking as proven by the study of the vibronic structure of the emission peak. The steep increase of the level of interchain interaction above the threshold enhances strongly the exciton diffusion length which must have a direct effect on the performance of any electronic device based on MEH-PPV due to its straightforward relation to the charge carrier mobility.

Conclusion of Chapter 7

In this Chapter, it was proved that significantly better alignment of σ-conjugated chains can be found in the thicker films than in the thin films. The characteristic feature for thick films is the extremely extended conjugation of PSis segments. The dependence of microstructure on thickness was shown as typical for thin films made from both PSi polymer materials and correlates with the material properties as well as with the susceptibility to UV degradation. For the thinnest films with thickness below 80 nm, a simple double-exponential decay is observed. With the increasing thickness over 80 nm, the exponential decay of PL displays a substantial slowdown above the thickness of 500 nm. Moreover, in case of 1 μm thick film made from the copolymer, the PL decay exhibits a minimum at 25 % of the initial

PL intensity followed by a PL enhancement until the saturation is reached at about 35 %. Such behavior was demonstrated to emerge on mesoscale and be not present in nanoscale thin films for the first time. The observed PL shifts unambiguously testify to the presence of a well aligned structure of polymer chains which can explain the stabilization and promotion of the self-healing of the material by the recovery of WBs even during the action of the degradation agent.

Conclusion of Chapter 8

In case of π-conjugated polymer, the mixtures of MEH-PPV with ZnO or CdS nanoparticles were prepared and studied. The purpose of such composite preparation was to balance the share of different charge carriers on electrical conductivity by enhancement of the mobility of electrons in the active layer with the aim to enhance the conversion efficiency in solar cells. On the other hand, the composite material from MEH-PPV and ZnO nanoparticles was prepared with the purpose to improve the light emissive characteristics of polymer/inorganic hybrid OLEDs. The highest achievable electroluminescence as well as the appearance of the emitting device was successfully improved using the new composite composition. The importance of demonstrated results is reflected in the fact, that these findings can have direct impact to practical applications in photovoltaic and in polymer electronic devices and the protection of the composition of the active layer was awarded by a patent.

General remarks

The optoelectronic properties of both σ- and π-conjugated polymers were investigated and the influence of thickness on the chains packing and structural ordering and thus the impact on the behavior of these kinds of material was observed, discussed and in detail described. In accord with the very first emerging publications of other research groups, it appears that this thickness threshold of structural ordering can be a general principle between nano- and microscale in polymer films. Moreover, experiments where the proofs of final applications were prepared and tested (i.e. polymer OLED, photovoltaic system) were carried out and resulted into the obtaining of one Patent and Utility model for inks for printed electronics (see Appendix I).

10. Suggestions for future research – polymer electronic

Achieved results and experience can help extend the use of σ- and π-conjugated polymer into the real application. Concretely, the thickness depending structural ordering of polymer chain in thin films can result into the possible application in polymer photovoltaic devices or polymer OLEDs, where the main problem is the conversion efficiency and material degradability. Experiences achieved during this study can help overcome these problems.

Based on the knowledge gathered in this dissertation, future research should be considered in four main directions.

First promising research route is expected to be the basic research oriented on the general study of structural ordering and chain conformation and packing development in thin films. It is suggested that the ordering of polymer chains between nano- and microscale is a more general phenomenon yet demonstrated on two types of polymer up to now. For this research the PL spectroscopy appears as a suitable method although it must include anisotropy measurements in future. Other appropriate method for thin films structure determination is low angle XRD analysis.

The second direction considers the prospective of material printing. From the technological point of view of sample preparation, the work should continue by studies on thin films deposited by any printing method, which is one of the last steps before mass production. Inkjet printing seems to be very proper method due to possibility of digital patterning and very easy processing.

The third direction has to be focused on the improving of material properties, which means optical and optoelectrical properties, stability, conductivity or transparency, whereas the original properties are preserved. Thus, the work has to be targeted on the preparation of composite material from σ- and π-conjugated polymers as a matrix and nanoparticles filler (ZnO, CdS, ZnS and other) because the synergy effect of nanoparticles and polymer is well known and the technology is mastered in our laboratory too.

The last, fourth course, derived from the basic research, has to be the preparation of the final application and devices, where the experiences from fundamental research work will be applied. Preparation of photovoltaic systems, large area light

sources, flexible and transparent display, flexible polymer sensors, all of the mentioned products seems to be possible.

The three applied directions shall be performed in cooperation with any private organization, which will push forward these experiences to applications on the real market with any product. For instance, the market with printed electronic is huge with estimated potential of 30 billion of USD.

List of symbols and acronyms

Ordered according to occurrence in text.

EL	Electroluminescence
OLED	Organic light emitting device
β_{gem}; β_{vic}	Resonance integrals – geminal, vicinal
HOMO	Highest occupied molecular orbital
LUMO	Lowest unoccupied molecular orbital
E_g	Energy of band gap (eV)
E_V	Energy of valence band
E_C	Energy of conductive band
E_F	Energy of Fermi level
1-D	One-dimensional
S^0	Neutral Soliton
S^-	Negative Soliton
S^+	Positive Soliton
P^-	Negative Polaron
P^+	Positive Polaron
BP^{--}	Negative Bipolaron
BP^{++}	Positive Bipolaron
tPA	*Trans*-polyacetylene
MEH-PPV	Poly[2-methoxy-5-(2-ethylhexyloxy)-1,4-phenylenevinylene]
PL	Photoluminescence
PSis	Polysilanes
PMPSi	Poly(methyl-phenyl)silane
P[DMSi-MPSi]	Co-polymer poly(dimethylsilane-methylphenylsilane)
UV/VIS	Ultraviolet and visible
λ	Wavelength (with scale in nanometers - nm)
ZnO	Zinc oxide
CdS	Cadmium sulfide
PPE-PPV	Poly[(p-phenylene-ethylene)-alt-(p-phenylene-vinylene)
WB	Weak bond
DOD	Drop-on-demand (kind of ink-jet print-head system)
I	Intensity
α	Absorption coefficient

A	Absorbance
S_0, S_1	Energy electronic states (ground, excited respectively)
SPV	Surface photovoltage
SCR	Space charge region
d	Bulk thickness
L	Exciton diffusion length
$\Delta n(x)$	Excess excitons concentration at depth x in the bulk
D	Exciton diffusion coefficient
g(x)	Photogeneration rate at depth x
I_0	Photon flux density
h	Total thickness of the layer
R_1, R_2	Reflectance
d	Thickness of the bulk
s	Surface recombination velocity
w	Thickness of the SCR
J	Current density
G	Factor representing recombination losses
V	Photovoltage
AFM	Atomic force microscopy
3-D	Three dimensional
(FT)-IR	(Fourier-transformed) infrared spectroscopy
DB	Dichlorobenzene
QG	Quartz glass
ITO	Indium-tin oxide
0-0	Peak related to transition between 0th vibronic excited state and 0th vibronic ground state
0-1	Peak related to transition between 0th vibronic excited state and 1st vibronic ground state
0-2	Peak related to transition between 0th vibronic excited state and 2nd vibronic ground state

List of Figures

List of Tables

References

[1] SKOTHEIM T. A.; Conjugated polymers: theory synthesis, properties and characterisation. 2007. Third edition. ISBN 978-1-4200-4358-7.

[2] ITO T., SHIRAKAWA H., IKEDA S.; Journal of Polymer Science Polymer Chemistry Edition 1974.

[3] CHIANG C. K. et al.; Physical Review Letters, 1977. 39. 1098.

[4] J.H.BURROUGHES, D.D.C. BRADLEY, A.R. BROWN, R.N. MARKS, K. MACKAY, R. H. FRIEND, P. L. BURNS, AND A.B. HOLMES, Nature, 347, 539 (1990).

[5] CACIALLI F.; Organic semiconductors for the new millenium. Philosophical Transactions of the Royal Society of London Series a-Mathematical Physical and Engeneering Sciences, 2000. 358 (1765) p173-192.

[6] SALANECK W.R.; Conjugated polymer and molecular interfaces: science and technology for photonic and optoelectronic applications. 2002, New York: Marcel Dekker. Xvi.

[7] KAFAFI Z.; Organic electroluminescence. Taylor and Francis 2005. ISBN 0-8247-5906-0.

[8] YANG Y. et al.; Electronic and Optical Properties of Conjugated Molecular Systems in Condensed Phases, 2003: 307-354, ISBN: 81-7736-083-3 Editor: Shu Hotta.

[9] NEŠPŮREK S.; Thin polysilylene films. Their electronic and photoelectrical propeerties. Materials Science and Engineering C 8-9 (1999) 319 - 327.

[10] POPE E., SWENBERG CH. E.; Electronic Processes in Organic Crystals and Polymers, Second Edition, Oxford University Press 1999, ISBN 0-19-512963-6.

[11] PEIERLS R.E.; Quantum theory of solids. International series of monographs on physics. 1964, Oxford. viii, p. 229.

[12] MIRZOV O., SCHEBLYKIN I.G.; Photoluminescence spectra of a conjugated polymer: from films and solution to single molecules. Physical Chemistry Chemical Physics. 2006, 8, 5569-5576.

[13] FAHLMAN M.; Experimental and Theoretical Studies of Organic Molecules for Electronic Devices. ISBN 91-7871-625-X.

[14] RICE M.J.; Phys. Lett., A71 (1979) 152.

[15] SU W.P., SCHRIEFFER J.R.; Proc. Natl. Acad. Sci. USA, 77 (1980) 5626.

[16] FESSER K., BISHOP A.R., CAMPBELL D.K.; Phys. Rev. B, 27 (1983) 4804.

[17] IUCCI G., XING K., LÖGDLUND M., FAHLMAN M., SALANECK W.R.; Chem. Phys. Lett., 244, (1995) 139.

[18] CHIANG, C.K., C.R. FINCHER, Y.W. PARK, A.J. HEEGER, H. SHIRAKAWA, E.J. LOUIS, S.C. GAU, AND A.G. MACDIARMID. 1977. Phys Rev Lett 39:1098.

[19] KAISER, A.B. 2001. Rep Prog Phys 64:1.

[20] EPSTEIN, A.J., H. ROMMELMAN, R. BIGELOW, H.W. GIBSON, D.M. HOFFMANN, AND D.B. TANNER. 1983. Phys Rev Lett 50:1866.

[21] BURROUGHES, J., D. BRADLEY, A. BROWN, R. MARKS, K. MACKAY, R. FRIEND, P.L. BURNS, AND A. HOLMES. 1990. Nature 347:539.

[22] SARICIFTCI, N.S., L. SMILOWITZ, A.J. HEEGER, AND F. WUDL. 1992. Science 258:1474.

[23] ONG, B.S., Y. WU, AND P. LIU. 2005. Proc IEEE 93:1412.

[24] PASVEER, W.F., J. COTTAAR, C. TANASES, R. COEHOORN, P.A. BOBBERT, P.W.M. BLOM, D.M. DE LEEUW, AND M.A.J. MICHELS. 2005. Phys Rev Lett 94:206601.

[25] WANG P., COLLISON C.J., ROTHBERG L.J.; J Photochem Photobiol A Chem 2001, 144:63.

[26] QUAN S. et al.; Solvent and concentration effects on fluorescence emission in MEH-PPV solution. European Polymer Journal 42 (2006) 228-233.

[27]   GETACHEW A. et al.; Mobility and photovoltaic performance studies on polymer blends: effects of side chains volume fraction. Journal of Material Chemistry. 2011. 21, 2594-2600.

[28]   JONES R. G.; Silicon-Containing Polymers; Michl, West, Chapter 18. ISBN 978-0-412-83110-2.

[29]   NEŠPŮREK S.; POLYSILANES - ADVANCED MATERIALS FOR OPTOELECTRONICS. Journal of Optoelectronics and Advanced Materials, Vol. 7, Nr. 1, 2005, 223-230.

[30]   KIPPING F.S.; Journal of the Chemical Society, 1921. 119 p. 830.

[31]   KIPPING F.S.; Journal of the Chemical Society, 1922. 125 p. 2291.

[32]   KASHIMURA, S.; Electroreductive Synthesis of Polysilanes, Polygermanes and Related Polymers with Magnesium Electrodes; J. Org. Chem. 1999, 64, 6615-6621.

[33]   NEŠPŮREK S.; From one dimensional organosilicon strucutures to polymeric semiconductors: optical and electrical properties. Journal of non-crystalline solids. 299-302 (2002) 1033-1041.

[34]   SCHAUER F et al; J. Phys.: Condens. Matter 19 (2007) 076101.

[35]   NEŠPŮREK; Visible Photluminescence in Polysilanes; Monatshefte für chemie 132. 159-168 (2001).

[36]   NEŠPŮREK S. et al; Charge carrier transport on molecular wire controlled by dipolar species: towards light-driven molecular switch. Thin solid films, 2003. 438 p. 268-278.

[37]   KURITKA I et al; UV degradability of polysilanes for nanoresists examined by electron spectroscopies and photoluminescence Czechoslovak Journal of Physics, Vol. 56 (2006), No. 1.

[38]   A MESZÁROŠ O., SCHMIDT P., POSPÍŠIL J., NEŠPŮREK S.; Phototriggered Atmospheric Degradation of Poly[methyl(phenyl)silandiyl] in the Presence of

Ultraviolet Absorbers; Journal of Polymer Science; Vol. 42; p. 714 – 721; 2004.

[39] SCHAUER, F.; KURITKA, I.; NESPUREK, S. UV degradability of aryl-substituted polysilylenes. Polymer Degradation and Stability, 2004. Vol. 84, č. 3, s. 383-391. ISSN 0141-3910.

[40] SCHAUER, F.; KURITKA, I.; SÁHA, P.; NESPUREK, S.; LIPSON, S.; UV created weak and dangling bonds in aryl-substituted polysilanes, Journal of Non-Crystalline Solids 352 (2006) 1679-1682.

[41] PIVRIKAS A., SARICIFTCI N. S., JUSKA G., OSTERBACKA R.; Progr. Photovolt.: Res. Appl., 2007, 15, 677.

[42] ANTONIADUS H.; Appl. Phys. Lett. 65, 2030 (1994).

[43] THANACHAYANONT C.; MEH-PPV/CdS Nanorod Polymer Solar Cells. Journal of the Korean Physical Society, Vol. 52, No. 5, May 2008.

[44] ÖZGÜR Ü.; A comprehensive review of ZnO materials and devices. J. Appl. Phys., 98 (2005), pp. 041103-041301.

[45] DA-WEI W.; The improvement of near-ultraviolet electroluminescence of ZnO nanorods/MEH-PPV heterostructure by using a ZnS buffer layer. Volume 12, Issue 1, January 2011, Pages 92-97.

[46] NORRMAN K.; Studies of spin-coated polymer films. Annu. Rep. Prog. Chem., Sect. C, 2005, 101, 174-201.

[47] WALKER P. H. AND THOMPSON J. G.; Proc. Am. Soc. Test. Mater. (Part 2), 1922, 22, 464.

[48] XU T., KIM H.-C., DEROUCHEY J., SENEY C., LEVESQUE C., MARTIN P., STAFFORD C. M. AND RUSSEL T. P., Polymer, 2001, 42, 9091.

[49] DE GANS B.J.; Inkjet printing of polymers: state of the art and future developments. Adv. Mater. 16(3): 203-213.

[50] MAGDASSI S.; The chemistry of Inkjet Inks. ISBN 978-981-281-821-8.

[51] TRACTON A.A.; Coatings Technology: Fundamentals, Testing, And Processing Techniques. ISBN 1-4200-4406-0.

[52] LAMBERT J.B. ET AL.; Organic Structural Spectroscopy, Prentice-Hall, Inc. 1998, ISBN 0-13-258690-8.

[53] LAKOWICZ J.R.; Principles of Fluorescence Spectroscopy, Third edition, Springer 2006, ISBN 978-0-387-31278-1.

[54] GOODMAN A.M., J. Appl. Phys. 32 (1961) 2550.

[55] TOUSEK J., TOUSKOVA J., KRIVKA I., PAVLACKOVA P., VYPRACHTICKY D., CIMROVA V.; Organic Electronics 2010;11(1):50-56.

[56] TOUSEK J., TOUSKOVA J.; Solar Energy Materials and Solar Cells 2008;92(9):1020-1024.

[57] TOUSEK J., TOUSKOVA J., REMES Z., KOUSAL J., GEVORGYAN S.A., KREBS F.C.; Synthetic Metals 2012;161(23-24):2727-2731.

[58] TOUSEK J., TOUSKOVA J., REMES Z., CERMAK J., KOUSAL J., KINDL D., KURITKA I.; Chemical Physics Letters 2012;552:49-52.

[59] BINNING G., QUATE C.F., GERBER C.; Atomic force microscope, Phys. Rev. Lett., 1986, 56(9): 930.

[60] SARID D.; Scanning Force Microscopy, Revised ed., 1994, New York: Oxford University Press, ISBN 0-19-509204-X.

[61] HAUGSTAD G.; Atomic Force Microscopy, Wiley, 2012, ISBN 978-0-470-63882-8.

[62] OVERNEY R.M. ET AL.; Friction measurements on phase-separated thin films with a modified atomic force microscope, Nature, 1992, 359, 133-135.

[63] HAUGSTAD G., HAMMERSCHMIDT J.A., GLADFELTER W.L.; Viscoelasticity in nanoscale friction on thin polymer films, in Interfacial Properties on the Submicrometer Scale. ISBN 978-0-8412-3691-2.

[64] TSUKRUK V.V., WAHL K.J.; Microstructure and Microtribology of Polymer Surfaces, ACS Symposium Series, Vol. 741, 2000.

[65] SILS S., OVERNEY R.M, Creeping friction dynamics and molecular dissipation mechanism in glassy polymers. Phys. Rev. Lett. 2003, 91(9): 1-4.

[66] NAKANASHI K.D., SOLOMON P.H.; Infrared absorption spectroscopy. 2d ed. San Francisco: Holden-Day. ISBN 978-1892803009.

[67] COURARD L., NELIS M.; Magazine of Concrete Research, 2003, 55 No. 4, 355-366.

[68] PEREZ F., BISSONNETTE B., COURARD L.; Magazine of Concrete Research, 2009, 61, No. 6. 389 – 400.

[69] NGUYEN T.Q., DOAN V., SCHWARTZ B.J.; J. Chem. Phys. 1999, 110:4068-78.

[70] QUAN S.Y., TENG F., XU Z., QIAN L., HOU Y.B., WANG Y.S. AND XU X.R.; European Polymer Journal 2006;42(1):228-233.

[71] SUN S.S. AND SARICIFTCI N.S., Organic Photovoltaics: Mechanisms, Materials, and Devices, Taylor & Francis Group 2005, USA, ISBN 978-0-8247-5963-6.

[72] SCHWARTZ B.J., Annual Review of Physical Chemistry 2003; 54:141-172.

[73] JENG U., HSU C.H., SHEU H.S., LEE H.Y., INIGO A.R., CHIU H.C., FANN W.S., CHEN S.H., SU A.C., LIN T.L., PENG K.Y., AND CHEN S.A.; Macromolecules 2005;38(15):6566-6574.

[74] LEE Y.J., KIM D.Y. AND BARBARA P.F.; Journal of Physical Chemistry B 2006;110(20):9739-9742.

[75] YANG C.Y., HIDE F., DIAZ-GARCIA M.A., HEEGER A.J. AND CAO Y.; Polymer 1998;39(11):2299-2304.

[76] SCHWARTZ B.J., HIDE F., ANDERSSON M.R. AND HEEGER A.J.; Chemical Physics Letters 1997;265(3-5):327-333.

[77] ROTHBERG L.J., YAN M., PAPADIMITRAKOPOULOS F., GALVIN M.E., KWOCK E.W. AND MILLER T.M.; Synthetic Metals 1996;80(1):41-58.

78

[78] DENTON G.J., TESSLER N., STEVENS M.A. AND FRIEND R.H.; Synthetic Metals 1999;102(1-3):1008-1009.

[79] MCBRANCH D.W., KRAABEL B., XU S., KOHLMAN R.S., KLIMOV V.I., BRADLEY D.D.C., HSIEH B.R. AND RUBNER M.; Synthetic Metals 1999;101(1-3):291-294.

[80] SCHAUER F., NESPUREK S., HORVATH P., ZEMEK J. AND FIDLER V.; Synthetic Metals 2000;109(1-3):321-325.

[81] YAMAGATA H., HESTAND N.J., SPANO F.C., KOEHLER A., SCHARSICH C., HOFFMANN S.T. AND BAESSLER H.; Journal of Chemical Physics 2013;139(11).

[82] HU D.H., YU J. AND BARBARA P.F.; Journal of the American Chemical Society 1999;121(29):6936-6937.

[83] HU D.H., YU J., WONG K., BAGCHI B., ROSSKY P.J. AND BARBARA P.F.; Nature 2000;405(6790):1030-1033.

[84] HUSER T., YAN M. AND ROTHBERG L.J.; Proceedings of the National Academy of Sciences of the United States of America 2000;97(21):11187-11191.

[85] HUSER T. AND YAN M.; Journal of Photochemistry and Photobiology a-Chemistry 2001;144(1):43-51.

[86] PEUMANS P., YAKIMOV A. AND FORREST S.R.; Journal of Applied Physics 2003; 93:3693.

[87] THEANDER M., YARTSEV A., ZIGMANTAS D., SUNDSTROM V., MAMMO W., ANDERSSON M.R., AND INGANAS O.; Physical Review B 2000;61(19):12957-12963.

[88] GOH C., SCULLY S.R. AND MCGEHEE M.D.; Journal of Applied Physics 2007;101(11).

[89] SHAW P.E., RUSECKAS A. AND SAMUEL I.D.W.; Advanced Materials 2008;20(18):3516.

[90] SCHAUER, F.; KURITKA, I.; SAHA, P.; NESPUREK, S. Journal of Physics-Condensed Matter 2007, 19 (7), 11.

[91]   ITO O., TERAZIMA M., AZUMI T., MATSUMOTO. N., TAKEDA K., FUJINO M.; Macromolecules 1989, 22 (4), 1718-1722.

[92]   SCHAUER F., SCHAUER P., KURITKA I., BAO H.; Materials Transactions 2010, 51 (2), 197-201.

[93]   ECKERTOVÁ L.; Physics of Thin Films, 2nd Edition, 1986, SNTL Prague, ISBN 0-306-41798-7.

[94]   KURITKA I., SCHAUER F., SAHA P., ZEMEK J., JIRICEK P., NESPUREK S.; Czechoslovak Journal of Physics 2006, 56 (1), 41-50.

[95]   HANDLIR R., SCHAUER F., NESPUREK S., KURITKA I., WEITER M., SCHAUER P.; Journal of Non-Crystalline Solids 1998, 227, 669-672.

[96]   NAKAYAMA Y., INAGI H., ZHANG M.; Journal of Applied Physics 1999, 86 (2), 768-773.

[97]   HAYASHI H., KURANDO T., OKA E., DOHMARU T., NAKAYAM Y.; Japanese Journal of Applied Physics Part 1-Regular Papers Short Notes & Review Papers 1996, 35 (7), 4096-4100.

[98]   FUJIKI M.; STRUCTURAL DEFECTS IN POLY(METHYLPHENYLSILYLENE); Chemical Physics Letters, 1992, 198.

[99]   PELIKAN P., KOSUTH M., BISKUPIC S., NOGA J., STRAKA M., ZAJAC A., BANACKY P.; Electron structure of polysilanes. Are these polymers one-dimensional systems?; Int. J. Quant. Chem., 84, 2, 2001.

[100] HAYASHI H., KURANDO T., NAKAYAM Y.; Japanese Journal of Applied Physics Part 1-Regular Papers Short Notes & Review Papers 1997, 36 (3A), 1250-1255.

[101] BURNHAM N. A., DOMINGUEZ D. D., MOWERY R. L., COLTON R. J.; Probing the surface forces of monolayer films with an atomic-force microscope; Phys. Rev. Lett. 64, 1931.

[102] LEE J., STEPANENKO V., YANG J., YOO H., SCHLOSSER F., BELLINGER D, ENGELS B., SCHEBLYKIN I.G., WUERTHNER F., KIM D.; Structure Property

Relationship of Perylene Bisimide Macrocycles Probed by Atomic Force Microscopy and Single-Molecule Fluorescence Spectroscopy, ACS Nano, Vol. 7, No. 6, 5064–5076, 2013.

[103] KNORR D.B. JR., WIDJAJA P., ACTON O., OVERNEY R.M.; Molecular friction dissipation and mode coupling in organic monolayers and polymer films, J. Chem. Phys. 134, 104502, 2011.

[104] REZEK B., ČERMÁK J., KROMKA A., LEDINSKÝ M., HUBÍK P., MAREŠ J., PURKRT A., CIMROVÁ V., FEJFAR A, KOČKA J.; Nanoscale Research Letters 2011, 6:238.

[105] YAHYA N.Z., RUSOP A.; Investigation on the Optical and SurfaceMorphology of Conjugated Polymer MEH-PPV:ZnO Nanocomposite Thin Films, Journal of Nanomaterials, 2012.

[106] MUSTAPHAA N., IBNAOUFA K.H., FEKKAIA Z., HENNACHEA A., PRASADB S., ALYAMANI A.; Improved efficiency of solar cells based on BEHP-co-MEH-PPV doped with ZnO nanoparticles; Optik, Vol. 124, Issue 22, November 2013.

[107] SCHARBER M.C., SARICIFTCI N.S.; Efficiency of bulk-heterojunction organic solar cells, Progress in Polymer Science, 38, 2013.

[108] RAMANA CH. V. V., MOODLEY M. K., KANNAN V.; Electrical Characteristics of ITO/MEH–PPV/ZnO/Al Structure, Nanoscience and Nanotechnology Letters, Volume 6, Number 3, March 2014, pp. 238-241(4).

Appendix I - Patents and Utility models

Patent Nr. 304387 Active layer for electroluminescence foils

PATENTOVÝ SPIS

(56) Relevantní dokumenty:
H.Benešová, J.Škorpil: Tandemové fotovoltaické články-jeden ze směrů výzkumu a vývoje v oblasti fotovoltaiky III.generace, Electroscope č.1, 2012.
KR 20110077524 A; 70567; 70569; 70570; 70571; 70572.

(73) Majitel patentu:
Univerzita Tomáše Bati ve Zlíně, Zlín, CZ
NWT a.s., Hulín, CZ

(72) Původce:
doc. Ing. et Ing. Ivo Kuřitka, Ph.D., Brno, CZ
Ing. Pavel Urbánek, Pitín, CZ
Ing. Petr Krčmář, Valašské Klobouky, CZ
Jakub Mráček, Holešov, CZ

(74) Zástupce:
Václav Müller, patentový zástupce, Filipova 2016,
148 00 Praha 4

(54) Název vynálezu:

Aktivní vrstva pro elektroluminiscenční fólie

(57) Anotace:
Aktivní vrstva pro elektroluminiscenční fólie sestává z
vodivého polymeru na bázi 2-methoxy- a 5-(2-
ethylhexyloxy)- substituovaného poly-1,4-
fenylenvinylenu v množství 85 až 90 % hmotn. a
anorganického plniva na bázi nanočástic oxidu
zinečnatého v množství 15 až 10 % hmotn. Vodivý
polymer má s výhodou molekulovou hmotnost Mn v
rozsahu 40 až 70 tis. a poměr Mw/Mn = 6. Anorganické
plnivo na bázi nanočástic ZnO má velikost částic s
výhodou menší než 50 nm.

CZ 304387 B6

Aktivní vrstva pro elektroluminiscenční fólie

<u>Oblast techniky</u>

Vynález se týká složení směsi pro aktivní vrstvu elektroluminiscenční fólie.

<u>Dosavadní stav techniky</u>

Průmyslové využití tenkých materiálových vrstev se v poslední době intenzivně rozrůstá. Tenké vrstvy se uplatňují v polymerní elektronice, organických světlo emitujících zařízeních, ale také ve flexibilních displejích.

Elektroluminiscenční fólie je založena na stejném principu jako světlo emitující zařízení (OLED), a je tedy složena z vrstev, které plní jednotlivé úlohy při přenosu elektrické energie do elektrického zdroje k aktivní vrstvě zařízení, na které dochází k rekombinaci nosičů opačného náboje doprovázené luminiscencí.

Základní vrstvu elektroluminiscenční fólie tvoří transparentní substrát, který je nosičem celého zařízení. Na substrátu je deponována kladná elektroda z transparentního vodivého materiálu. Na kladné transparentní elektrodě je nanesena vrstva z materiálu s děrovou vodivostí, která zajišťuje injekci děr do aktivní vrstvy. Z opačné strany k transparentnímu substrátu je na povrchu zařízení záporná elektroda a pod ní následuje vrstva z materiálu s elektronovou vodivostí pro injekci elektronů do aktivní vrstvy. Aktivní vrstva zařízení je deponována mezi vrstvou s děrovou vodivostí a vrstvou s elektronovou vodivostí, tedy uprostřed sledu vrstev. V aktivní vrstvě pak dochází k emisi světla na základě rekombinace doprovázené luminiscencí, tedy tzv. zářivé rekombinace nosičů opačných nábojů k ní dopravených, tj. děr a elektronů.

Aktivní vrstva u světlo emitujících diod bývá tvořena z několika druhů materiálů. Buď může být tato vrstva z anorganických fosforescenčních materiálů, nebo může být z vodivých elektroluminiscenčních polymerů. Oba druhy materiálů lze úspěšně použít, nicméně s jistými nevýhodami.

Jako anorganický fosforescentní materiál se pro aktivní vrstvu například často využívají anorganické polovodiče. U anorganických fosforescentů je problematická jejich depozice na nosnou vrstvu, především pak chemické napařování, které může vést k devastaci vrstvy, na kterou se anorganický fosforescent deponuje.

Jako vodivý polymer pro aktivní vrstvu se například často využívá materiál odvozený od poly-1,4-fenylenvinylenu (PPV). Použití vodivého polymeru jako materiálu pro aktivní vrstvu představuje technologicky méně náročné řešení, především z toho důvodu, že umožňuje místo problematického napařování pracovat s roztokem. Kromě toho je možno volit ze spektra kombinací různých rozpouštědel tak, aby vrstvy předchozí nebyly erodovány nově deponovanou vrstvou. Ovšem i u tohoto typu řešení existuje řada nevýhod. Problémy vznikají například při extrémně rychlém odpařování rozpouštědla z roztoku a související změně jeho koncentrace, která se pak odlišuje od požadované hodnoty. Dále může být na závadu nevhodná viskozita a hustota roztoku, která neumožní dosažení dostatečné tloušťky aktivní vrstvy.

Samotné anorganické fosforescenční materiály, stejně jako samotné polymerní luminiscenční materiály, mají vždy jeden charakteristický typ vodivosti – děrové nebo elektronové. To při jejich použití ve funkci aktivní vrstvy vede k nerovnováze mezi oběma způsoby vedení elektrického proudu aktivní vrstvou, a tedy i přebytek nosičů náboje jedné polarity na úkor nosičů náboje druhé polarity. Tato nerovnováha snižuje efektivitu zařízení, protože k účinné zářivé rekombinaci, která je vlastní podstatou funkce aktivní vrstvy, je zapotřebí vyrovnané nábojové bilance, tedy vždy jednoho kladného nosiče náboje (díry) a jednoho negativního nosiče náboje (elektronu).

Podstata vynálezu

Uvedené nevýhody a nedostatky dosud známých řešení aktivních vrstev OLED zařízení do značné míry odstraňuje aktivní vrstva pro elektroluminiscenční fólie podle vynálezu. Podstata vynálezu spočívá v tom, že aktivní vrstva sestává z vodivého polymeru na bázi 2–methoxy– a 5–(2–ethylhexyloxy)– substituovaného poly–1,4–fenylenvinylenu v množství 85 až 90 % hmotn. a anorganického plniva na bázi nanočástic oxidu zinečnatého v množství 15 až 10 % hmotn.

Výhodou aktivní vrstvy pro elektroluminiscenční fólie podle technického řešení je zejména skutečnost, že přídavek anorganické látky – nanočástic oxidu zinečnatého – ve vhodném rozsahu koncentrací způsobuje zlepšený přenos elektronů do aktivní vrstvy a zároveň blokaci děr tak, aby mohla být zvýšena jejich zářivá rekombinace přímo v aktivní vrstvě, jejíž matrice je tvořena vodivým polymerem, na bázi 2–methoxy– a 5–(2–ethylhexyloxy)– substituovaného poly–1,4– fenylenvinylenu. Nanočástice díky své velikosti, která je až 50 nm, také způsobují rozptyl emitovaného záření, což se na výsledném optickém vjemu při pozorování emitovaného světla projevuje dojmem zvláštní živosti a jasu barvy, a umožňuje to pozorovat emisi z velkého úhlového rozsahu.

Pro správnou funkci je výhodné, že vodivý polymer má molekulovou hmotnost Mn v rozsahu 40 až 70 tis. a poměru Mw/Mn = 6 a že anorganické plnivo na bázi nanočástic ZnO má velikost částic menší než 50 nm.

Přehled obrázků na výkresech

Charakteristiky aktivní vrstvy pro elektroluminiscenční fólie podle vynálezu jsou znázorněny na přiloženém výkrese, kde značí:

– obr. 1 – Voltampérová charakteristika diody, příklad 1

– obr. 2 – Voltampérová charakteristika diody, příklad 2

– obr. 3 – Spektrum světla emitovaného diodou, příklad 1

– obr. 4 – Spektrum světla emitovaného diodou, příklad 2

Příklady provedení vynálezu

Příklad 1

Aktivní vrstva ve světlo emitující diodě byla získána cestou disperze, která se připravila s využitím směsi rozpouštědel. Nejdříve se provedlo rozpuštění poly[2–methoxy–5–(2–ethylhexyloxy)–1,4–fenylenvinylenu] (MEH–PPV) ve směsi rozpouštědel. Dále se k dobře rozpuštěnému MEH–PPV přidala disperze nanočástic ZnO ve směsi rozpouštědel. Poměr ZnO ku MEH–PPV v této směsi činil 11,8 % hmotn. ku 88,2 % hmotn. Po smíchání roztoku polymeru s disperzí nanočástic a navazující homogenizaci byla směs pomocí metody spin coatingu nanesena na připravený substrát. Odpařením rozpouštědel byla získána funkční elektro–luminiscenční vrstva.

Na obr. 1 je voltampérová charakteristika diody s touto elektro–luminiscenční vrstvou. Obr. 3 představuje spektrum emitovaného světla diodou s aktivní vrstvou tohoto složení při napětí 13 V. Při pozorování pouhým okem se emise diody jeví jako velice jasné a živě působící žlutooranžové vyzařování, jehož intenzita je rovnoměrně rozložená v ploše diody a je pozorovatelná z velkého úhlového rozsahu.

Příklad 2

Aktivní vrstva ve světlo emitující diodě byla získána cestou disperze, která se připravila s využitím směsi rozpouštědel. Nejdříve se provedlo rozpuštění poly[2–methoxy–5–(2–ethylhexyloxy)–1,4–fenylenvinylenu] (MEH–PPV) ve směsi rozpouštědel. Dále se k dobře rozpuštěnému MEH–PPV přidala disperze nanočástic ZnO ve směsi rozpouštědel. Poměr ZnO ku MEH–PPV v této směsi činil 14,3 % hmotn. ku 85,7 % hmotn. Po smíchání roztoku polymeru s disperzí nanočástic a navazující homogenizaci byla směs pomocí metody spin coatingu nanesena na připravený substrát. Odpařením rozpouštědel byla získána funkční elektro–luminiscenční vrstva.

Na obr. 2 je voltampérová charakteristika diody s touto elektro–luminiscenční vrstvou. Obr. 4 představuje spektrum emitovaného světla diodou s aktivní vrstvou tohoto složení při napětí 13 V. Při pozorování pouhým okem se emise diody jeví jako velice jasné a živě působící žlutooranžové vyzařování, jehož intenzita je rovnoměrně rozložená v ploše diody a je pozorovatelná z velkého úhlového rozsahu.

Průmyslová využitelnost

Směs pro elektroluminiscenční aktivní vrstvu podle vynálezu umožňuje přípravu světlo emitujících zařízení, která naleznou uplatnění v polymerní elektronice, flexibilních displejích a flexibilních zdrojích světla pro osvětlení.

PATENTOVÉ NÁROKY

1. Aktivní vrstva pro elektroluminiscenční fólii, **v y z n a č u j í c í s e t í m**, že sestává z vodivého polymeru na bázi 2–methoxy– a 5–(2–ethylhexyloxy)– substituovaného poly–1,4–fenylenvinylenu v množství 85 až 90 % hmotn. a anorganického plniva na bázi nanočástic oxidu zinečnatého v množství 15 až 10 % hmotn.

2. Aktivní vrstva pro elektroluminiscenční fólii podle nároku 1, **v y z n a č u j í c í s e t í m**, že vodivý polymer má molekulovou hmotnost Mn v rozsahu 40 až 70 tis. a poměr Mw/Mn = 6.

3. Aktivní vrstva pro elektroluminiscenční fólii, podle nároku 1, **v y z n a č u j í c í s e t í m**, že anorganické plnivo na bázi nanočástic ZnO má velikost částic menší než 50 nm.

2 výkresy
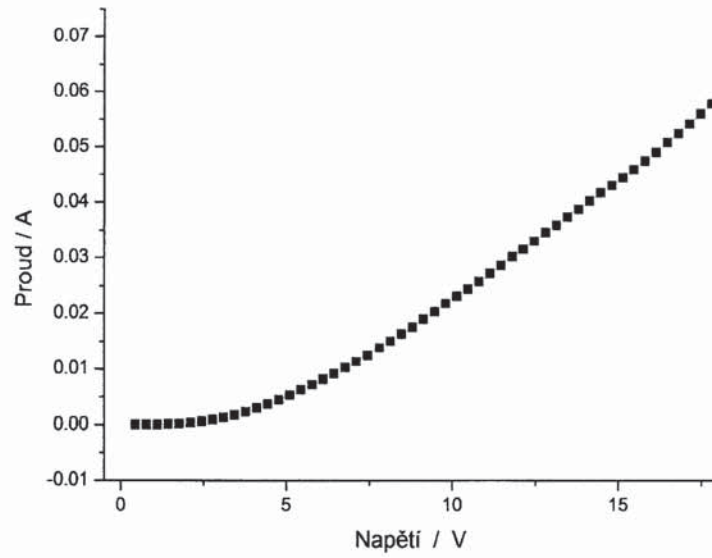
Obr. 1
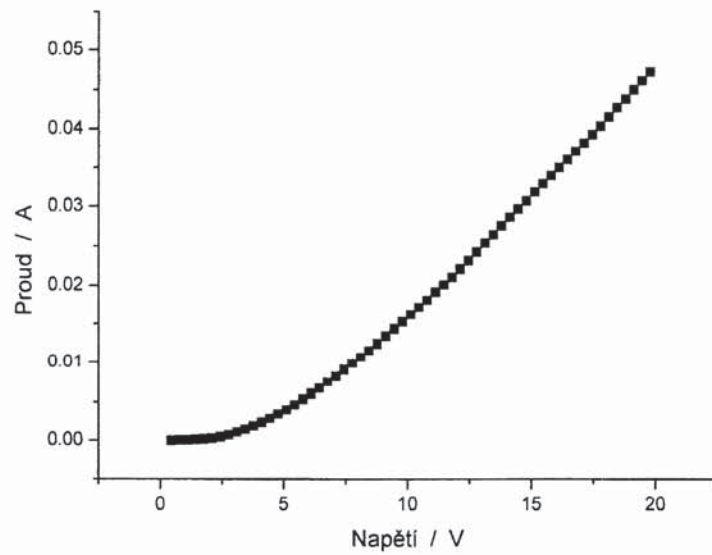
Obr. 2
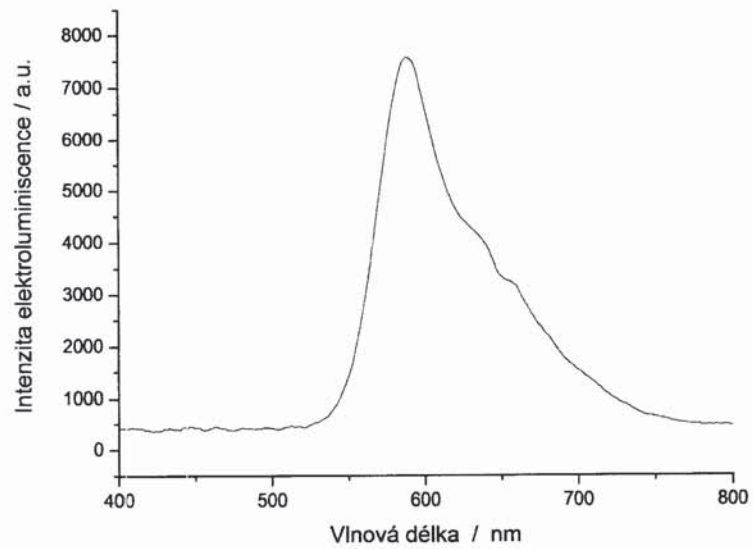
Obr. 3
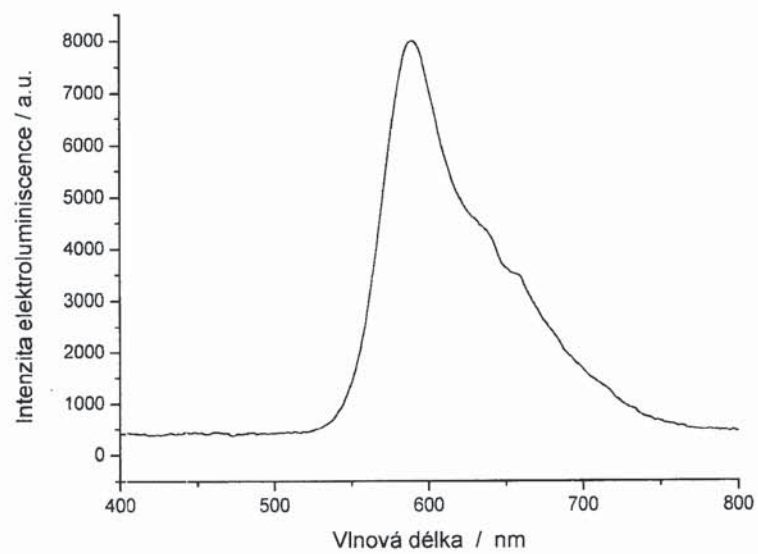
Obr. 4

Konec dokumentu

Utility model Nr. 26729 - Polymer ink for material printing

UŽITNÝ VZOR

(73) Majitel:
Univerzita Tomáše Bati ve Zlíně, Zlín, CZ

(72) Původce:
doc. Ing. et Ing. Ivo Kuřitka, Ph.D.et Ph.D., Brno, CZ
Ing. Pavel Urbánek, Pitín, CZ
Ing. Petr Krčmář, Valašské Klobouky, CZ
Ing. Jan Mašlík, Zlín, CZ

(74) Zástupce:
UTB ve Zlíně, Univerzitní institut, Ing. Dana Kreizlová, nám. T.G. Masaryka 5555, 760 01 Zlín

(54) Název užitného vzoru:
Polymerní inkoust pro materiálový tisk

CZ 26729 U1

Polymerní inkoust pro materiálový tisk

<u>Oblast techniky</u>

Technické řešení se týká složení polymerního inkoustu pro materiálový tisk.

<u>Dosavadní stav techniky</u>

5   V posledních letech se pozornost výzkumníků i výrobců obrací ke slibné technice výroby plošných elektronických struktur - k materiálovému tisku. Do této technologie lze zahrnout dílčí metody (sítotisk, inkjetový tisk, flexotisk, kapičkový tisk). Z nich pak jsou nejvýznamnější sítotisk a inkjetový tisk. To souvisí především s kvalitou deponované vrstvy, dále také s opakovatelností a možností soutisku. Tyto dvě technologie (sítotisk a inkjetový tisk) byly úspěšně použity pro vý
10   robu různých elektronických součástek, senzorů, optických komponent flexibilních displejů a dalších světlo emitujících zařízení.

Pro tisk složitějších struktur a motivů má velké výhody inkjetový tisk. Oproti sítotisku je výhodný především proto, že není potřeba před každou změnou tisknutého motivu konstrukce nového síta, ale tištěný motiv se nastaví přes digitální rozhraní.

15   Materiálové inkjetové tiskárny se od běžných uživatelských inkoustových tiskáren značně liší svými funkcemi. Především je to přesnost a opakovatelnost mechanických posunů, která umožňuje pracovat s tiskovým rozlišením až do 5080 dpi. Tiskovou hlavu lze také vyhřívat a snižovat tak viskozitu polymerních roztokových inkoustů používaných pro tisk.

Co se týká samotného procesu, při depozici je roztok (inkoust), obsahující látku určenou
20   k nanesení, zaveden do tiskové hlavy, odkud je například pomocí mechanicky se deformujících piezoelektrických prvků vystřikován směrem k substrátu. Vhodný profil elektrických signálů přiváděných na piezoelektrické prvky zaručí, že tiskovou hlavu opouští pravidelný proud jednotně zformovaných kapiček o určitém objemu. Tyto parametry jsou rozhodující pro dosažení potřebné kvality tisku.

25   Pro dokonalý tisk je přitom třeba brát v úvahu celý tiskový systém, jmenovitě tiskovou hlavu, typ substrátu, na který je deponován tištěný vzor, především však samotný inkoust. Existují čtyři hlavní druhy inkoustů pro materiálový tisk: taveniny neboli inkousty se změnou skupenství, inkousty UV tvrditelné, dále inkousty na bázi vody a inkousty na bázi rozpouštědel.

Inkousty na bázi taveniny vstupují do systému v pevné fázi a před samotným tiskem se zahřejí,
30   čímž se převedou do kapalného stavu. Výhoda těchto inkoustů spočívá ve velmi rychlém vytvrzení. Používají se především k tisku čárových kódů na neporézní substráty. Nevýhodou je materiálové omezení na termoplasty.

UV tvrditelné inkousty se úspěšně používají v tiskařství řadu let. Omezení se však týká oblasti potravinářství. Jejich nevýhody dále spočívají ve vysokých nákladech.

35   Inkousty na bázi vody jsou rozšířené především na domácích tiskárnách. Jejich výhodou je možnost využití i v biologických a potravinářských aplikacích. Tyto inkousty však vyžadují pórovité substráty nebo substráty se speciálně upraveným povrchem. Adheze s nepórovitým substrátem není dokonalá.

Inkousty na bázi rozpouštědel jsou široce používány pro velkoformátové aplikace s důrazem na
40   kvalitu tisku, odolnost obrazu a kompatibilitu se substrátem. Obecně se považují za nízkonákladové. Výhody dále zahrnují kompaktnost s různými typy substrátů a v pohotovém schnutí (často urychleném zahřátím). Nevýhody spočívají u některých těchto inkoustů v rychlém odpaření rozpouštědel, čímž může dojít k ucpání trysek tiskové hlavy.

Mezi nejdůležitější aplikační vlastnosti polymerního rozpouštědlového inkoustu patří viskozita
45   a povrchové napětí. Nevýhodou metody materiálového inkjetového tisku je její velká citlivost na tyto parametry, které určují rozmezí použitelnosti inkoustu. Viskozita by měla být v poměrně úzkém rozsahu $6\text{-}12 \times 10^{-3}$ Pas a povrchové napětí mezi 30×10^{-3} Nm^{-1} v závislosti na typu tiskové

hlavy (pod $3x10^{-3}$ Pas u tepelných tiskových hlav). Viskozita má zásadní vliv na tryskání a nanášení na substrát a její hodnota závisí především na přítomnosti a koncentraci polymeru, složení rozpouštědla a případné koagulaci. Viskozita může narůstat vlivem koagulace částic nebo v případě UV inkoustů i během skladování, kdy složky inkoustu mohou podléhat polymerním reakcím.

Povrchové napětí závisí především na složení inkoustu. Povrchové napětí je klíčové pro velikost a tvar kapky a dále pro smáčení povrchu substrátu inkoustem při dopadu kapky a rozlivu inkoustu po substrátu. To vše do značné míry ovlivňuje výkon a kvalitu tisku při použití inkjetové tiskové hlavy. Úzké rozmezí hodnot povrchového napětí je přitom obtížné dodržet a to může mít rozhodující dopad na dosažené parametry a nižší kvalitu tisku, zejména u funkčně citlivých plošných elektronických struktur nebo velkoformátových aplikací.

Podstata technického řešení

Uvedené nedostatky a nevýhody co se povrchového napětí inkoustu, a s tím spojenou adhezí na substrát, týká, do značné míry odstraňuje polymerní inkoust pro materiálový tisk podle technického řešení. Podstata technického řešení spočívá v tom, že polymerní inkoust pro materiálový tisk sestává z vodivého polymeru – poly[2-methoxy-5-(2-ethylhexyloxy)-1,4-phenylenvinylenu] o koncentraci 0,2 až 0,4 % hmotn. ve směsi organických rozpouštědel a povrchově aktivního činidla – polyethylenglykol-p-(1,1,3,3-tetramethylbutyl)-phenyl-etheru v množství 3 až 4 % hmotn.

Polymerní inkoust pro materiálový tisk podle technického řešení má s výhodou vodivý polymer o molekulové hmotnosti Mn v rozsahu 40 000 až 70 000 a poměru Mw/Mn = 6.

Výhodou polymerního inkoustu pro materiálový tisk podle technického řešení je především skutečnost, že se u něj dosahuje rapidního zlepšení tryskání kapek z tiskové hlavy a zvýšení samotné adheze na substrát, čímž se pak dosahuje tisku precizních homogenních a kvalitních vrstev, což je v oblasti materiálového tisku nejdůležitější.

Přehled obrázků na výkresech

Ukázky tryskání kapek z tryskové hlavy a nastavení parametrů procesu na trysce tiskové hlavy (waveformy) pro polymerní inkoust pro materiálový tisk podle technického řešení jsou znázorněny na přiložených obrázcích, kde značí:

Obr. 1 – tryskání kapek z tryskové hlavy pro konkrétní tiskovou hlavu (Dimatix DMP 2831)

Obr. 2 – waveforma (tj. parametry režimu provozu tiskové hlavy), 2a při tryskání, 2b bez tryskání inkoustu pro konkrétní tiskovou hlavu (Dimatix DMP 2831)

Příklady provedení technického řešení

Příklad 1

Složení směsi – tabulka 1:

Směs rozpouštědel	MEH-PPV	surfaktant
96,3353% hmotn.	0,2398% hmotn.	3,4249%hmotn.

Polymerní inkoust pro materiálový tisk byl připraven tak, že se nejdříve provedlo rozpuštění vodivého polymeru na bázi MEH-PPV(= poly[2-methoxy-5-(2-ethylhexyloxy)-1,4-phenylenvinylen]) ve směsi rozpouštědel tak, aby byl dodržen hmotnostní poměr obou složek vyplývající z tabulky 1. Po důkladném rozpuštění se k roztoku přidal surfaktant polyethylenglykol p-(1,1,3,3-tetramethylbutyl)-phenyl ether v množství odpovídajícím hmotnostním % uvedeným v tabulce. Výsledný inkoust měl optimální viskozitu, spadající do ideálního tiskařského rozsahu, tedy v oblasti $6-12x10^{-3}$ Pas, a optimální povrchové napětí menší než $30x10^{-3}$ Nm^{-1}.

Takto připravený inkoust byl již připraven pro naplnění inkjetové cartridge a k následnému tisku.

Na obr. 1 je znázorněn průběh tryskání – svislý směr drah kapiček z jednotlivých trysek takto upraveného inkoustu (odpovídá příkladu 1). Je patrné, že díky úpravě povrchového napětí dle technického řešení je průběh tryskání rovnoměrný s vysokou přesností danou konstantním objemem kapiček a konstantní rychlosti tryskání. Experiment byl proveden na zařízení Dimatix DMP 2831, dráhy tryskání jednotlivých kapiček zachyceny jako printscreen.

Na obr. 2 je znázorněna „wave-forma" (pracovní režim tiskové hlavy) pro polymerní inkousty dle technického řešení (pro všechny uvedené příklady). Konkrétní provedení je v SW ovládajícím tiskárnu Dimatix DMP 2831, zachyceno jako printscreen.

Příklad 2

Složení směsi – tabulka 2:

Směs rozpouštědel	MEH-PPV	surfaktant
96,2583% hmotn.	0,3195% hmotn.	3,4222% hmotn.

Polymerní inkoust pro materiálový tisk byl připraven analogickým postupem, jak je již uvedeno v příkladu 1, za dodržení aktuálních hmotnostních poměrů složek vyplývajících z tabulky 2. Výsledný inkoust měl optimální viskozitu, spadající do ideálního tiskařského rozsahu, tedy v oblasti 6-12x10^{-3} Pas, a optimální povrchové napětí menší než 30x10^{-3} Nm^{-1}.

Takto připravený inkoust byl již připraven pro naplnění inkjetové cartridge a k následnému tisku.

Příklad 3

Složení směsi – tabulka 3:

Směs rozpouštědel	MEH-PPV	surfaktant
96,1815% hmotn.	0,3991% hmotn.	3,4194% hmotn.

Polymerní inkoust pro materiálový tisk byl připraven analogickým postupem, jak je již uvedeno v příkladu 1, za dodržení aktuálních hmotnostních poměrů složek vyplývajících z tabulky 3. Výsledný inkoust měl optimální viskozitu, spadající do ideálního tiskařského rozsahu, tedy v oblasti 6-12x10^{-3} Pas, a optimální povrchové napětí menší než 30x10^{-3} Nm^{-1}.

Takto připravený inkoust byl již připraven pro naplnění inkjetové cartridge a k následnému tisku.

Průmyslová využitelnost

Polymerní inkoust pro materiálový tisk podle technického řešení umožňuje přípravu aktivní elektroluminiscenční vrstvy v elektronických a elektrických zařízeních pomocí inkjetového materiálového tisku, která nalezne uplatnění v polymerní elektronice, zejména flexibilních zdrojích světla pro osvětlení a flexibilních displejích. Další možnosti využití polymerního inkoustu pro materiálový tisk jsou v oblasti senzorů, elektrod, analytických a diagnostických pomůcek, proužků, popř. kitů; v obalové technice pro zajištění kontroly nad stavem baleného předmětu, bezpečnosti obalu, indikace otevření nebo porušení obalu.

NÁROKY NA OCHRANU

1. Polymerní inkoust pro materiálový tisk, **vyznačující se tím**, že sestává z vodivého polymeru – poly[2-methoxy-5-(2-ethylhexyloxy)-1,4-phenylenvinylenu] o koncentraci 0,2 až 0,4 % hmotn. ve směsi organických rozpouštědel a povrchově aktivního činidla – polyethylenglykol-p-(1,1,3,3-tetramethylbutyl)-phenyl-etheru v množství 3 až 4 % hmotn.
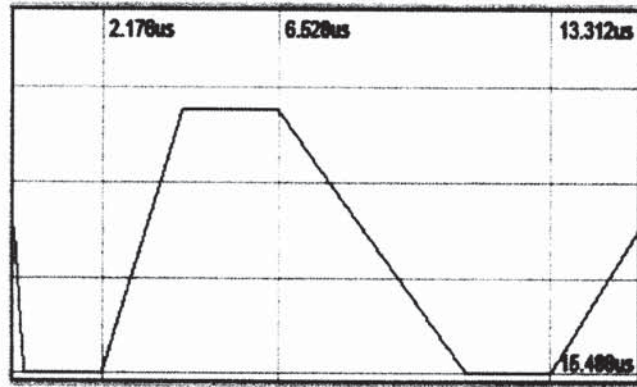
2. Polymerní inkoust pro materiálový tisk podle nároku 1, **v y z n a č u j í c í s e t í m** , že vodivý polymer má molekulovou hmotnost Mn v rozsahu 40 000 až 70 000 a poměr Mw/Mn = 6.
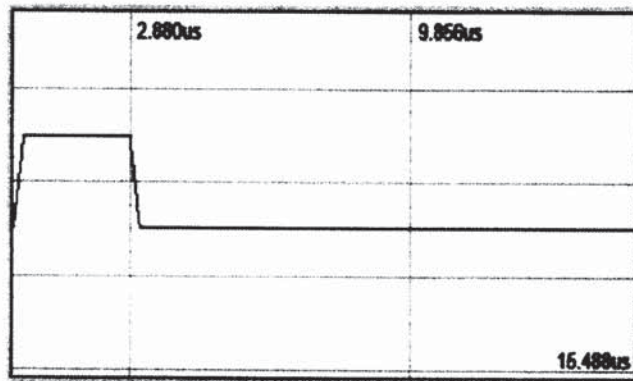
2 výkresy

Obr. 1

Obr. 2a

Obr. 2b

Konec dokumentu

Appendix II – Photovoltage method for the research of CdS and ZnO nanoparticles and hybrid MEH-PPV/nanoparticle structures

RESEARCH PAPER

Photovoltage method for the research of CdS and ZnO nanoparticles and hybrid MEH-PPV/nanoparticle structures

**J. Toušková · J. Toušek · J. Rohovec ·
A. Růžička · O. Polonskyi · P. Urbánek ·
I. Kuřitka**

Abstract The paper demonstrates an application of photovoltaic effect in the research of nanomaterials and hybrid structures of polymers with nanoparticles. Photovoltage (PV) measurement was utilized for estimating the size of CdS and ZnO nanoparticles and diagnostics of hybrid structures with poly[2-methoxy-5-(2-ethylhexyloxy)-1,4-phenylenevinylene] (MEH-PPV), namely nano-CdS/MEH-PPV and nano-ZnO/MEH-PPV. CdS average nanocrystal diameters 4.0 and 4.8 nm were calculated from the onset values of energies corresponding to the steep increase in the PV signals using the effective mass model. The range of size of ZnO particles was from about 5 up to 50 nm. Nanoparticle distribution obtained by transmission electron microscopy (TEM) measurements shows that the calculated diameters agree fairly well with the size of nanoparticles with the highest occurrence. The PV spectrum represents a sum of the spectra corresponding to the various nanoparticle sizes. The distribution of the nanoparticles was also obtained by a simple mathematical treatment of the PV spectra, and agreement with the results of TEM was found. PV and TEM measurements were performed on commercial CdS and ZnO nanoparticles and on CdS nanoparticles prepared in our laboratory. We employ triethanolamine as a protective agent to cover the surface of CdS nanoparticles. Nano-CdS/MEH-PPV and nano-ZnO/MeH-PPV hybrid structures were prepared, and influence of the particles on charge transport was shown by the PV spectra measurements.

Keywords Nanoparticles · CdS · ZnO · MEH-PPV · Photovoltage spectra · Transmission electron microscopy · Energy conversion

J. Toušková (✉) · J. Toušek · A. Růžička · O. Polonskyi
Department of Macromolecular Physics, Faculty of Mathematics and Physics, Charles University in Prague, V Holešovičkách 2, 180 00 Prague 8, Czech Republic
e-mail: jana.touskova@mff.cuni.cz

J. Rohovec
Institute of Geology of the Academy of Sciences of the Czech Republic, Rozvojová 269, 165 00 Prague 6, Czech Republic

P. Urbánek · I. Kuřitka
Faculty of Technology, Tomas Bata University in Zlin, Nam. T.G.Masaryka 275, 762 72 Zlin, Czech Republic

Introduction

In view of their practical applications in optoelectronics and photonics, strong effort has been expended during the past decade to prepare semiconductor nanoparticles. Combinations of organic materials and inorganic nanoparticles are being extensively studied in the field of photovoltaic hybrid solar cells. Inorganic nanoparticles in polymers firstly facilitate the charge transport, and secondly, they can extend the spectral response of the cells.

The nanoparticles have unique properties following from the quantum confinement effect. Their energy band gap exhibits significant size dependence. By controlling the particle size, the gap can be tuned and optical and electronic properties can be altered according to practical demands. Among nanosized particles, CdS and ZnO were intensively studied, e.g., (Brus 1984; Huang et al. 2004; Murray et al. 1993; Rossetti et al. 1984; Yadav et al. 2010) and (Musa et al. 2012; Yahya and Rusop 2012; Monticone et al. 1998; Lin et al. 2005). CdS semiconductor has many applications in photodiodes, light-emitting diodes, hybrid solar cells, or nonlinear optics, to mention only some of the uses (Kowshik et al. 2002; Masala et al. 2011; Jiang et al. 2010). The ZnO nanoparticles were developed (Womelsdorf et al. 1999, 2000, 2004) and later used also in hybrid solar cells (Sekine et al. 2009; Beek et al. 2004, 2006; Krebs et al. 2008; Hagemann et al. 2008) and especially in inverted structures (e.g., Hau et al. 2008; Wang et al. 2010; Tan et al. 2013).

We studied CdS and ZnO nanoparticles purchased from Sigma-Aldrich Company. These particles have a quite thick surfactant layer limiting their function. Besides, CdS nanoparticles based on a principle similar to that used by Unni et al. (2009) were investigated. In order to improve their physical properties, we used triethanolamine $N(CH_2CH_2OH)_3$ (TEA) as a protective agent to cover the surface (Rohovec et al. 2011).

Absorption spectra measurements relying on the transmission of the particle layers are usually used for determining the nanoparticle size (Murray et al. 1993; Kagan et al. 1996). We employ the method of photovoltage (PV) spectra measurements. This method is simpler and cheaper as compared with the absorption measurements. Another advantage of the PV method lies in the fact that the measurement depends only on absorbed light so that it is not influenced by a possible discontinuity and/or contamination of the nanoparticles. Details of the PV method have been published elsewhere (Toušek et al. 2010).

Experimental

CdS and ZnO nanoparticles

Lumidot CdS nanoparticles No. 662372 were purchased from Sigma-Aldrich. The company states that the nanoparticles with carboxylic acids used as the capping agent were organically stabilized in toluene. Hereafter, these particles are denoted as A-type. ZnO nanoparticles No. 677450 were also delivered by this company.

The surfactant of A-type CdS particles proved to be rather thick. Because thin surfactant on CdS nanocrystals is needed for charge transport in optoelectronic devices, we have used CdS nanoparticles with TEA surface layer. The alkanolamine molecule remains in touch with the nano-CdS particle, stabilizing the particle against coagulation. Short alkyl-OH chains present in the alkanolamine molecules should not interfere in the electron transfer between CdS nanocrystals (Rohovec et al. 2011). These nanocrystals were denoted D-type particles.

Preparation of samples and arrangement of experiment

The layers of nanocrystalline CdS and ZnO were prepared by casting of suspensions containing the nanoparticles on ITO-covered glass electrode and dried at 100 °C in vacuum oven for 2 h. On some of them, [2-methoxy-5-(2-ethylhexyloxy)-1,4-phenylenevinylene] (MEH-PPV) polymer layer was spin-coated to obtain a hybrid structure. The spin-coating conditions were set up on 3,500 rpm, and the duration time was 30 s. Specimens with the spin-cast polymer layers were annealed in vacuum oven at the same temperature and for the same time as the nanoparticles. The thickness of this structure was 50–60 nm.

To characterize the nanoparticles, we have employed the method of PV spectra measurement. A-type CdS and ZnO nanoparticle layers with a thicker surfactant layer needed measurement in an electrochemical cell (Fig. 1a). Iodine-containing electrolyte was put between the glass/ITO electrodes, facilitating the charge transport. Electric field is formed as a result of the difference between the work functions of the nanoparticles and the substrate, and it separates electrons and holes from the light-generated excitons. The electrons are transported into ITO substrate, and the free places are replenished with the electrons carried by iodine ions from the top electrode to the nanoparticles. The situation suggests the processes in Graetzel cells (O'Regan and Graetzel 1991; Grätzel 2003). However, it must be noted that in contrast to Graetzel cells, no dye is present, which leads to recombination losses at the nanoparticle

surface and, consequently, lowers the PV signal. A more simple arrangement could be used for the measurement of PV of the D-type CdS layers, with Mylar sheet separating the layers from another ITO/ glass electrode to form a capacitive coupling (Fig. 1b). After illumination, the electrons are transported into ITO substrates, leaving the holes in the particles. The PV is formed between the substrate and positively charged nanoparticles. Light from a monochromator was chopped with frequency 11 Hz. In our experiment, this frequency was sufficiently low to obtain saturated pulses of the PV not influenced by relaxations. The PV spectra of all samples were detected by Lock-in Amplifier. The PV signal was recalculated for constant impinging photon flux density and corrected for transparency of the glass/ITO electrodes. The measurement was performed at room temperature.

The PV of the hybrid structures with both types of CdS and/or ZnO nanoparticles and MEH-PPV polymer was measured in the arrangement shown in Fig. 1b, with active layer of the composite. The electric field at the nanoparticle/polymer interface separates electrons and holes from excitons generated in the polymer as well as in the nanoparticles. As a result, the holes are transported through the polymer into the ITO substrate, while electrons are conducted to the opposite side by a chain of nanoparticles. A PV is created, indicating that the polymer probably filled the free space among nanoparticles at least in some places, giving rise to a blend structure.

D-type CdS nanoparticles yielded quite strong PV signals ~10 µV. We have found that sufficient PV signal (>5 µV) was also obtained from nanoparticles with a thick surfactant (A-type CdS and ZnO) if covered with electrolyte. This also holds for the hybrid structure with such particles. It is probably due to a contact area formed between the particles and surrounding conducting medium, which lowers the total resistivity of the sample.

Another method used for investigation of the nanoparticles was transmission electron microscopy (TEM) using Jeol 2000 FX transmission electron microscope.

Results and discussion

CdS and ZnO particle size

Figure 2 shows the PV spectra of the samples with A- and D-type of CdS nanoparticles.

The spectra in Fig. 2a, b indicate a clear blue shift from the bulk material band-gap (2.42 eV, which corresponds to 512 nm) due to the quantum confinement effect. The band gaps (E) of the CdS nanoparticles are related to the radius of the particles according to the Brus equation (Brus 1984; Lippens and Lannoo 1989) following from the effective mass model and including Coulomb attraction of the electron and the hole (the correlation term is neglected):
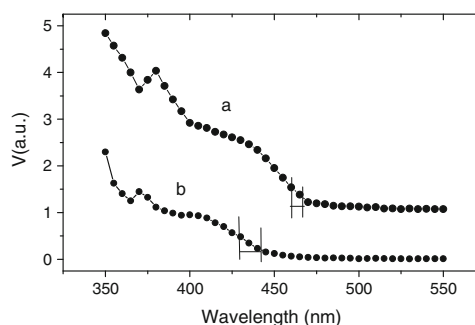
Fig. 2 Photovoltage spectra of CdS nanoparticles. *a* A-type samples, *b* D-type samples. The *bars* show the range of the threshold wavelengths of all measured samples (see text)

Fig. 1 Schematic arrangement of the samples for photovoltage measurements. **a** A-type of CdS and ZnO nanoparticles, **b** D-type of CdS nanoparticles
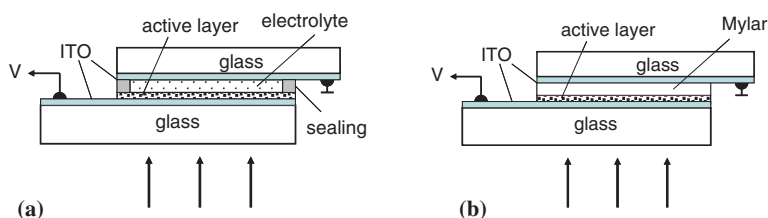
$$E = E_g + \frac{\hbar^2 \pi^2}{2r^2}\left[\frac{1}{m_e^*} + \frac{1}{m_h^*}\right] - \frac{1.8e^2}{4\pi\varepsilon_0\varepsilon_r r} \qquad (1)$$

E_g is the bulk band-gap energy, ε_0 is the permittivity of vacuum, ε_r is the relative permittivity (a high-frequency value 4.6 was used) (Zhou 2003), m_e^*(0.18 m_e), and m_h^*(0.53 m_e) are the electron and the hole effective masses, respectively (Lippens and Lannoo 1989), and $2r$ is the diameter of the particles. Equation (1) was used for the evaluation of the nanoparticle sizes.

In fact, the PV spectra represent a sum of the spectra corresponding to the various nanoparticle sizes similarly as in Rossetti et al. (1984) where absorption spectra were employed. Let us note that for thin layers, where the product of the absorption coefficient and the thickness of the layer are less than one, the PV signal is proportional to absorbance. Important advantage is that the PV signal is not influenced by the non-absorbed light and depends only on the light absorbed in the nanocrystals. To analyze the PV spectra, we have used the method and the relations published in Pesika et al. (2003). Under an assumption of spherical nanoparticles and assuming that the absorption coefficient is not dependent on nanoparticle size, the PV is proportional to the total volume of all particles bigger than or equal to the particles with the size corresponding to the PV threshold:

$$PV \sim \int_r^\infty \frac{4}{3}\pi r^3 n(r)\, dr \qquad (2)$$

where $n(r)$ is the size distribution, and r is the radius of the nanoparticles.

The particle size distribution was found in the case of PV measurement similarly as for absorbance using the derivative of the signal with respect to the particle radius (Pesika et al. 2003). The full lines in Fig. 3 represent the distributions calculated using the PV spectra. The particles size with the highest occurrence can be also found from the threshold wavelength of the steep increase in the PV signal.

Fig. 3 TEM images of A- and D-type of CdS nanoparticles. Histograms showing particle size distribution are at the right side of the images: *a* A-type nanoparticles, *b* D-type nanoparticles. The *solid line* is the distribution acquired from the PV measurement
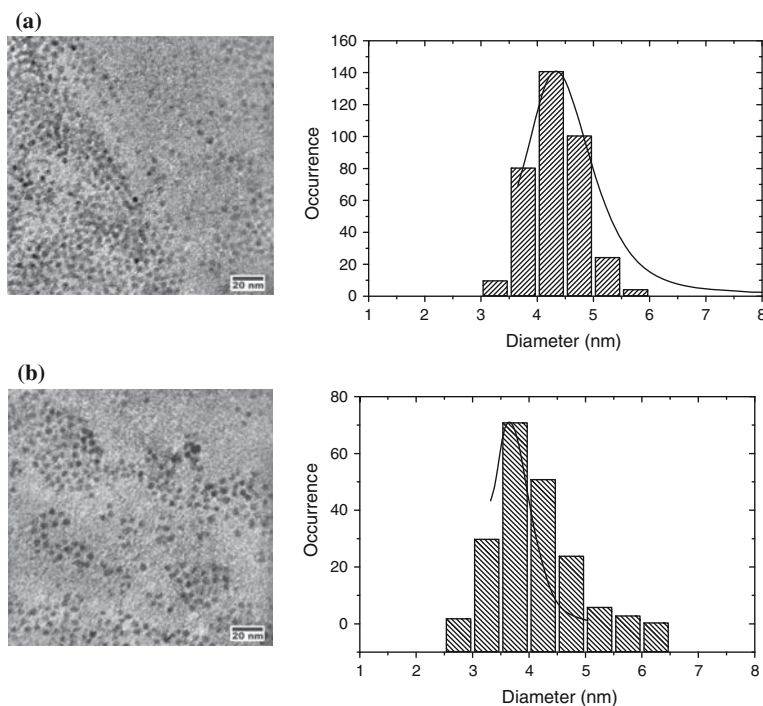
The threshold wavelengths of A-samples were found using the derivative of the fast increasing part of the spectra with respect to the wavelength. They ranged from 460 to 467 nm corresponding to nanoparticle diameters from 4.7 to 4.9 nm. The interval of the threshold wavelengths of measured A-samples is depicted in Fig. 2a with the bars. Figure 2a shows the PV of A-sample with threshold wavelength of 464 nm, which gives the calculated diameter of 4.8 nm. The Aldrich Company reports the size of 5.0 nm. The PV signal of D-sample (Fig. 2b) increases strongly from the threshold wavelength of 440 nm. The diameter calculated using this value is 4.0 nm. The threshold wavelengths ranging from 430 to 443 nm with corresponding diameters from 3.9 to 4.1 nm were obtained in a similar way as in the case of A-samples. This means that the inaccuracy of the determination of the threshold wavelengths in the PV spectra leads to ±0.1 nm inaccuracy of the diameters.

The results obtained from the PV spectra were compared with the measurements acquired from the transmission electron microscope. Figure 3 shows TEM images for A- and D-type CdS nanoparticles taken at the indicated magnification along with the histograms showing particle size distribution. Good agreement of the distribution calculated using the PV spectra with the distribution from the histograms is seen. The histograms depict various sizes of the particles in individual samples yielding "effective band-gaps" of the nanoparticles (Rossetti et al. 1984). Using Eq. (1), these band-gaps (E) of the CdS nanoparticles were calculated. The range of energies corresponding to the respective diameters of the particles is in Table 1. The threshold wavelengths estimated from the PV spectra and the calculated diameters d_{PV} fall within the intervals specified by the quite narrow histograms of samples A and D.

Figure 4 depicts the TEM image of ZnO nanoparticles, and a markedly broad size distribution is shown by the histogram.

The PV spectrum of ZnO nanoparticles is in Fig. 5. The PV increases for wavelengths shorter than 375 nm, i.e., for energy higher than that of band-gap of the bulk material. In this case, a blue shift is not apparent because of very weak confinement due to the presence of large particles indicated by the histogram (Fig. 4), and relation (2) cannot be used for the particles distribution. The Aldrich Company declares the sizes up to 50 nm. The increase in the PV signal in Fig. 5 points to the presence of nanoparticles with small size from 5.7 to 4.3 nm as calculated using Eq. (1) and parameters m_e^* (0.24 m_e) and m_h^* (0.45 m_e) (Brus 1984), ε_r (3.7) (Monticone et al. 1998), and E_g (3.3 eV).

Table 1 The range of nanoparticle diameters obtained from the histograms (d_{TEM}) and calculated energies (E) and wavelengths (λ) of the appropriate "effective band-gaps"

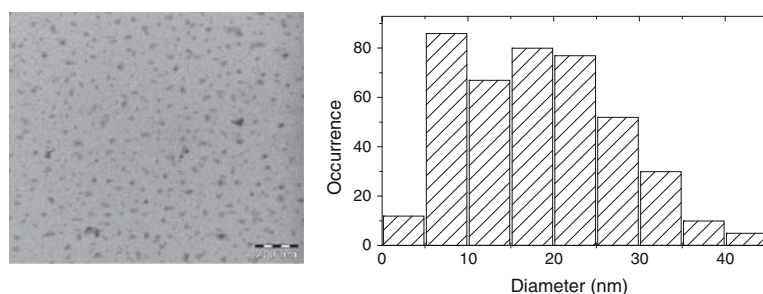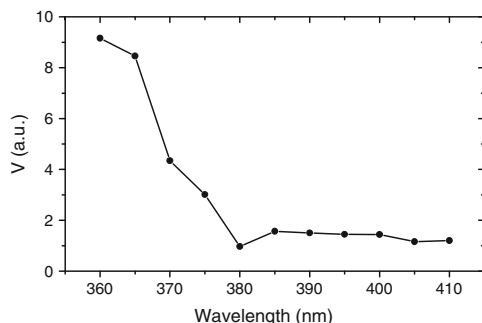| Samples	A	D
d_{TEM} (nm)	3.0–6.0	2.5–6.5
E (eV)	3.29–2.54	3.76–2.49
λ (nm)	377–488	330–498
d_{PV} (nm)	4.8 ± 0.1	4.0 ± 0.1

The diameters estimated from the threshold wavelengths in the PV spectra (d_{PV}) are in the last row

Fig. 4 TEM image of ZnO nanoparticles. Histogram showing particle size distribution is at the *right side* of the image

Fig. 5 Photovoltage spectrum of ZnO nanoparticles

Fig. 6 Photovoltage spectra of pristine MEH-PPV (*a*) and MEH-PPV with CdS nanoparticles (*b*)

Fig. 7 *a* MEH-PPV photovoltage spectrum. *b* Spectrum of the polymer with ZnO nanoparticles

Fig. 8 PV spectra in UV region *a* pristine MEH-PPV, *b* MEH-PPV/ZnO blend

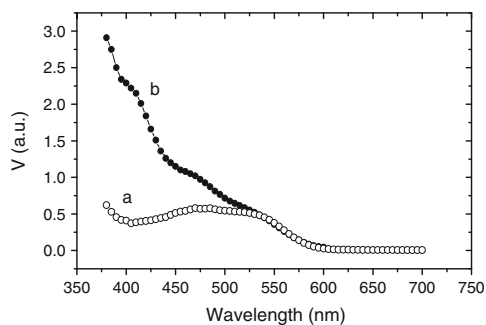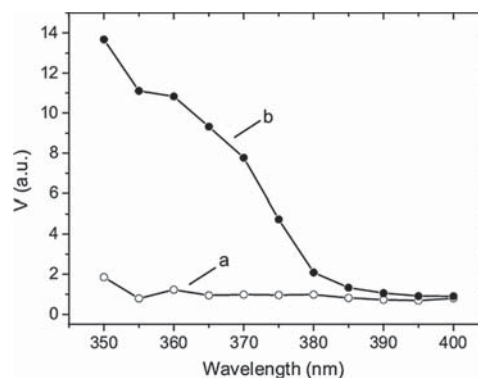### Hybrid structure of MEH-PPV with CdS or ZnO nanoparticles

Figure 6 shows the PV spectra of pristine MEH-PPV and of composite MEH-PPV with CdS nanoparticles. After achieving maximum at 480 nm, which corresponds to the maximum of absorbance, the spectrum of the pristine MEH-PPV (curve a) decreases, whereas the spectrum of the composite increases over the whole measured spectral region by the action of the nanoparticles. This situation is illustrated on MEH-PPV/D-type of CdS structure (curve b). The presence of the nanoparticles in composite raises the PV signal from about 530 nm, i.e., for much higher wavelengths than that corresponding to the onset of the CdS spectrum (Fig. 2). This is a consequence of the transport of electrons coming from the polymer through the nanoparticles toward the top surface

which is, for example, known to improve the function of hybrid solar cells.

Comparison of MEH-PPV PV spectrum with the spectrum of the polymer with ZnO nanoparticles is shown in Fig. 7. In the part where the PV of pristine material decreases (curve a), curve b keeps increasing. In fact, the PV signal of the composite increases throughout the whole wavelength range from about 600–400 nm above the values of PV measured on the pristine polymer. Also, in this case, ZnO nanoparticles act as a transporter of electrons.

The signal from ZnO nanoparticles in MEH-PPV polymer can be expected in UV region. This is clearly seen in Fig. 8.

Figure 8 shows a strong increase in PV signals for wavelengths lower than about 380 nm in agreement with the result of measurement of the spectrum of ZnO particles (Fig. 5). It is therefore evident that the increase belongs to ZnO particles.

Conclusions

The PV method for estimation of nanoparticle size and for determination of the size distribution used here is an alternative to the commonly employed absorbance measurement. There are several advantages of the PV method. The PV signal depends only on the light absorbed in the nanocrystals in contrast to transmittance measurement, which is also influenced by the light possibly unabsorbed in the nanocrystals. The PV relies on separation of light-generated charge carriers and includes in itself information on charge transport in measured layers or in a composite. This is similar to the data obtained from EQE measurement in solar cells but without the necessity of formation of a complete device. Besides, the PV method is simple and less time-consuming; therefore, it is quite cheap. Our PV method in the arrangement shown in Fig. 1 gives reliable results with good reproducibility, as has been verified by many measurements. The method was employed for estimating CdS and ZnO particle size and the size distribution. The effective mass model was used for calculating the particle size. Nanoparticle size distributions were derived from the PV spectra. The distributions agree fairly well with the distributions following from TEM data. The sizes of nanoparticles with the maximum occurrence are in agreement with those calculated from the onset values of wavelengths corresponding to the steep increase in the PV signal. Appropriate diameters of A-type CdS nanoparticles with carboxylic acids surfactant and D-type CdS nanoparticles with TEA surfactant were estimated at 4.8 and 4.0 nm, respectively. Sigma-Aldrich Company reports the size of 5 nm for A-type CdS particles. The PV spectra of ZnO particles show that besides the reported large particle size of up to 50 nm, also small nanoparticles are present with a size from 4.3 to 5.7 nm, which is confirmed by TEM results. The inaccuracy of size determination of all particles is ± 0.1 nm.

With a view to future use especially in hybrid solar cells, nano-CdS/MEH-PPV and nano-ZnO/MEH-PPV were prepared. Effect of the nanoparticles is shown in the PV spectra of these structures. The photovoltage is formed as a consequence of the transport of electrons and holes separated by the electric field, which is created on the interface of the nanoparticles and the polymer.

References

Beek WJE, Wienk MM, Janssen RAJ (2004) Efficient hybrid solar cells from zinc oxide nanoparticles and a conjugated polymer. Adv Mater 16:1009–1013

Beek WJE, Wienk MM, Janssen RAJ (2006) Hybrid solar cells from regioregular Polythiophene and ZnO. Adv Funct Mater 16:1112–1116

Brus LE (1984) Electron-electron and electron-hole interactions in small semiconductor crystallities: the size dependence of the lowest excited electronic state. J Chem Phys 80:4403–4409

Grätzel M (2003) Dye-sensitized solar cells. J Photochem Photobiol 4:145–153

Hagemann O, Bjerring M, Nielsen NCh, Krebs FC (2008) All solution processed tandem polymer solar cells based on thermocleavable materials. Sol Energy Mater Sol Cells 92:1315–1327

Hau SK, Yip HL, Baek NS, Zou J, O'Malley K, Jen AKY (2008) Air-stable inverted flexible polymer solar cells using zinc oxide nanoparticles as an electron selective layer. Appl Phys Lett 92:2533011–2533013

Huang NM, Kan CS, Khiew PS, Radiman S (2004) Single w/o microemulsion templating of CdS nanoparticles. J Mater Sci 39:2411–2415

Jiang X, Chen F, Qiu W, Yan Q, Nan Y, Xu H (2010) Effect of molecular interface modification in CdS/polymer hybrid bulk heterojunction solar cells. Sol Energy Mater Sol Cells 94:2223–2229

Kagan CR, Murray CB, Bawendi MG (1996) Long-range resonance transfer of electronic excitations in close-packed CdSe quantum-dot solids. Phys Rev B 54:8633–8644

Kowshik M, Desmukh N, Vogel W, Urban J, Kulkarni SK, Paknikar KM (2002) Microbial synthesis of semiconductor CdS nanoparticles, their characterization, and their use in the fabrication of an ideal diode. Biotechnol Bioeng 78:583–588

Krebs FC, Thomann Y, Thomann R, Andereasen JW (2008) A simple nanostructured polymer/ZnO hybrid solar cell-preparation and operation in air. Nanotechnology. doi:10.1088/0957-4484/19/42/424013

Lin KF, Chehg HM, Hsu HCh, Lin LJ, Hsieh WF (2005) Band gap variation of size-controlled ZnO quantum dots synthesized by sol–gel method. Chem Phys Lett 409:208–211

Lippens PE, Lannoo M (1989) Calculation of the band gap for small CdS and ZnS crystallites. Phys Rev B 39:10935–10942

Masala S, Del Gobbo S, Borriello C et al (2011) Hybrid polymer-CdS solar cell active layers formed by in situ growth of CdS nanoparticles. J Nanopart Res 13:6537–6544

Monticone S, Tufeu R, Kanaev AV (1998) Complex nature of the UV and visible fluorescence of colloidal ZnO nanoparticles. J Phys Chem 102:2854–2862

Murray CB, Norris DJ, Bawendi MG (1993) Synthesis and characterization of nearly monodisperse CdE (E = S, Se, Te) semiconductor nanocrystallites. J Am Chem Soc 115:8706–8715

Musa I, Massuyeau F, Faulques E, Nguyen T-P (2012) Investigation of optical properties of MEH-PPV/ZnO nanocomposites by photoluminescence spectroscopy. Synth Metals 162:1761–1765

O'Regan B, Graetzel M (1991) A low-cost, high efficiency solar cell based on dye-sensitized colloidial TiO_2 films. Nature 353:737–740

Pesika NS, Stebe KJ, Searson PC (2003) Relationship between absorbance spectra and particle size distributions for quantum-sized nanocrystals. J Phys Chem B 107:10412–10415

Rohovec J, Toušková J, Toušek J, Schauer F, Kuřitka I (2011) New cadmium sulfide nanomaterial for heterogeneous organic photovoltaic cells. World Renewable Energy Congress Sweden 2011 Linköping, Sweden 2815–2822

Rossetti R, Ellison JL, Gibson JM, Brus LE (1984) Size effects in the excited electronic states of small colloidal CdS crystallites. J Chem Phys 80:4464–4469

Sekine N, Chou Ch-H, Kwan WL, Yang Y (2009) ZnO nanoridge structure and its application in inverted polymer solar cell. Org Electron 10:1473–1477

Tan MJ, Zhong S, Li J, Chen Z, Chen W (2013) Air-stable efficient inverted polymer solar cells using solution processed nanocrystalline ZnO interfacial layer. ACS Appl Mater Interf 5:4696–4701

Toušek J, Toušková J, Křivka I, Pavlačková P, Cimrová V, Výprachtický D (2010) Surface photovoltage method for evaluation of exciton diffusion length in fluorene-thiophene based copolymers. Org Electron 11:50–56

Unni C, Philip D, Smitha SL, Nissamudeen KM, Gopchandran KG (2009) Aqueous synthesis and characterization of CdS, CdS: Zn^{2+} and CdS: Cu^{2+} quantum dots. Spectrochim Acta A Mol Biomol Spectrosc 72:827–832

Wang JCh, Weng WT, Tsai MY, Lee MK, Horng SF, Perng TP, Kei ChCh, Yu ChCh, Meng HF (2010) Highly efficient flexible inverted organic solar cells using atomic layer deposited ZnO as electron selective layer. J Mater Chem 20:862–866

Womelsdorf H, Hoheisel W, Passing G (1999) Nanopartikuläres, redispergierbares Fällungsoxid. German Patent (filing date 23.02.1999), DE 19907704 A1

Womelsdorf H, Hoheisel W, Passing G (2000) Process for producing nanoparticulate, redispersible zinc oxide gels, European patent (filing date 11.02.2000) EP 1157064

Womelsdorf H, Hoheisel W, Passing G (2004) Nanoparticulate, redispersible zinc oxide. United States patent (patent date 23.03.2004) US 6,710,091 B1

Yadav RS, Mishra P, Mishra R, Kumar M, Pandey AC (2010) Growth mechanism and optical property of CdS nanoparticles synthesized using amino-acid histidine as chelating agent under sonochemical process. Ultrason Sonchem 17:116–122

Yahya NZ, Rusop M (2012) Investigation on the optical and surface morphology of conjugated polymer MEH-PPV: ZnO nanocomposite thin films. J Nanomater 2012:793679–793683

Zhou SM (2003) Dielectric properties of phase-size control CdS nanoparticles and conventional powders. Phys Stat Sol A 200:423–428

List of publications

Papers

Pavel Urbánek, Ivo Kuřitka, Stanislav Daniš, Jana Toušková, Jiří Toušek; Thickness Threshold of Structural Ordering in Thin MEH-PPV Films; submitted to Polymer journal at 7th of March 2014, accepted at 19th of May 2014.

J. Toušková, J. Toušek, J. Rohovec, A. Růžička, O. Polonskyi, P. Urbánek, I. Kuřitka; Photovoltage method for the research of CdS and ZnO nanoparticles and hybrid MEH-PPV/nanoparticle structures; Journal of Nanoparticle Research, DOI: 10.1007/s11051-014-2314-5.

V. Sedlařík, A. Vesel, P. Kucharczyk, P. Urbánek; A NOVEL APPROACH FOR QUALITATIVE DETERMINATION OF RESIDUAL TIN BASED CATALYST IN POLY(LACTIC ACID) BY X-RAY PHOTOELECTRON SPETROSCOPY; Materials and technology 45 (2011) 3.

Conference contributions

Urbanek, P., Kuritka, I., Krcmar, P. and Maslik, J. (2013), Paper No P31: Optoelectronic Properties of MEH-PPV Thin Films Influenced by their Thickness. SID Symposium Digest of Technical Papers, 44: 105–107. doi: 10.1002/sdtp.32

Maslik, J., Urbanek, P., Kuritka, I. and Krcmar, P. (2013), Paper No P20: Surface Modification of ITO-Coated PET Foil for Material Printing. SID Symposium Digest of Technical Papers, 44: 70–71. doi: 10.1002/sdtp.33

Pavel Urbánek, Ivo Kuřitka, Petr Krčmář , Jan Maslik and Jiri Bartos; Polysilanes Thin Films Doped by Coumarin; In NANOCON 2012 Conference proceedings; ISBN 978-80-87294-32-1, p.103.

Petr Krčmář, Pavel Urbánek, Ivo Kuřitka, Jan Mašlík, Jiří Bartoš; The Effect of The Exalite on Photoluminescence of Poly(methylphenylsilane) in Thin Films, In NANOCON 2012 Conference proceedings; ISBN 978-80-87294-32-1, p.133.

Pavel Urbánek, Petr Krčmář, Ivo Kuřitka; The Influence of Process Conditions on the Thickness and Photoluminescence of the PMPSi Thin Films; Plastko 2012 Conference, Fulltext in Conference Proceeding, ISBN 978-80-7454-137-7, p.236-239.

Petr Krčmář, Pavel Urbánek, Ivo Kuřitka; The influence of the substrate surface on deposition of thin layers from PEDOT:PSS; Plastko 2012 Conference, Fulltext in Conference Proceeding, ISBN 978-80-7454-137-7, p.307-311.

URBÁNEK, Pavel; KUŘITKA, Ivo; URBÁNEK, Michal. The Influence of Thickness and Used Solvent on Luminescence and Photodegradation of Polysilane Thin Films; In NANOCON 2011 Conference proceedings; 2011. ISBN 978-80-87294-23-9, p. 34-35.

Pavel Urbánek, Ivo Kuřitka, and Petr Krčmář. The Influence of ZnO content on optoelectronic properties of films from MEH-PPV/ZnO composite. In Proceedings of the 13th WSEAS international conference on Mathematical and computational methods in science and engineering (MACMESE'11), 2011, 411-414, ISBN: 978-1-61804-046-6.

Patents and utility models

Patent Nr. 304387 „Active layer for electroluminescence foils"

Utility model Nr. 25048 „Active layer for electroluminescence foils"

Utility model Nr. 26391 „Inorganic ink based on nanoparticles, especially for material print"

Utility model Nr. 26729 „Polymer ink for material printing"

CURRICULUM VITAE

Name: Pavel Urbánek

Date of birth: 26. 11. 1985

Place of birth: Uherské Hradiště

Permanent address:

Pitín 239, 687 71, Czech Republic

Nationality: Moravian

Affiliation: Polymer Centre, Faculty of Technology, Tomas Bata University in Zlín, Náměstí T. G. Masaryka 275, 762 72 Zlín, Czech Republic

Centre of Polymer Systems, University Institute, Tomas Bata University in Zlin, Nad Ovcirnou 3685, 760 01 Zlín, Czech Republic

Phone: (+420)-57-603-8049

E-mail: urbanek@ft.utb.cz

Education and stays:

May 2014 - stay at Charles University in Prague, Faculty of Mathematics and Physics, Department of Macromolecular Physics, Conductivity of thin films measurements

September 2013 – stay at Charles University in Prague, Faculty of Mathematics and Physics, Department of Macromolecular Physics, Photovoltage surface spectra measurements

2010 – to date

Doctoral study program at Tomas Bata University in Zlin,

Faculty of Technology, Technology of Macromolecular Compounds

2008 - 2010

Master program at Tomas Bata University in Zlin, Faculty of Technology, Polymer Engineering

15th sept. 2008 - 31th January 2009

Erasmus study stage, coordinator prof. Sariciftci,

Linz Institute of Solar Cells,

Johannes Kepler Universität Linz, Austria

2007 july/august Language study stage in Dresden, Kästner College

2005 - 2008

Bachelor programme at Tomas Bata University in Zlin, Faculty of Technology, Polymer Engineering

Projects: IGA/FT/2012/025 "Modifikované polymerní materiály pro tenké vrstvy" – project leader

IGA/4/FT/11/D – "Tenké hybridní kompozitní vrstvy" – project leader

FR-TI3/424 - "Elektroluminiscenční fólie pro bezpečnostní interiérové osvětlení" – Junior researcher in team

CZ.1.07/2.2.00/15.0363 - "Inovace vzdělávání v technologiích a aplikacích polymerů" - member of research team

Grant IAA100100622 of Grant Agency of the Academy of Sciences of the Czech Republic – "Konjugované křemíkové polymery pro rezisty v nanotechnologiích" - member of research team

Grant GA202/09/1206 of Grant Agency of the Academy of Sciences of the Czech Republic – "Nanokrystalické heterogenní sluneční fotovoltaické články" – member of research team

Work experience: 2007 – 2008 marketing manager, LUKO strojírny s.r.o.